東海大學化學工程與材料研究所

博士論文

指導教授 ： 黃琦聰 博士

指導教授 ： 程學恆 博士

Design and Control of a Complete Azeotropic Distillation System Incorporating Stripping Columns for Isopropyl Alcohol Dehydration

研究生 ： 張文騰 撰

中華民國一〇二年二月

博士學位論文指導教授推薦書

化學工程與材料工程研究所 張文騰 君所提供之論文

Design and Control of a Complete Azeotropic Distillation System Incorporating Stripping Columns for Isopropyl Alcohol Dehydration

係由本人指導撰述，同意提付審查

此致

化學工程與材料工程研究所所長

指導教授：

日期：102年 1月 16日

博士學位論文口試委員會審定書

化學工程與材料工程研究所 張文騰 君所提供之論文

Design and Control of a Complete Azeotropic Distillation System Incorporating Stripping Columns for Isopropyl Alcohol Dehydration

經本委員會審定通過，特此證明。

論文口試委員會

委　　員：程萬里　喬儒明

張煖　謝孫未

王聖漢

指導教授：程萬里

中華民國 102 年 1 月 16 日

Abstract

Wen-Teng Chang
Ph. D. of Department of Chemical and Material Engineering

Because the reflux ratio used either in the pre-concentration column or the recovery column of the three-column heterogeneous distillation sequence for IPA dehydration system is quite small demonstrated by Arifin and Chien (2007), these two conventional distillation columns are both replaced by a stripping column in this study and a new separation scheme called Scheme 3 is thereby developed. The economic analysis of the proposed system shows it is more energy efficient and lower capital costs as compared to the two and three-column sequences afore-mentioned.

Further, in developing a plant-wide control structure, a tray temperature control loop is implemented in each of the three columns which regulates reboiler duty in order to maintain the bottom product compositions for Scheme 3, and ratio control of the organic reflux flow to the feed flow rate of the azeotropic column is used to reject feed rate disturbance. Closed-loop responses to ±20% changes in fresh feed rate and feed H_2O composition show that the proposed strategy has good control performance. This proposed scheme can be achieved three goals that are more energy saving, less total annual cost, and process easily controlled.

謝致

首先感謝吾師 黃琦聰博士，在專業知識上的傳授與待人處世啟發， 程學恆博士 和 謝樹木博士在化材領域的諄諄教導，師恩沒齒難忘；感謝 喬緒明博士、淡江大學 陳錫仁博士、 張煖博士和大華技術學院 王聖潔博士在論文研究方面的指導幫助，謹此特別致上最誠摯的謝意。在研究學習期間，非常感謝工研院材化所 何宗仁學長於本研究之資料提供與多方面的建議和東海大學化材系所有老師的關懷與提攜教導。

在攻讀博士學位期間，感謝同實驗室的黃莊弘信、張式奇、吳浚銘、林妤軒、甘嘉玲、李嘉祥、吳紹秦、連晨宇、製程研究室的官政銳、林祺偉、張永長、陳正翰、陳玟羽、化工程序模擬實驗室的陳國粹、高分子及流變實驗室的蕭家蓉、蘇郁雅、蘇鵬仁、蔡憲麒、呂鎮宇、林思羽和奈米材料與模擬實驗室的郭弘毅等學弟妹的陪伴與鼓勵，讓我深深體會到同窗情誼之可貴；感謝 王英招學姐、 陳瑞秀學姊、韓怡娟學姊、 林月華學姊和 林印模先生在研究教學上給予極大的幫助與協助，再次非常感謝東海大學化材系上各位學姐先進。

最後，僅將本文獻給我的媽媽 潘綉蕊，這位偉大的母親無怨無悔、無私奉獻，我才能盡全力攻讀博士學位，如果沒有這偉大女性的同行相伴，我將無法堅持走到最後，願大家在未來的人生道路上健健康康、平平安安、前程似錦、一路風順。

Table of contents

List of tables

List of figures

Chapter 1 Introduction

1.1 Background

Isopropyl alcohol (IPA, 2-propanol) is commonly used as a cleaning agent in semiconductor industries, and a typical waste IPA liquid stream contains IPA and water. IPA-water mixture has minimum boiling azeotrope at 80.00℃ (68.88 mol% IPA)[1]. The components of this mixture are difficult and expensive to separate.

In order to separate the azeotrope, several distillation techniques are developed such as heterogeneous azeotropic distillation, extractive distillation, and pressure swing distillation etc.

- Heterogeneous azeotropic distillation is a distillation-based separation which involves the addition of a third component, called an extrainer, to facilitate the separation by inducing a liquid-phase separation in the ternary mixture. In general, a light entrainer is used. One of the components to be separated gone overhead with this entrainer in a column and are typically separated in a decanter. One advantage of heterogeneous azeotropic distillation is that one can utilize a decanter to cross a distillation boundary for obtaining high purity products. It is oftentimes a continuous process in which entrainer selection is a critical element in maintaining the product quality. One often applies this technique in industrial

dehydration processes, such as alcohol dehydration and acetic acid dehydration processes. Widagdo and Seider[2] gave a review on azeotropic distillation. Pham and Doherty[3] studied three different separation sequences for ethanol-water-benzene system, which include four-column, three-column, and two-column heterogeneous distillation sequences. The four-column sequence, shown in Figure 1-1, contains a pre-concentration column, an azeotropic column, an entrainer recovery column, and a purification column. The last two columns of the four-column sequence are replaced by a single column and this sequence actually is three-column sequence. The three-column sequence, shown in Figure 1-2, contains a pre-concentration column, an azeotropic column, and an entrainer recovery column. The two-column sequence (Figures 1-3), in fact, combines the pre-concentration column and the recovery column as one. Later, Ryan and Doherty[4] pointed out that the four-column sequence has no advantage over the three-column sequence, and that the three-column sequence has lower operating costs but higher capital costs than two-column sequence, so that the total annualized cost is about the same for both sequences. Recently, Luyben[5] proposed a control strategy of three-column sequence for ethanol dehydration. For IPA dehydration, Chien et al.[6] proposed a design and control system for a two-column sequence. Furthermore, Arifin and Chien[7] compared two-column

and three-column sequences of IPA dehydration for a diluted IPA feed (50 mol% IPA) shown in Figure 1-4 and 1-5. They found that the operating cost of three-column sequence is slightly less than that of the two-column sequence, but the capital cost of the former is more than that of the latter. Their results are almost the same as that of Ryan and Doherty[4].

- Extractive distillation is a special case of homogeneous azeotropic distillation in which liquid entrainers do not induce a liquid-phase separation in the ternary mixture. A typical extractive distillation column sequence, shown in Figure 1-6, contains an extractive column, an entrainer recovery column, and a condenser to cool down the temperature of recycle stream to avoid the flash occurrence on the stage of the recycle stream feed. The heavy entrainer, also called solvent, with one of the components out the bottom of the extractive column is separated in the entrainer recovery distillation column and recycled to the extractive column. For IPA dehydration, ethylene glycol[8] and dimethyl sulfoxide (DMSO)[8, 9] are used as a solvent.

- Pressure-swing azeotropic distillation is a system of columns operating at different pressures can be used to separate an azeotropic mixture into nearly pure components for the composition of the azeotrope changes significantly with pressure.A pressure-swing azeotropic distillation column sequence contains a

low-pressure column, and a high-pressure column[10, 11]. In general, the reflux drum temperature of a high-pressure column is higher than the base temperature of the low-pressure column, so heat integration could be attractive in terms of energy consumption[10, 11]. For pressure-swing pressure azeotropic distillation, the numerical example is the tetrahydofuran (THF)/water system. For IPA-water system, the azeotrope is hardly dependent on pressure shown in Figure 1-7[12]. Hence, a pressure-swing distillation is not effectively to separate IPA-water mixture.

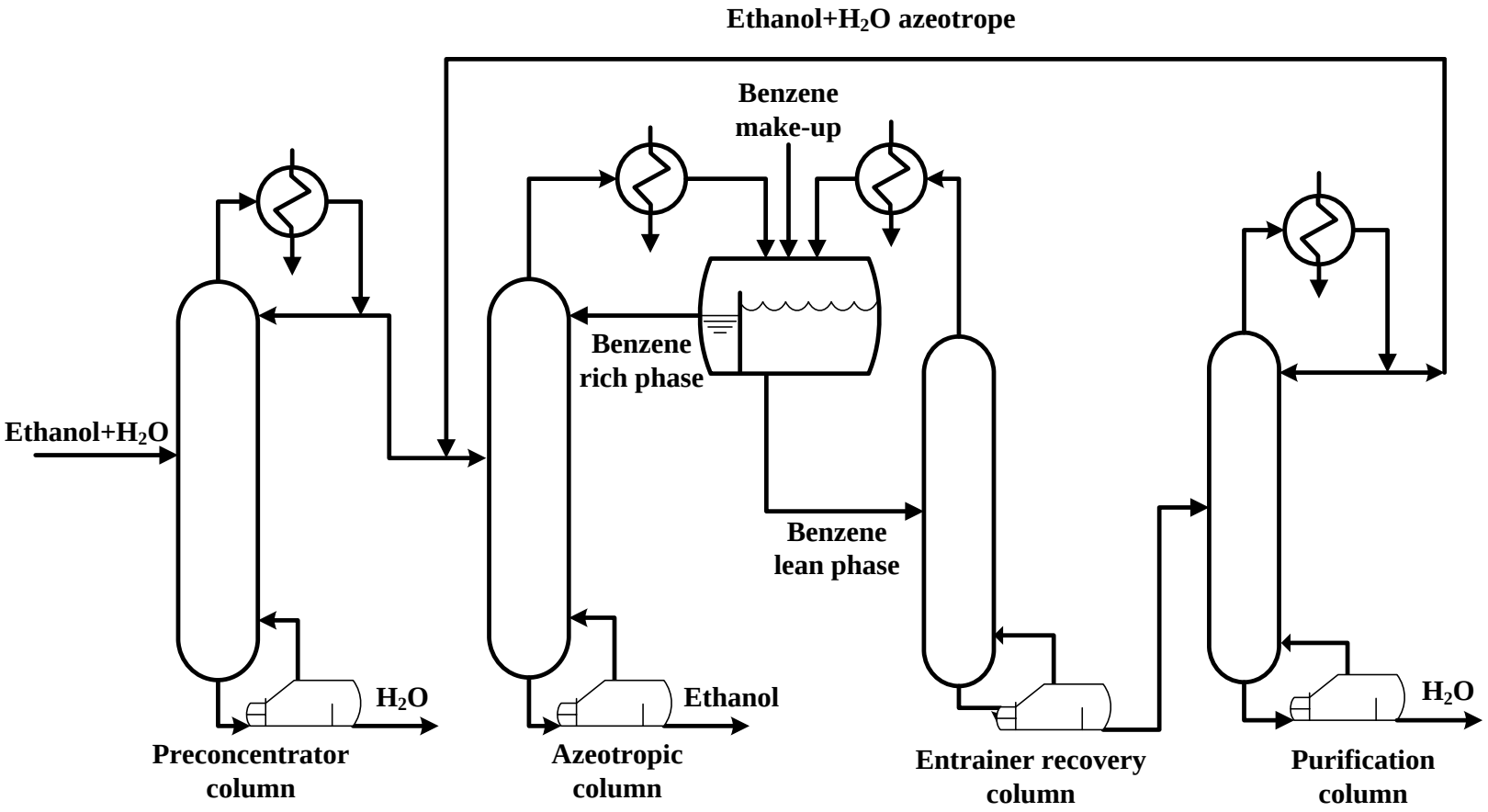

Figure 1-1 Four-column sequence of heterogeneous azeotropic distillation for ethanol/benzene/H_2O[3].

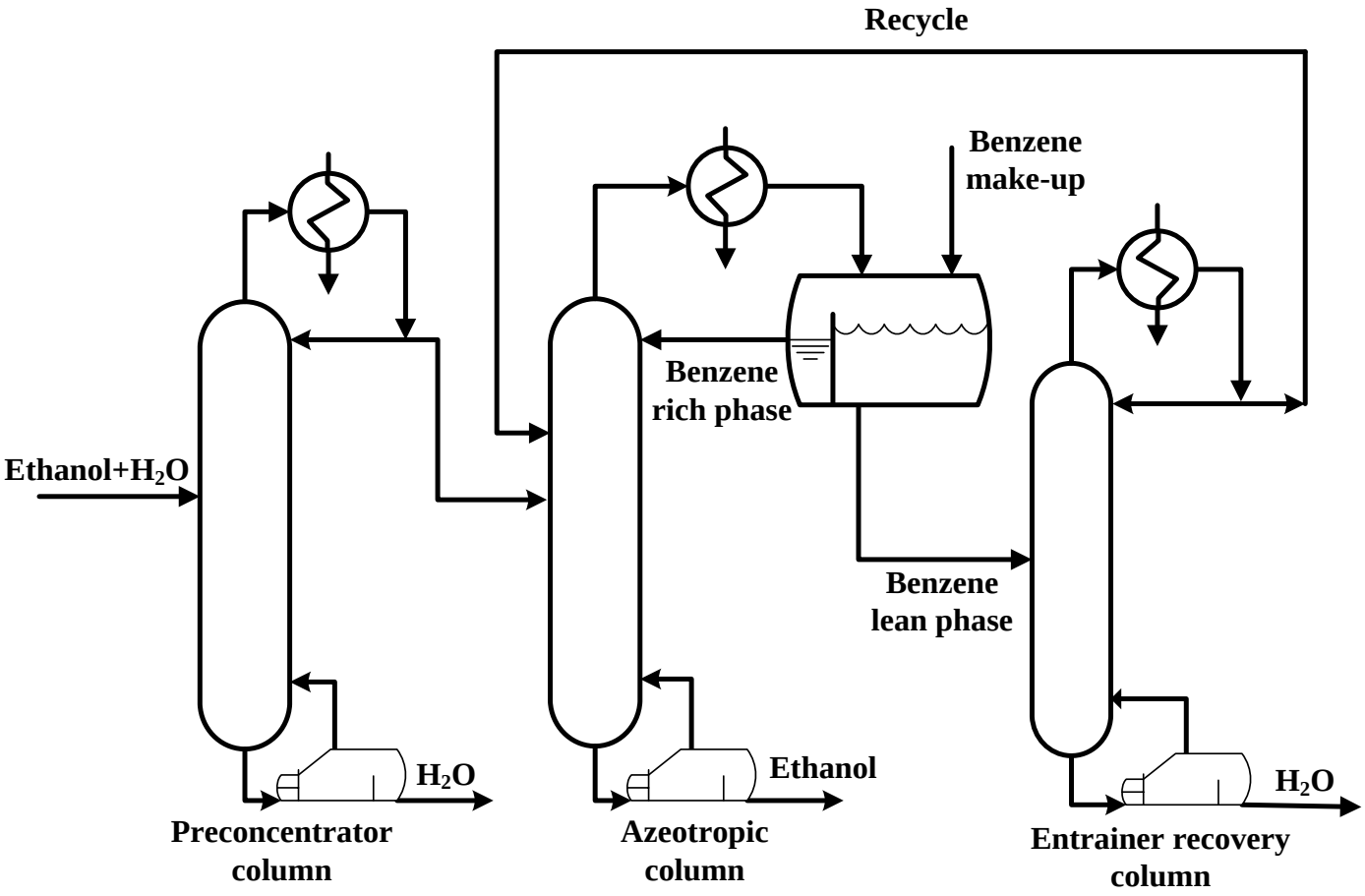

Figure 1-2 Three-column sequence of heterogeneous azeotropic distillation for ethanol/benzene/H_2O[3].

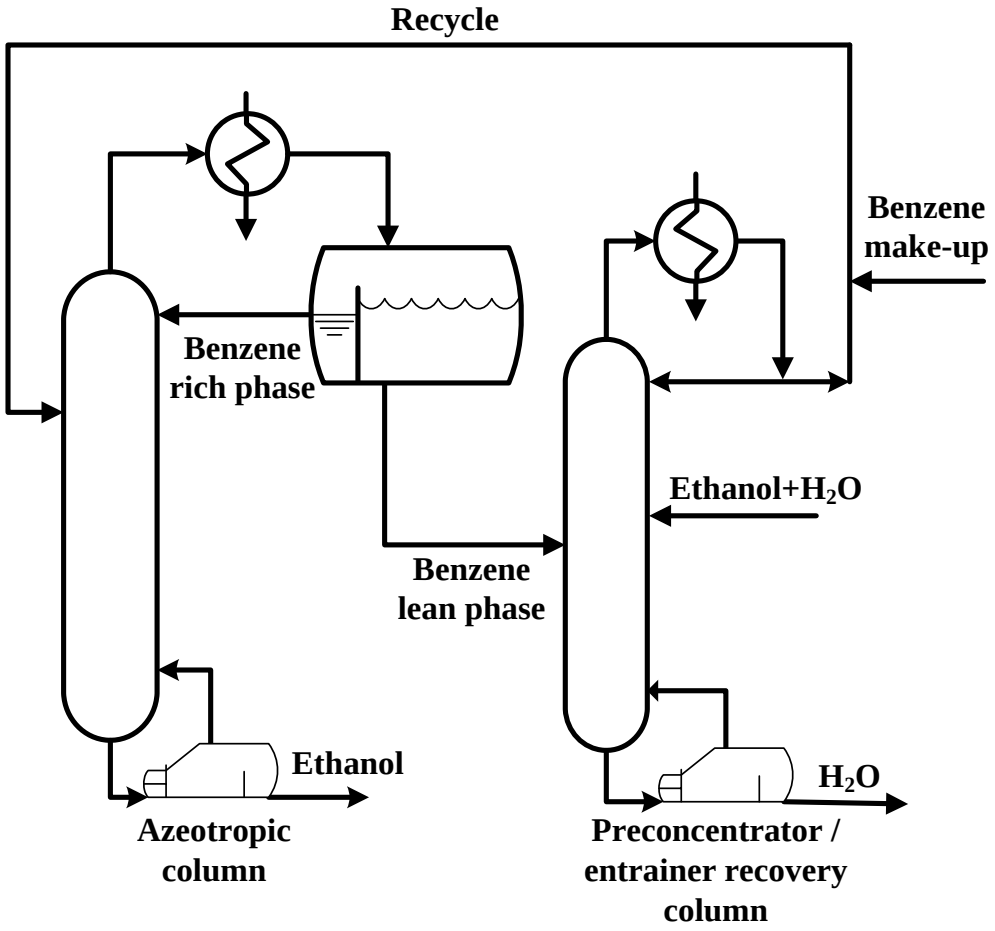

Figure 1-3 Two-column sequence of heterogeneous azeotropic distillation for ethanol/benzene/H_2O[4].

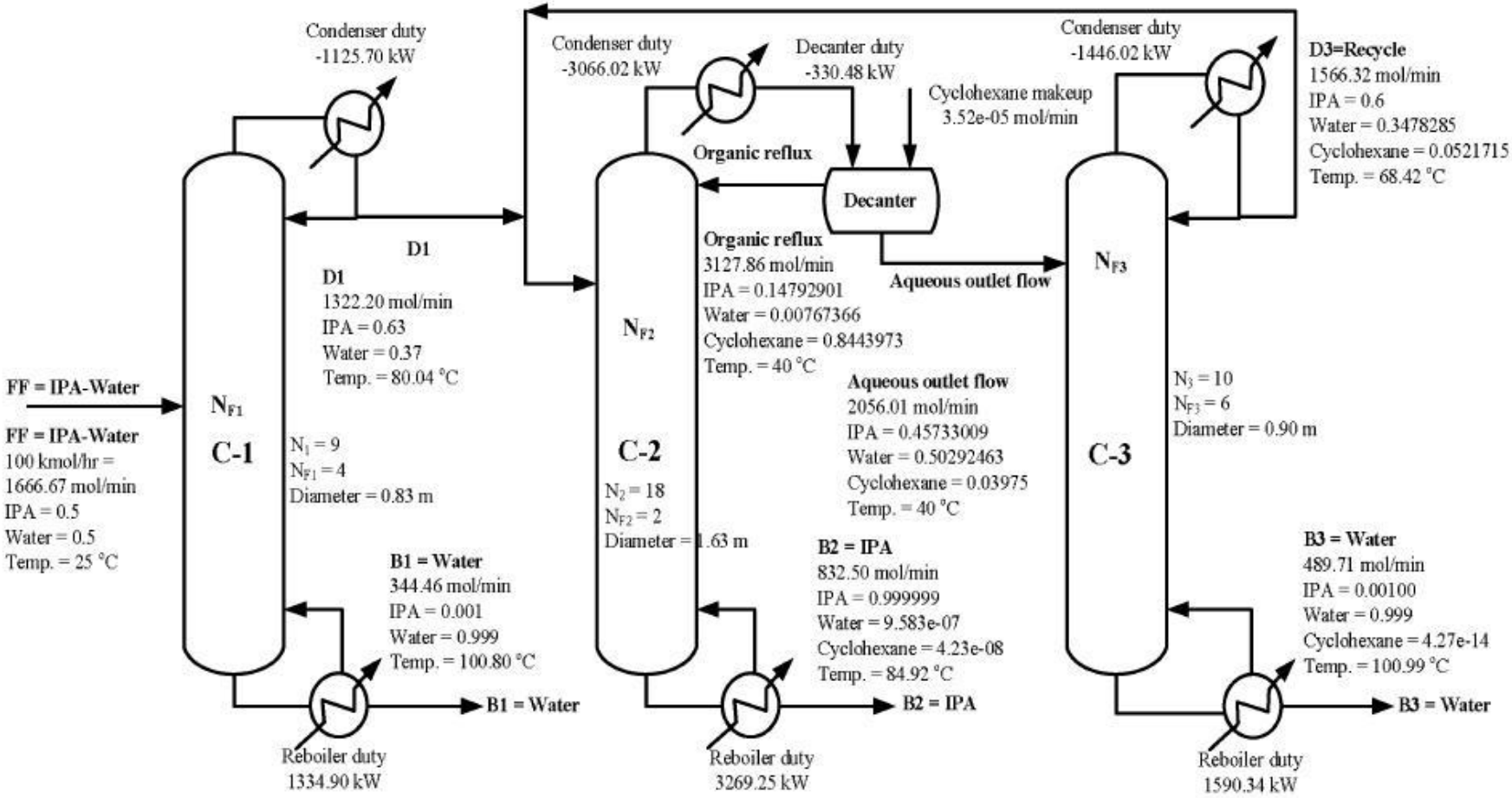

Figure 1-4 Three-column sequence of heterogeneous azeotropic distillation for IPA/cyclohexane/H_2O[7].

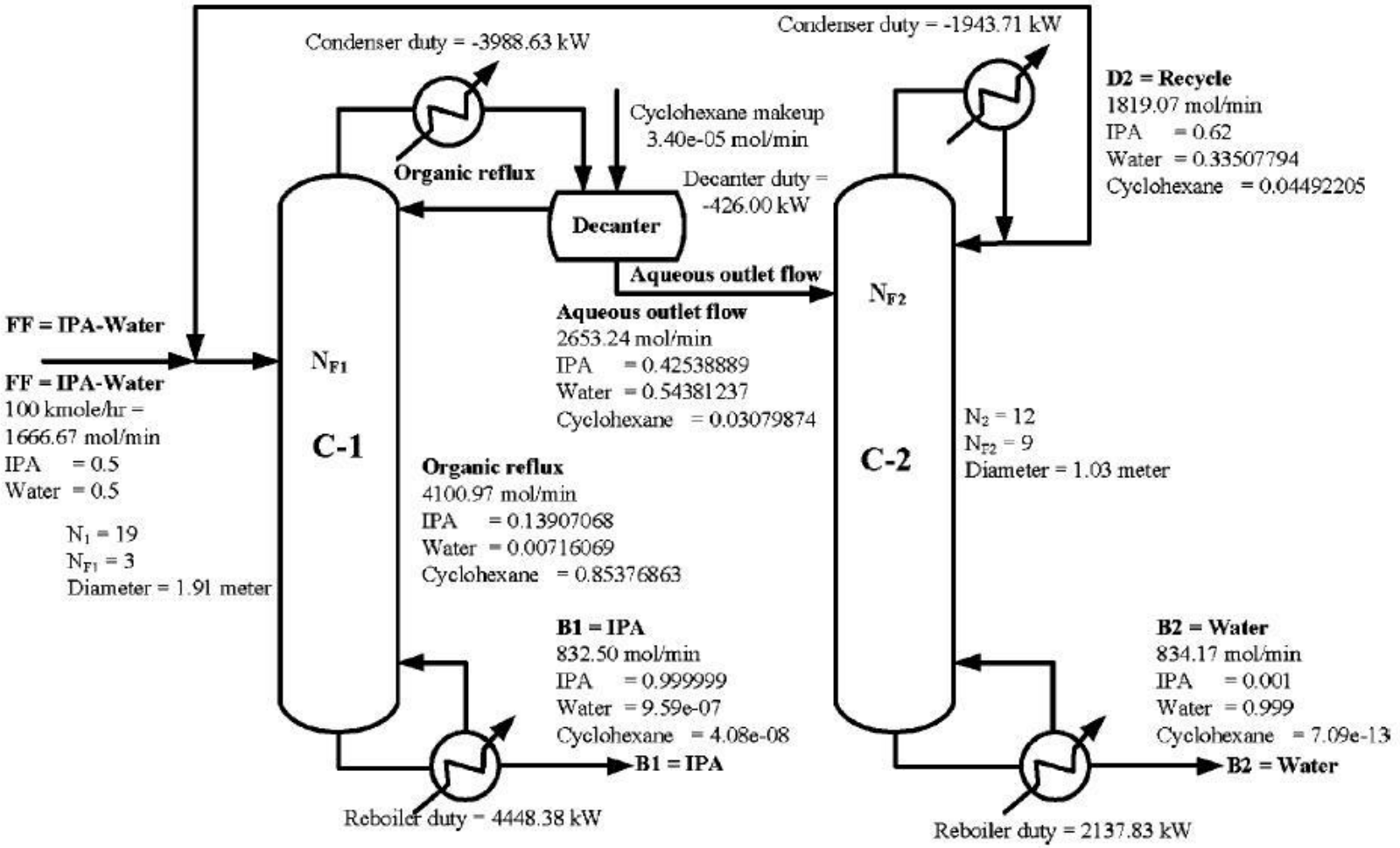

Figure 1-5 Two-column sequence of heterogeneous azeotropic distillation for IPA/cyclohexane/H_2O[7]

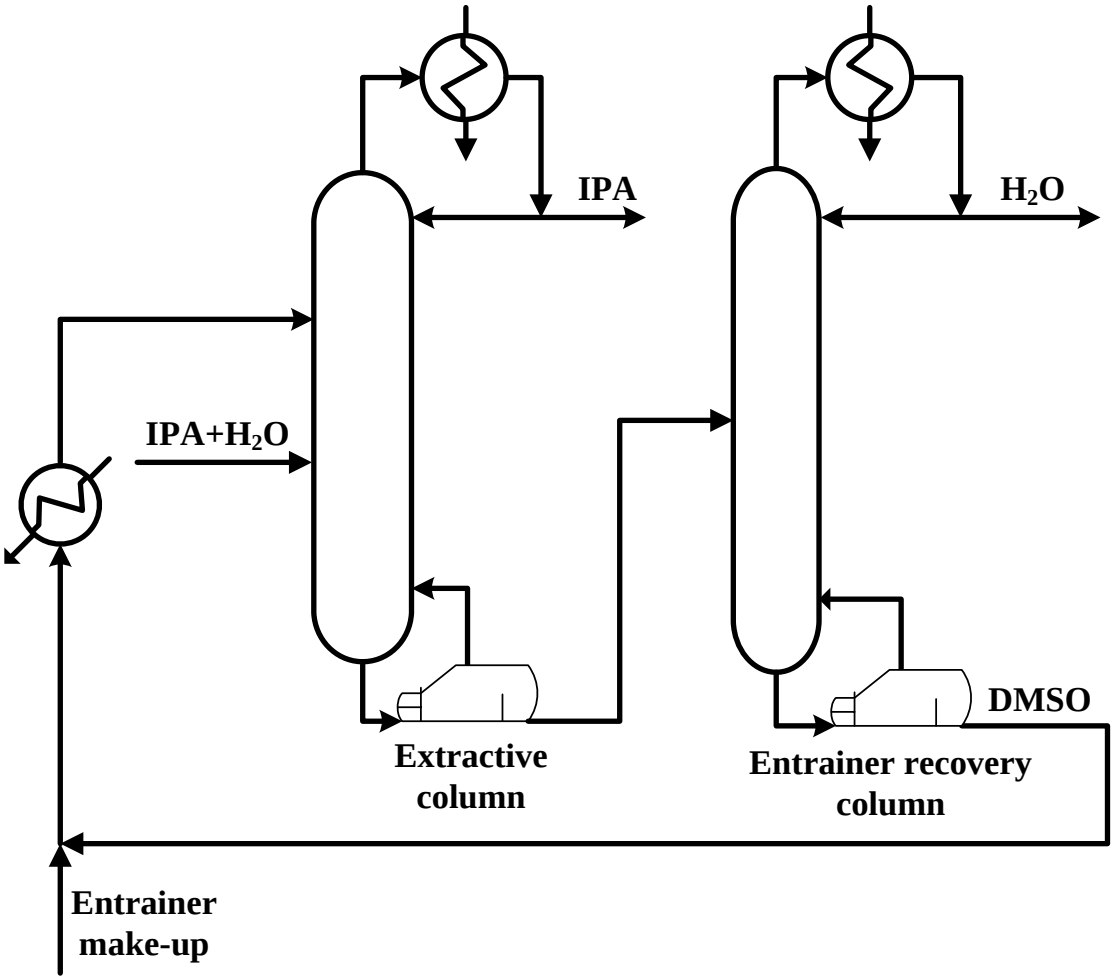

Figure 1-6 Column sequence of extractive distillation for IPA/DMSO/H_2O[9].

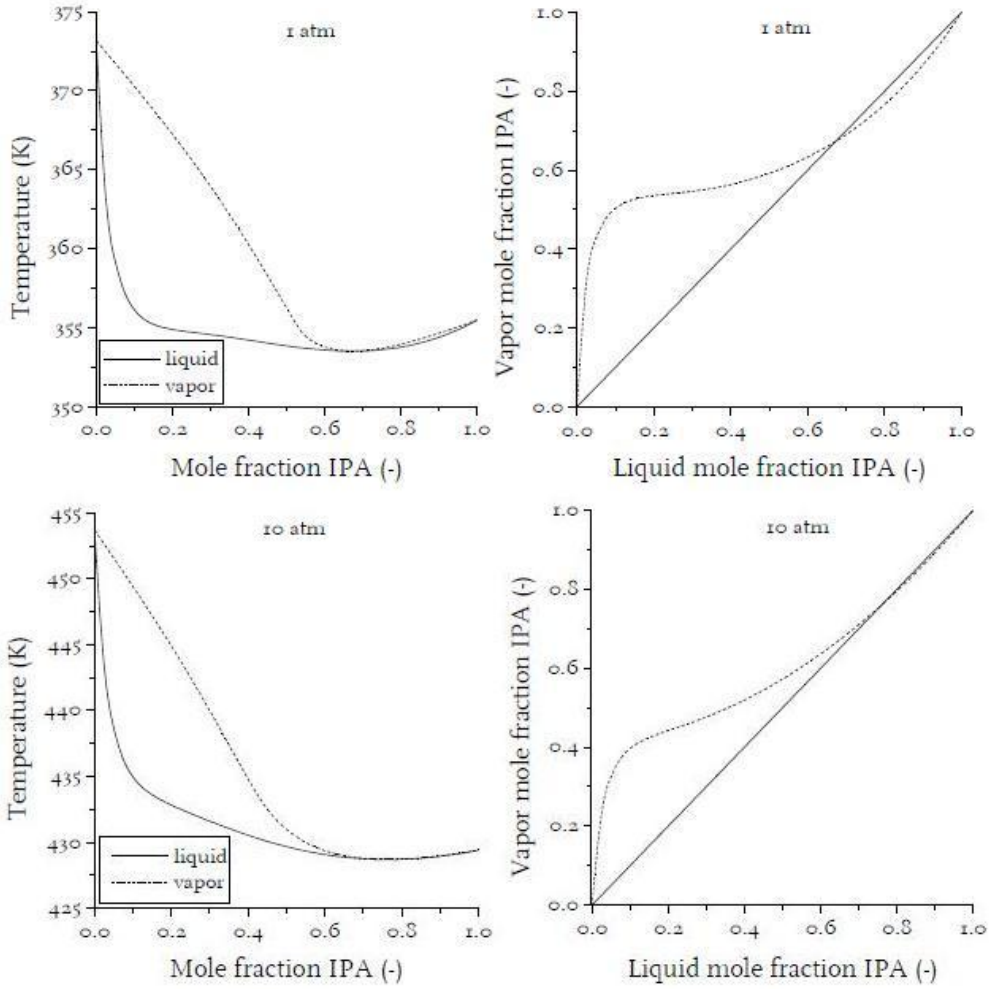

Figure 1-7 Txy-diagram (left) and xy-diagram (right) for the binary system IPA-water at 1atm and 10 atm[12].

However, distillation is the most energy-intensive unit operation and demand for energy in distillation is more than 45% of total energy consumption in chemical industries[13]. Due to rising oil prices and increasing demand for reducing CO_2 emissions, recent process design technology tend to go for energy-saving options. In recent years, thermally coupled distillation system, like dividing-wall columns (DWC), and pervaporation are discussed and presented.

- The dividing wall column (DWC) system is a practical way to implement the

topology of the Petlyuk column that features two columns. One column is a prefractionator into which the feed in introduced and another column is a main column from which a sidestream product is withdrawn. These two columns are coupled together with interconnected vapor and liquid streams arising from a single reboiler and a single condenser. Figure 1-8 presents the DWC system to separate a ternary mixture with components being A, B, and C in order of increasing boiling point. Besides the three design degrees of freedom (reflux flow, boilup flow, and side draw flow), there are two additional degrees of freedom that are liquid split ratio and vapor split ratio with three product specifications. These two degrees of freedom are important to the energy efficiency of the column[14]. DWC is a promising energy-saving alternative (about 35% operating cost)[15] for the separation of multi-component mixture. In recent years, industrial applications of the DWC for separating of ternary mixtures have increased and there are 40 columns reported to be in service. For IPA dehydration, DWC is implemented in extractive distillation[15], and two-column heterogeneous distillation sequences[16]. However, control for DWC is more difficult than with a conventional two-column separation sequence due to more interaction between controlled and manipulated variables of the four sections in DWC.[17, 18, 19]

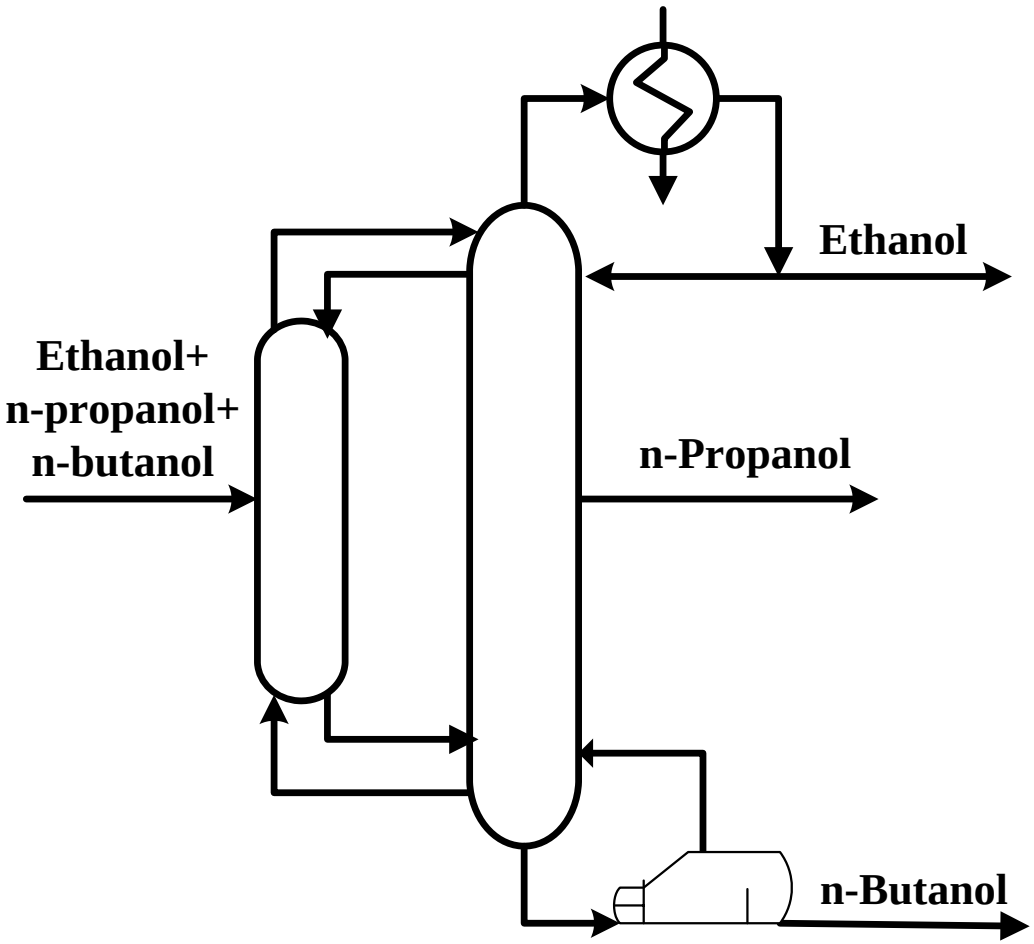

Figure 1-8 Column sequence of DWC for ethanol/n-propanol/n-butanol[17].

- Pervaporation is a membrane separation process that combines the technologies of permeation and vaporization. A liquid mixture is placed in contact with one side of a non-porous polymeric membrane or molecularly porous and other side of membrane is low pressure or vacuum condition. By the pressure force, the miscible components in the liquid sorb into the membrane, permeate through the membrane, and evaporate into the vapor phase. A schematic diagram of the pervaporation process is shown in Figure 1-9[20]. Depending on the permeating component two main areas of pervaporation can be identified hydrophilic pervaporation and organophilic pervaporation[21]. Organophilic pervapration can be divided into hydrophobic pervaporation and target-organophilic pervaporation. The main advantages of pervaporation are the major potential to save energy (above 50% energy saving) and high selectivity. Thus, pervaporation combined with distillation or with a chemical reactor have been realized on an industrial-scale[22]. Figure 1-10[23] shows integrating a pervaporation-distillation hybrid process with a pervaporation unit as final step for IPA dehydration. However, the membranes and membrane installations (need for vacuum) are currently relatively expensive. Thanks to considerable energy saving, the investment is sometime still economically viable for complex distillations.

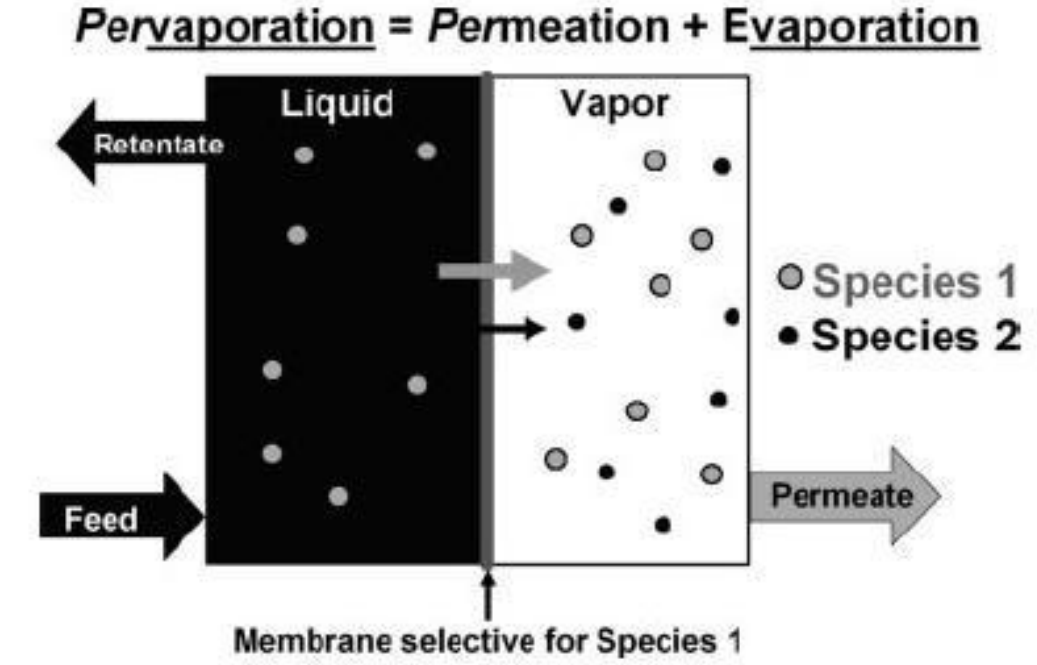

Figure 1-9 Schematic diagram of pervaporation process[20].

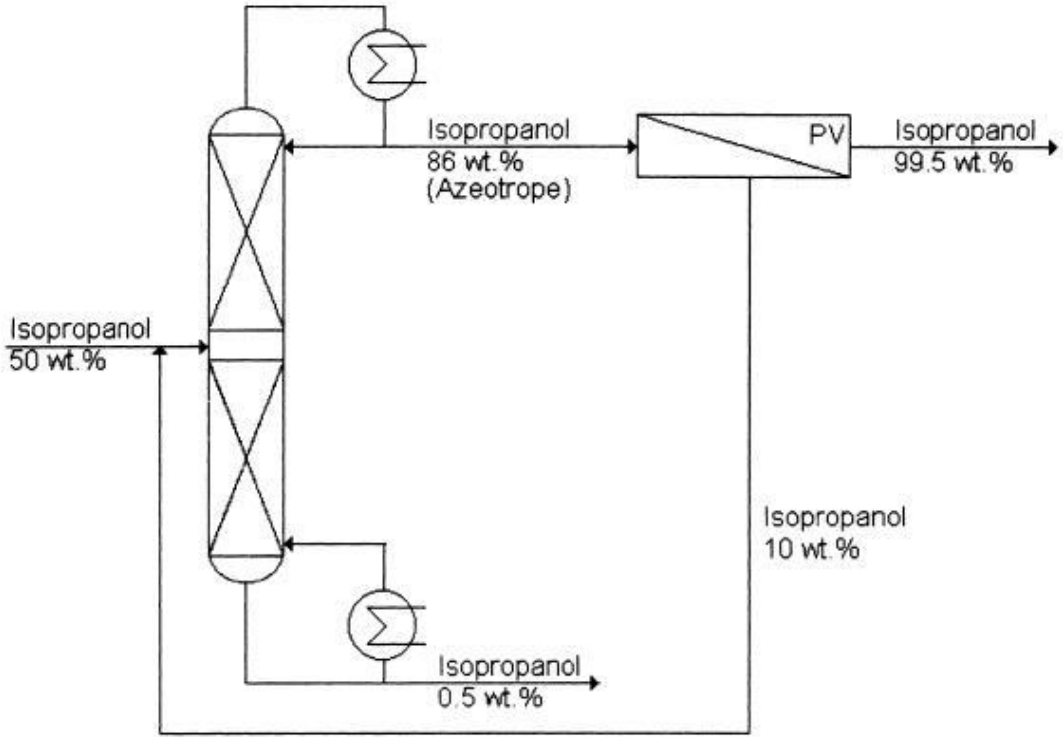

Figure 1-10 Iso-propanol production integrating a pervaporation-distillation.[23]

1.2 Motivation of this work

For IPA dehydration, all kinds of separation technology are summarized in Table 1-1. As demonstrated by Pham and Doherty[3] in an ethanol dehydration process and by Arifin and Chien[7] in an isopropyl alcohol (IPA) dehydration process, a three-column heterogeneous distillation sequence which contains a pre-concentration column, an azeotropic column, and an entrainer recovery column is more energy saving than two-column and four-column sequences. The three-column sequence for isopropyl alcohol (IPA) dehydration process, according to Arifin and Chien[7], consumes less energy than two-column sequence, but the capital cost of the entire sequence is more expensive than that of the two-column sequence.

To cope with the rising oil prices and increasing demand for reducing CO_2 emissions, this study explores the possibility of improving the design and control of an existing heterogeneous azeotropic distillation system designed for the separation of IPA and water using cyclohexane as entrainer. Besides DWC system applied in two-column heterogeneous distillation sequences[16] for IPA/CyH/H_2O process, this study presents a study of designing a three-column heterogeneous azeotropic distillation configuration of IPA dehydration process, featuring energy saving, cost effective and controllability. Further, the basic and simple control for Scheme 3 has also been looked into. Furthermore, the control strategy of Scheme 3 will be tested

with fresh feed rate or water composition in the feed subjected to a ±20% change.

Table 1-1. Summary of Separation Technologies of IPA Dehydration

Kind of separation	Reference	Entrainer or membrane	Descriptions
Azeotropic Distillation	[6]	Cyclohexane	For 69 mol% IPA fresh feed (approach IPA-water azeotrope), three-column sequence (same as four-column sequence in [3]) is much more economical than two-column sequence (same as three-column sequence in [3]).
Azeotropic Distillation	[7]	Cyclohexane	For 50 mol% IPA fresh feed (diluted waste IPA stream), operating cost of three-column sequence is slightly less than two-colunm sequence (about 0.77%), but the capital cost of the former is more than that of the latter as the payback period is assumed 3 years.
Azeotropic Distillation	[21]	Benzene	For 10 mol% IPA fresh feed, the total reboiler heat duties are optimized minimum with the concentration of IPA at concentrator top as a manipulated variable for three-column sequence.
Extraction Distillation	[8]	Ethylene glycol, DMSO	For 80 wt% IPA fresh feed, the plantwide control of IPA dehydration has been studied, and a unique control scheme is developed to give effective control by eliminating the lag of change of feed to solvent flow rate.
Extraction Distillation	[9]	DMSO	For 50 mol% IPA fresh feed, the optimal design flowsheet of the complete process has been established and a very simple overall control strategy has also been proposed which requires only one tray temperature control loop in each column to hold the specifications of the two products.
DWC - Extraction Distillation	[15]	DMSO	Extractive dividing wall distillation has been designed using a constrained stochastic multi-objective optimization technique to determine the design that minimizes energy consumption and total annualized cost.
DWC - Azeotropic Distillation	[16]	Cyclohexane	For two-column heterogeneous distillation sequence, the design and optimization procedures of DWC have been investigated and the optimal values of the design variables are detected to guarantee the minimum energy consumption.
Hybrid process	[23]	Hydrophilic	For high IPA concentration fresh feed, prevaporation becomes more effective than distillation. For 50% IPA fresh feed, hybrid process combined of distillation and pervaporatoin is best.

Chapter 2 Steady-State Design of IPA Dehydration Process

This study considers the design of an isopropyl alcohol dehydration system with a feed composition of 50 mol% IPA and 50 mol% water (H_2O), and a feed rate of 100 kmol/h at 25 ^oC. Cyclohexane (CyH) is used as an entrainer for the system and a decanter is employed for the scheme and is operated at 40 ^oC. Purities are set at 99.9999 mol% IPA for the IPA product stream and 99.9 mol% H_2O for the waste water stream. These specifications were, in fact, adopted by Arifin and Chien[7]. Similar to the approach by Arifin and Chien[7], Aspen Plus is employed for the rigorous steady-state simulation in this study.

2.1 Property and thermodynamic model

Because components differ in relative volatility, distillation process can be used to separate mixture by evaporation and condensation step by step. In a distillation column, vapor and liquid phases must be vapor-liquid equilibrium (VLE) or vapor-liquid-liquid equilibrium. Therefore, it is important to select appropriate thermodynamic models in order to simulate VLE and VLLE on a stage accurately.

In this study, modified Raoult's law is used to calculate VLE and VLLE. The formulation of modified Raoult's law in low pressure condition is shown as:

$$K_i = \frac{y_i}{x_i} = \frac{\gamma_i P_i^{sat}}{P} \tag{2-1}$$

where y_i and x_i are liquid and vapor molar fraction of component i. P_i^{sat} and γ_i are vapor pressure and activity coefficient of component i at a certain temperature. P is the pressure in a stage. The vapor phase of the system is assumed to be ideal, and the nonrandom two-liquid model (NRTL)[25] is used to describe the non-ideality of the liquid phase. The formulation of NRTL is shown as:

$$\ln \gamma_i = \frac{\sum_j x_j \tau_{ji} G_{ji}}{\sum_k x_k G_{ki}} + \sum_j \frac{x_j G_{ij}}{\sum_k x_k G_{kj}} \left[\tau_{ij} - \frac{\sum_m x_m \tau_{mj} G_{mj}}{\sum_k x_k G_{kj}} \right]$$

$$G_{ij} = \exp(-\alpha_{ij} \tau_{ij})$$

$$G_{ii} = 1 \tag{2-2}$$

$$\tau_{ii} = a_{ij} + b_{ij} / T(K)$$

$$\alpha_{ij} = \alpha_{ji}$$

$$\tau_{ii} = \tau_{jj} = 0$$

where τ_{ij} and τ_{ij} are the dimensionless interaction parameters. a_{ij}, b_{ij}, and α_{ij} are the non-randomness parameters. A set of the non-randomness parameters of NRTL for this ternary system (IPA/CyH/H_2O) are obtained from Wang et al.[26] shown in Table 2-1. In addition, All other physical properties are obtained from the Aspen Plus data bank[27].

Table 2-1. NRTL Parameters for IPA/CyH/H_2O system[26]

Component *i*	CyH	CyH	IPA
Component *j*	IPA	H_2O	H_2O
a_{ij}	0.0	0.0	0.0
a_{ji}	0.0	0.0	0.0
b_{ij}	662.5507	1629	185.4495
b_{ji}	294.5264	2328	777.3484
α_{ij}	0.5	0.242	0.5

According to Dean[28], the boiling points of pure substances for the ternary system are 80.8℃ (CyH), 82.2℃ (IPA), and 100℃ (H_2O) at atmospheric pressure. Figure 2-1 and Figure 2-2 are sketched by Aspen Plus using the NRTL model with those parameters (Table 2-1) in vapor-liquid-liquid equilibrium condition. Figure 2-1 shows T-x-y and x-y diagrams of binary components of IPA/CyH/H_2O at 1 atm. Three binary azeotropes are observed for IPA/CyH/H_2O system. Judging from the shapes of T-x-y and x-y diagram for CyH/H_2O, this binary azeotrope is heteroazeotrope. Figure 2-2 is the residue curve map of IPA/CyH/H_2O at 1 atm. It displays the ternary heteroazeotrope of a minimum boiling azeotrope and an unstable node, and the three binary azeotropes are all saddle nodes.

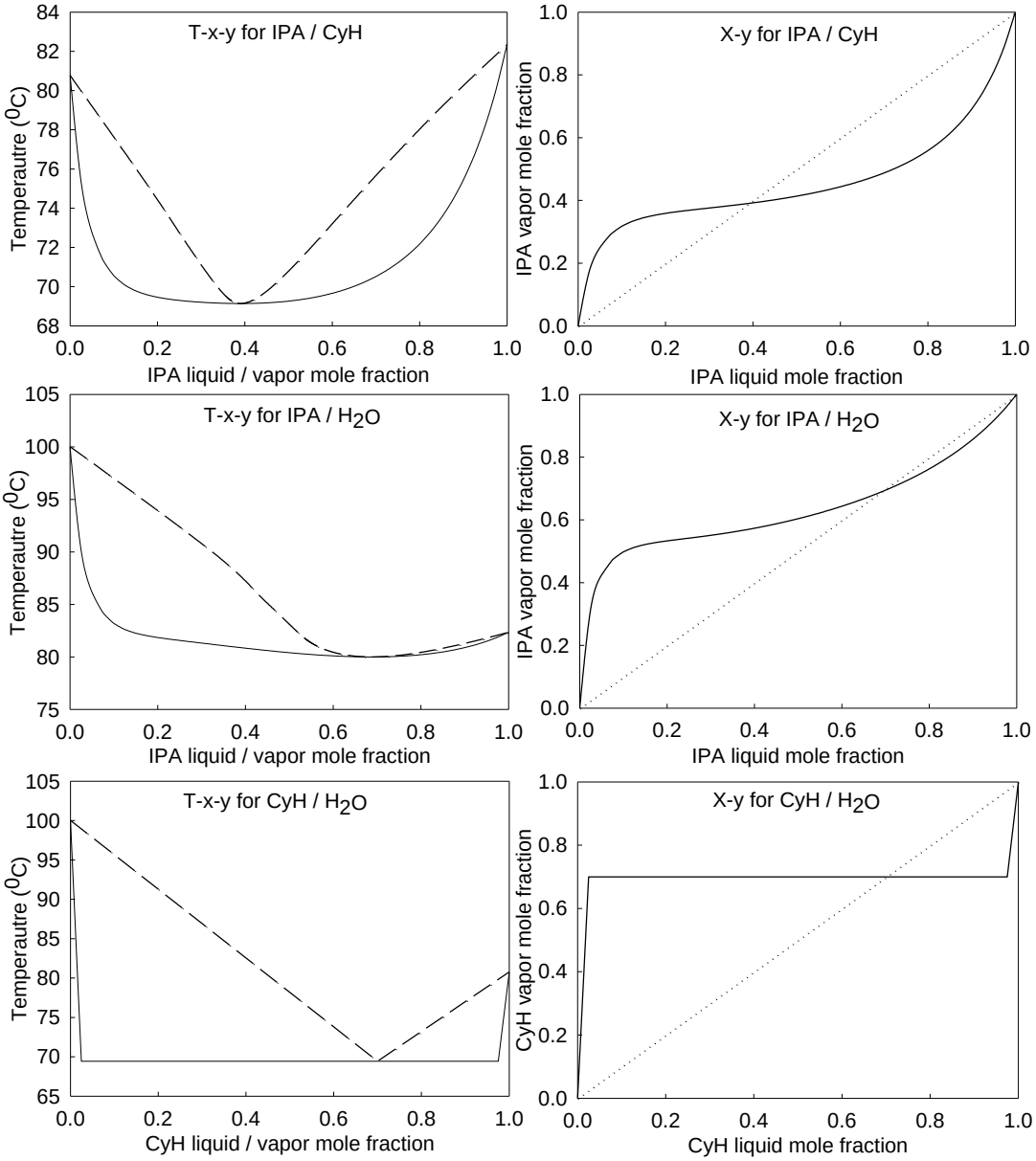

Figure 2-1 T-x-y and x-y diagrams of binary components of IPA/CyH/H_2O at 1 atm.

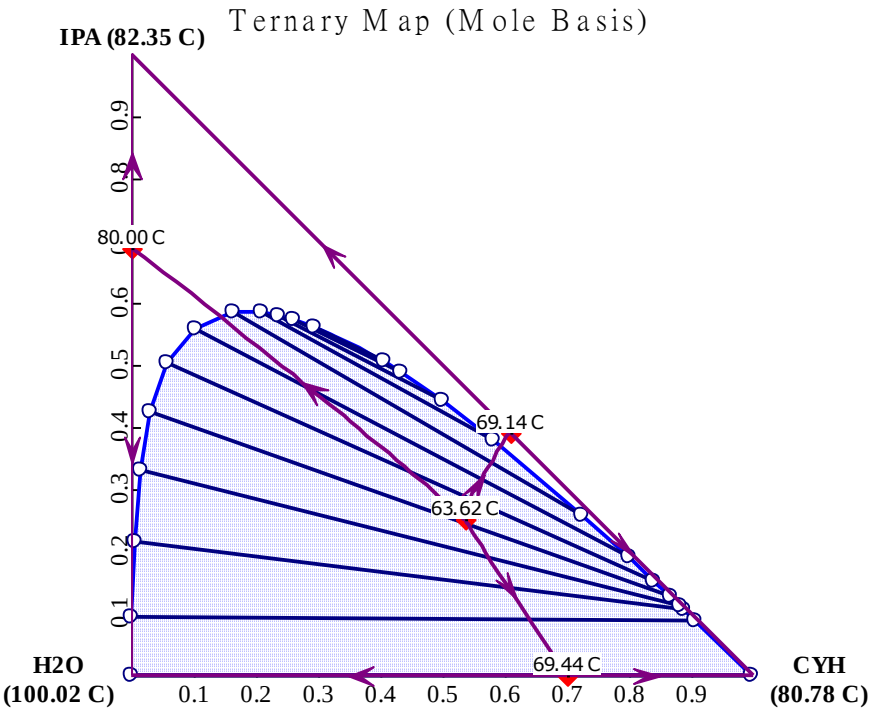

Figure 2-2 Residue curve map of IPA/CyH/H_2O at 1 atm.

These four azeotropes constitute three distillation boundaries and the zone is dividing to three distillation regions. Liquid-liquid equilibrium region stretches over two distillation regions. Therefore, the distillation boundaries can go across by liquid-liquid separated phase if a composition locates in the liquid-liquid equilibrium region. The important azeotrope information of experimental[28] and calculation using NRTL of these three components at atmospheric pressure are listed in Table 2-2. The calculated results of all azeotrope information from using NRTL model are about the same as the results from experimental. In Table 2-2, it is also shown that there are one ternary heteroazeotrope, one binary heteroazeotrope, and two binary homogeneous azeotropes.

Table 2-2. Experimental and Calculated Normal Boiling Point Ranking of Pure Components, and Azeotropes for IPA/CyH/H_2O system

	Boiling point(℃)	IPA (mol%)	H_2O(mol%)	CyH (mol%)
Pure component				
CyH	80.8	—	—	—
IPA	82.2	—	—	—
H_2O	100.0	—	—	—
Azeotrope				
IPA / H_2O /CyH	64.3 (63.62)	19.20 (25.13)	25.96 (21.35)	54.84 (53.52)
IPA / CyH	69.4 (69.14)	39.72 (39.06)	—	60.28 (60.94)
IPA / H_2O	80.3 (80.00)	67.53 (68.78)	32.47 (31.22)	—
H_2O / CyH	69.5 (69.44)	—	29.99 (30.03)	70.01(69.97)

*Values in small bracket are calculated using NRTL model[26].

2.2 Conceptual steady-state design

In terms of those previous literatures, a three-column sequence, which was studied by Arifin and Chien[7], is shown in Figure 2-3 and is named as Scheme 1 in this study. As shown in Figure 2-3, the fresh dilute feed stream flows into a pre-concentration column (C101). The bottom product of the pre-concentration column is 99.9 mol% of water. The distillate of the pre-concentration column is mixed with a recycle stream from an entrainer recovery column (C301) and flows into a heterogeneous azeotropic column (C201). The distillate composition of the pre-concentration column is close to that of IPA-water azeotrope. A small amount of make-up entrainer stream is added to the decanter. The organic entrainer-rich phase of

the decanter is refluxed back to the heterogeneous azeotropic column, and the aqueous phase is sent to the recovery column. Their respective bottom products are 99.9999 mol% IPA and 99.9 mol% water. An alternative two-column sequence, proposed by Arifin and Chien[7], is shown in Figure 2-4 and named as Scheme 2 in this study. One difference from these two schemes is that the feed stream of Scheme 2, mixed with the aqueous-phase of the decanter, flowing directly into the pre-concentrationor column is close to that of IPA-water azeotrope. One difference from these two schemes is that the feed stream of Scheme 2, mixed with the aqueous-phase of the decanter, flows directly into the recovery column, and there is no pre-concentration column in Scheme 2. According to Ryan and Doherty[4] and Chien et al.[6], the three-column sequence (Scheme 1) can save more energy than the two-column sequence (Scheme 2). From the simulation results of Arifin and Chien[7], it can be found that the reflux ratio used either in the pre-concentration column or the recovery column in Scheme 1 is quite small. Also, the variation of the reflux ratio in either of these two distillation columns may not be so important, since there is no rigid specification in the top product stream. This can be interpreted as that both of these two columns requires a very pure bottoms product, but a pure top product is not needed. Thus, these two conventional distillation columns can be replaced by two stripping columns.

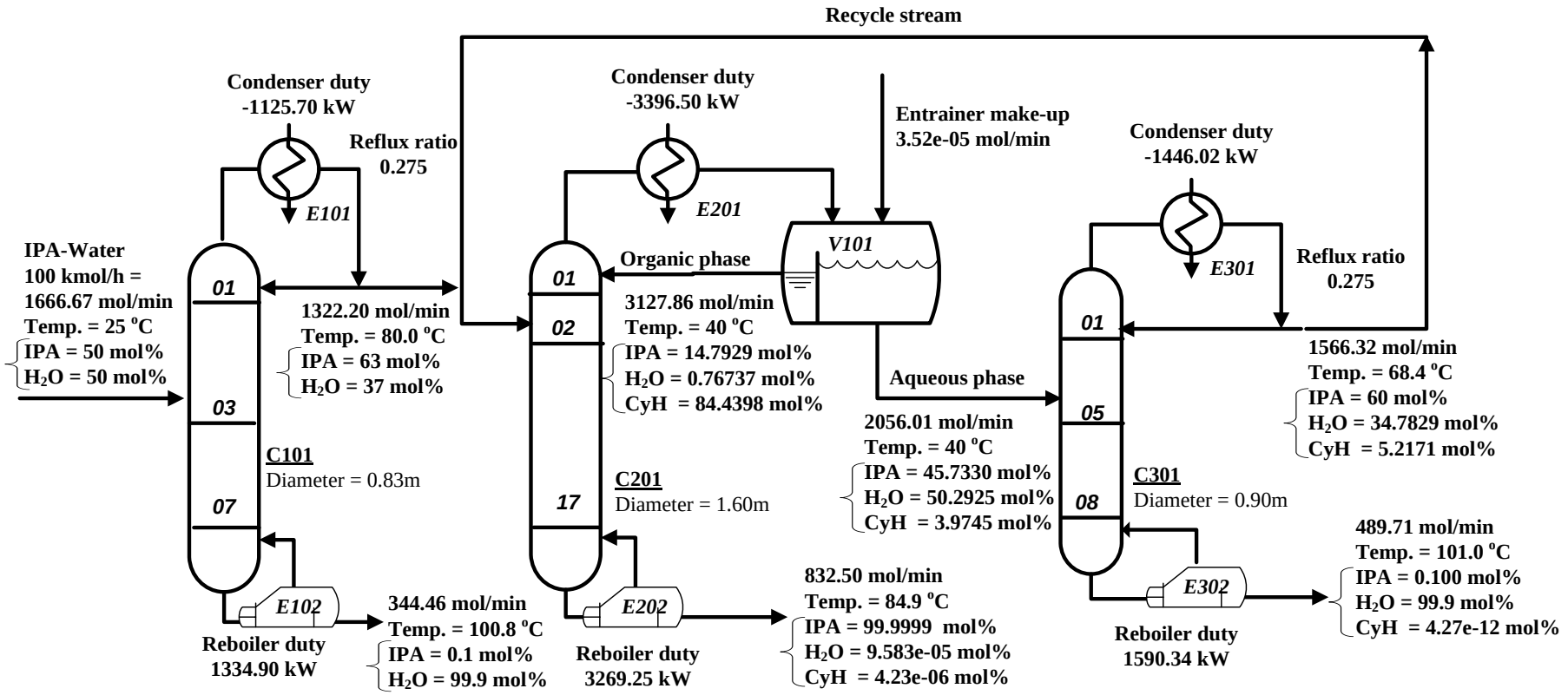

Figure 2-3 Operating conditions for Scheme 1[7].

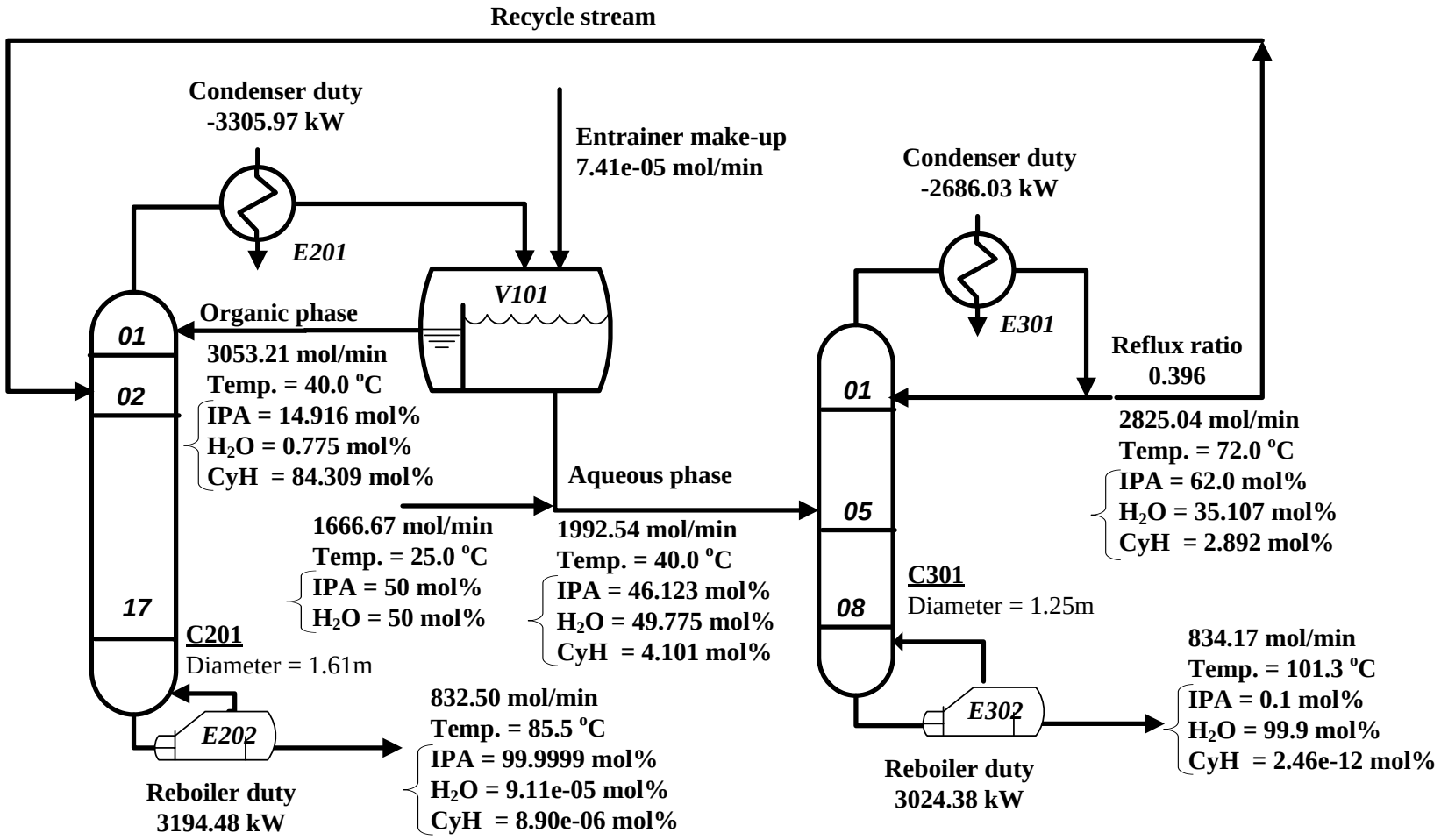

Figure 2-4 Operating conditions for Scheme 2[7].

A stripping column can be thought of as a conventional distillation column with no external reflux in the rectifying section. In contrast, one shortcoming associated with the conventional distillation column is that it has a reboiler to vaporize liquid in the stripping section and also has a condenser to condense vapor in the rectifying section. From the perspective of energy conservation, a stripping column is a tower without a condenser, in which energy carried by the overhead vapor is conserved instead of being removed in a condenser, and is considered to be more energy-efficient here than the conventional distillation. In addition, using the stripping column to replace the conventional distillation column can not only reduce energy cost but also cut capital cost. Accordingly, a modified separation system, named Scheme 3 here, is proposed in this study, for which a simple process flow diagram (PFD) is presented in Figure 2-5. According to the same reasons, the pre-concentrationor/entrainer recovery column of the two-column sequence[7] is replaced by a stripping column. This two-column sequence is named Scheme 4 and shown in Figure 2-6.

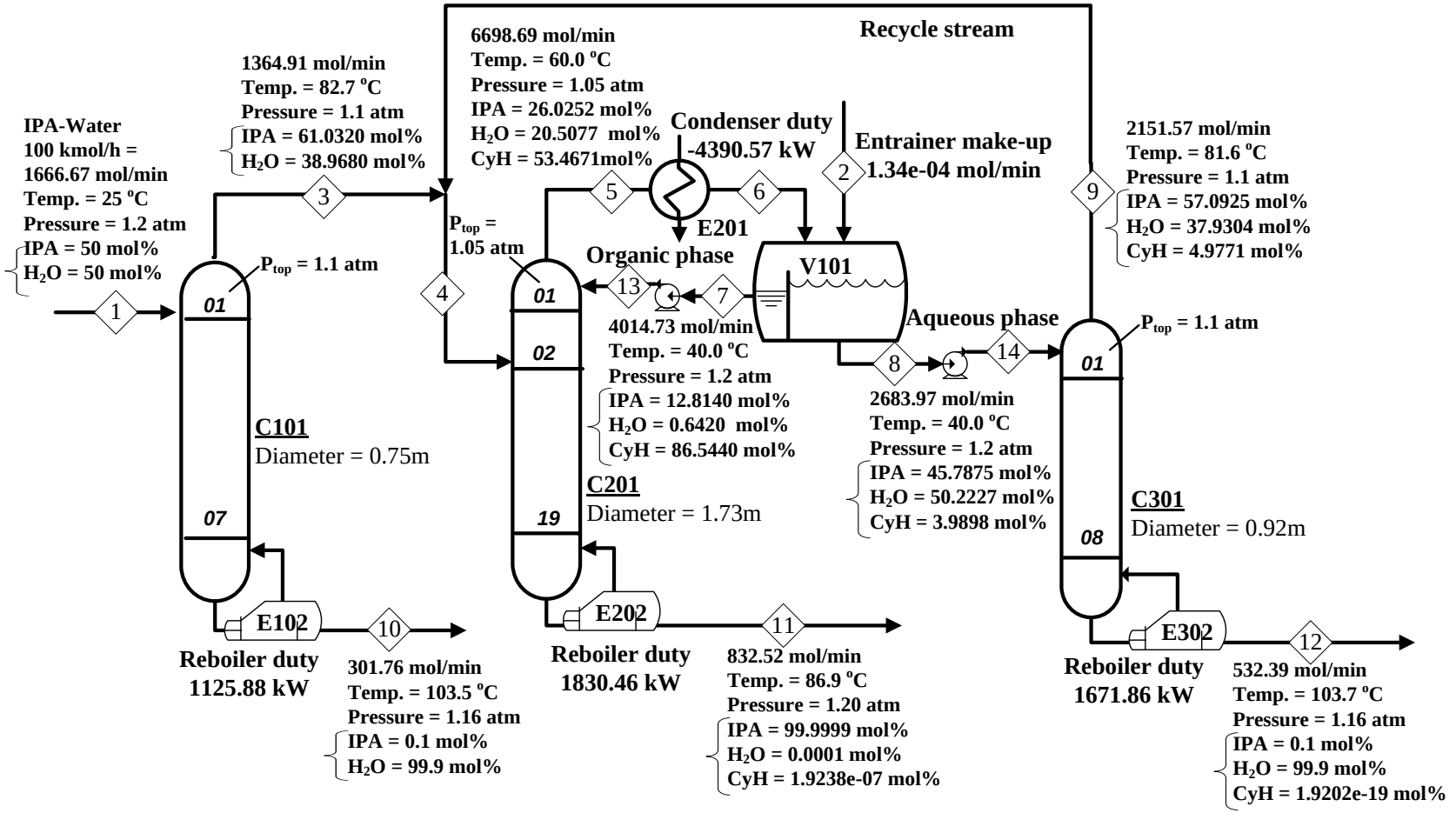

Figure 2-5 Operating conditions for Scheme 3.

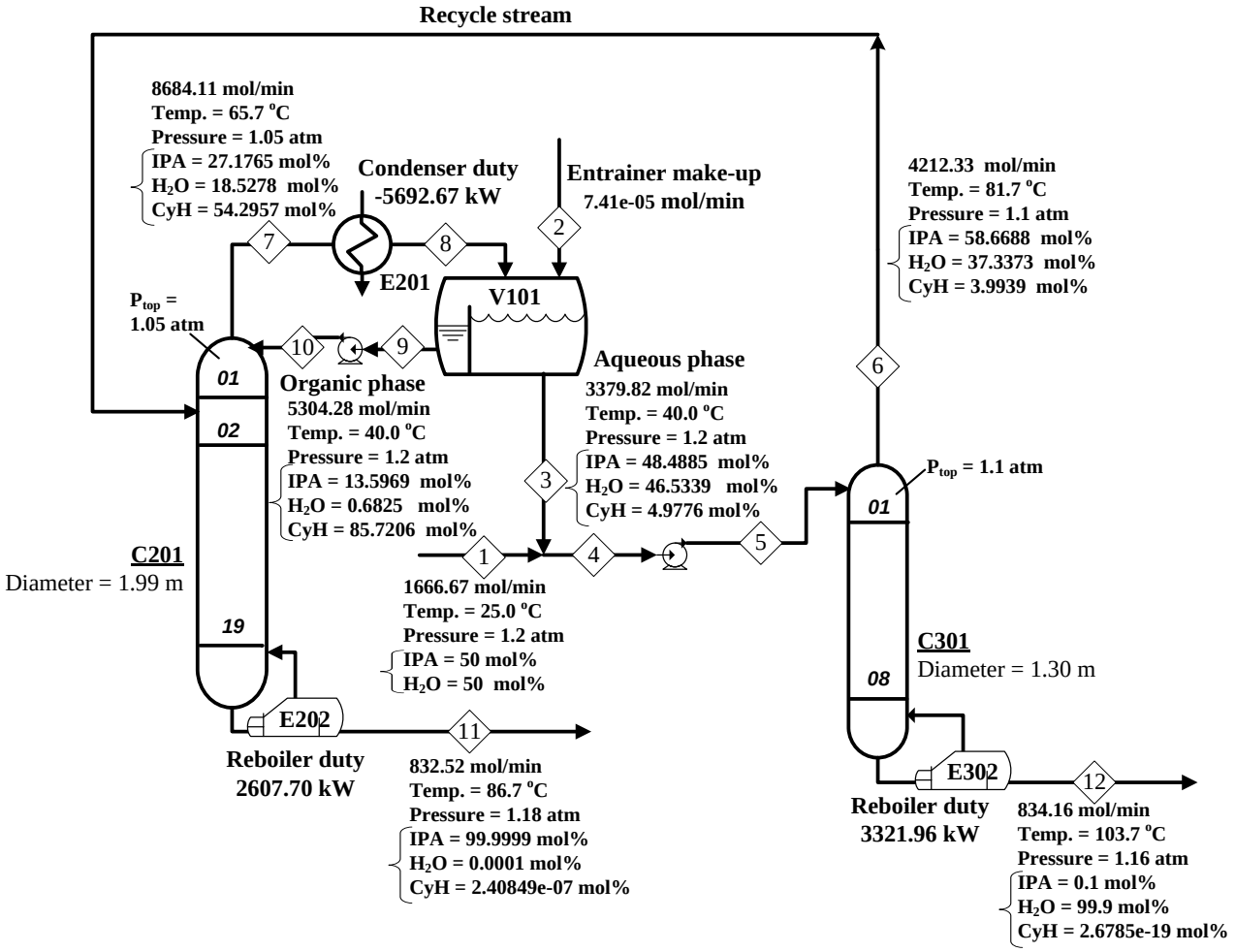

Figure 2-6 Operating conditions for Scheme 4.

For Scheme 3, as shown in Figure 2-5, the fresh feed (stream 1) flows into a pre-concentration stripping column (C101), yielding a high-purity water stream (99.9 mol%) at the bottom (stream 10) and an overhead vapor stream (stream 3). This vapor stream then mixes with the overhead stream (stream 9) of another stripping column (C301) to form a feed stream (stream 4) to a heterogeneous azeotropic column (C201). An ultra-high purity (99.9999 mol%) IPA product, i.e, stream 11, can be obtained in the bottoms. The overhead vapor of C201 (stream 5), whose composition is close to that of the ternary azeotrope, then passes through a total condenser and is cooled to 40 ^{o}C. The condensate from the condenser is split into two liquid phases at the decanter where the organic phase (stream 7) is refluxed to the top of the heterogeneous azeotropic column and the aqueous phase (stream 8) flows into the entrainer-recovery stripping column (C301). A product stream (stream 12) containing 99.9 mol% water can be easily obtained at its bottoms of this stripping column. In order to facilitate the transport of overhead vapor streams from C101 and C301, the top pressures of C101 and C301 are both set at 1.1 atm, while that of C201 is set at 1.05 atm, instead of fixing all column pressures at 1 atm as in the work of Arifin and Chien[6]. A stream summary for this flowsheet based on rigorous simulation results with Aspen Plus is presented in Table 2-3. Residue curve map (RCM) and conceptual material balance (MB) lines for Scheme 3 including MB lines for Columns C101, C201, and C301 can

be visualized in Figure 2-7 with major process streams being labeled. For Scheme 4, as shown in Figure 2-6, the fresh feed (stream 1) which mixes with the aqueous phase (stream 3) from the decanter to form a feed stream (stream 4) flows into a pre-concentration/entrainer-recovery stripping column (C301), yielding a high-purity water stream (99.9 mol%) at the bottom (stream 12) and an overhead vapor stream (stream 6). This vapor stream flows into a heterogeneous azeotropic column (C201). An ultra-high purity (99.9999 mol%) IPA product, i.e, stream 11, can be obtained in the bottoms. The overhead vapor of C201 (stream 7) passes through a total condenser and is cooled to 40 ^{o}C. The condensate from the condenser is split into two liquid phases at the decanter where the organic phase (stream 9) is refluxed to the top of the

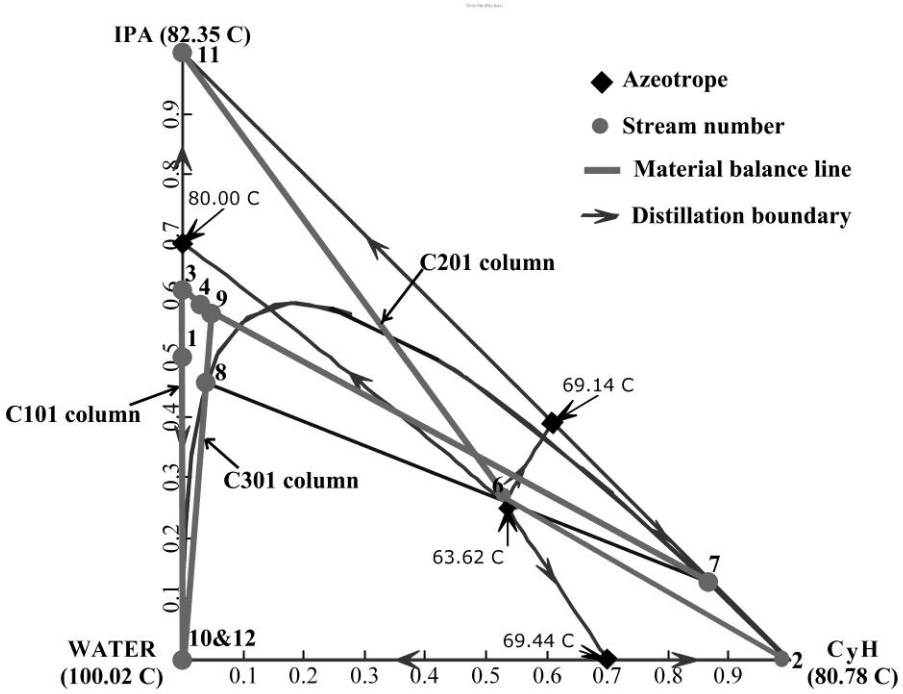

Figure 2-7 RCM and material balance lines for Scheme 3.

Table 2-3. Stream Summary Based on Simulation Results for Scheme 3

Stream number	1	2	3	4	5	6	7
Pressure (atm)	1.20	1.00	1.10	1.10	1.05	1.00	1.00
Temperature (℃)	25.0	25.0	82.7	82.0	65.0	40.0	40.0
Vapor Fraction	0	0	1	0.99998	1	0	0
Mole Fraction							
CyH	0	1	0	0.030453	0.534671	0.534671	0.865440
IPA	0.5	0	0.610320	0.586216	0.260252	0.260252	0.128140
H2O	0.5	0	0.389680	0.383331	0.205077	0.205077	0.006420
Total Flow (mol/min)	1666.67	1.34E-04	1364.91	3516.48	6698.69	6698.69	4014.73

Stream number	8	9	10	11	12	13	14
Pressure (atm)	1.00	1.10	1.16	1.20	1.16	1.20	1.20
Temperature (℃)	40.0	81.6	103.5	86.9	103.7	40.0	40.0
Vapor Fraction	0	1	0	0	0	0	0
Mole Fraction							
CyH	0.039899	0.049771	0.000000	trace	trace	0.865440	0.039899
IPA	0.457875	0.570925	0.001000	0.999999	0.001000	0.128140	0.457875
H2O	0.502227	0.379304	0.999000	0.000001	0.999000	0.006420	0.502227
Total Flow (mol/min)	2683.97	2151.57	301.76	832.52	532.39	4014.73	2683.97

Table 2-4. Stream Summary Based on Simulation Results for Scheme 4

Stream number	1	2	3	4	5	6
Pressure (atm)	1.00	1.00	1.00	1.00	1.20	1.10
Temperature (℃)	25.0	25.0	40.0	35.2	35.2	81.7
Vapor Fraction	0	0	0	0	0	1
Mole Fraction						
CyH	0	1	0.049776	0.033337	0.033337	0.039939
IPA	0.5	0	0.484885	0.489877	0.489877	0.586688
H2O	0.5	0	0.465339	0.476786	0.476786	0.373373
Total Flow (mol/min)	1666.67	7.41E-05	3379.82	5046.49	5046.49	4212.33

Stream number	7	8	9	10	11	12
Pressure (atm)	1.05	1.00	1.00	1.20	1.18	1.16
Temperature (℃)	65.7	40.0	40.0	40.0	86.7	103.7
Vapor Fraction	1	0	0	0	0	0
Mole Fraction						
CyH	0.542957	0.542957	0.857206	0.857206	0.000001	trace
IPA	0.271765	0.271765	0.135969	0.135969	0.999999	0.001000
H2O	0.185278	0.185278	0.006825	0.006825	trace	0.999000
Total Flow (mol/min)	8684.11	8684.11	5304.28	5304.28	832.50	834.16

heterogeneous azeotropic column and the aqueous phase (stream 3) which mixes with the fresh feed (stream 1) flows into the C301. Also, in order to facilitate the transport of overhead vapor streams from C301, the top pressures of C301 is set at 1.1 atm, while that of C201 is set at 1.05 atm. A stream summary for this flowsheet based on rigorous simulation results with Aspen Plus is presented in Table 2-4. Residue curve map (RCM) and conceptual material balance (MB) lines for Scheme 4 including MB lines for Columns C201, and C301 can be visualized in Figure 2-8 with major process streams being labeled.

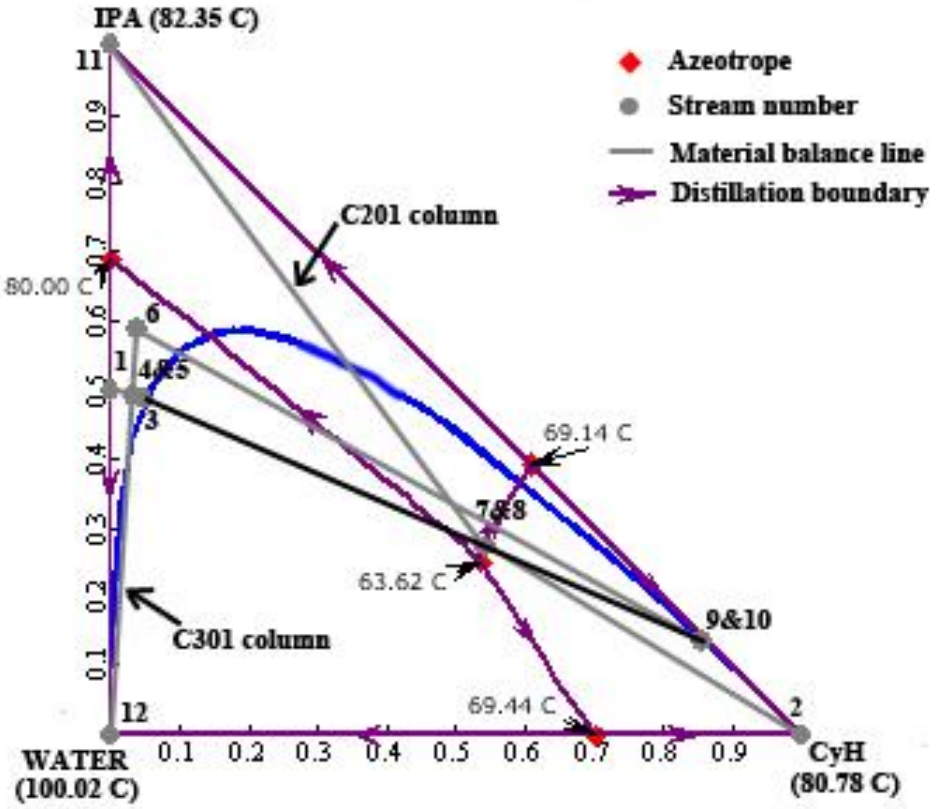

Figure 2-8 RCM and material balance lines for Scheme 4.

Ratio of total reboiler duties is shown in Figure 2-9 and Scheme 3 is the most energy-saving distillation sequence. Because the dilute waste stream of IPA and water mixture is considered as a feed of an isopropyl dehydration system in this study, the total reboiler duty is discussed using Scheme 2 and Scheme 3 with the range of from 20% to 40% dilute IPA waste stream. Figure 2-10, Figure 2-11, Figure 2-12, Figure 2-13, Figure 2-14, and Figure 2-15 are shown the operating conditions for Scheme 2 and Scheme 3 using 20%, 30%, and 40% IPA feed. A comparison of all the total reboiler duties of Scheme 2 and Scheme 3 are summarized in Table 2-5, and shows Scheme 3 is still the most energy saving distillation sequence. Next, the economic analysis of these four schemes focused on 50 mol% IPA feed are discussed and calculated.

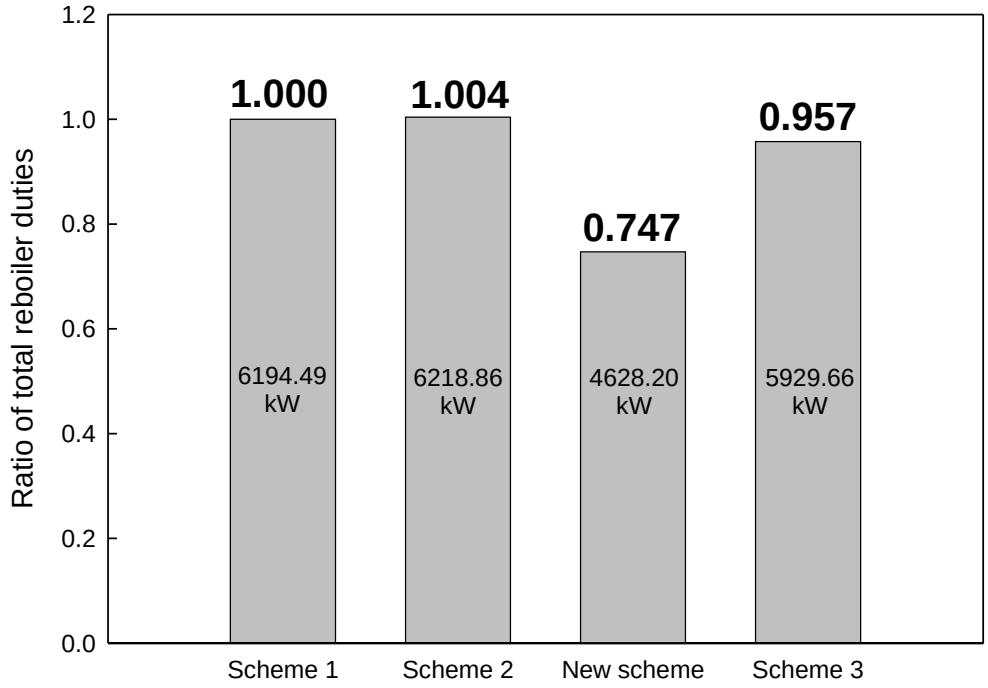

Figure 2-9 Ratio of total reboiler duties of four schemes.

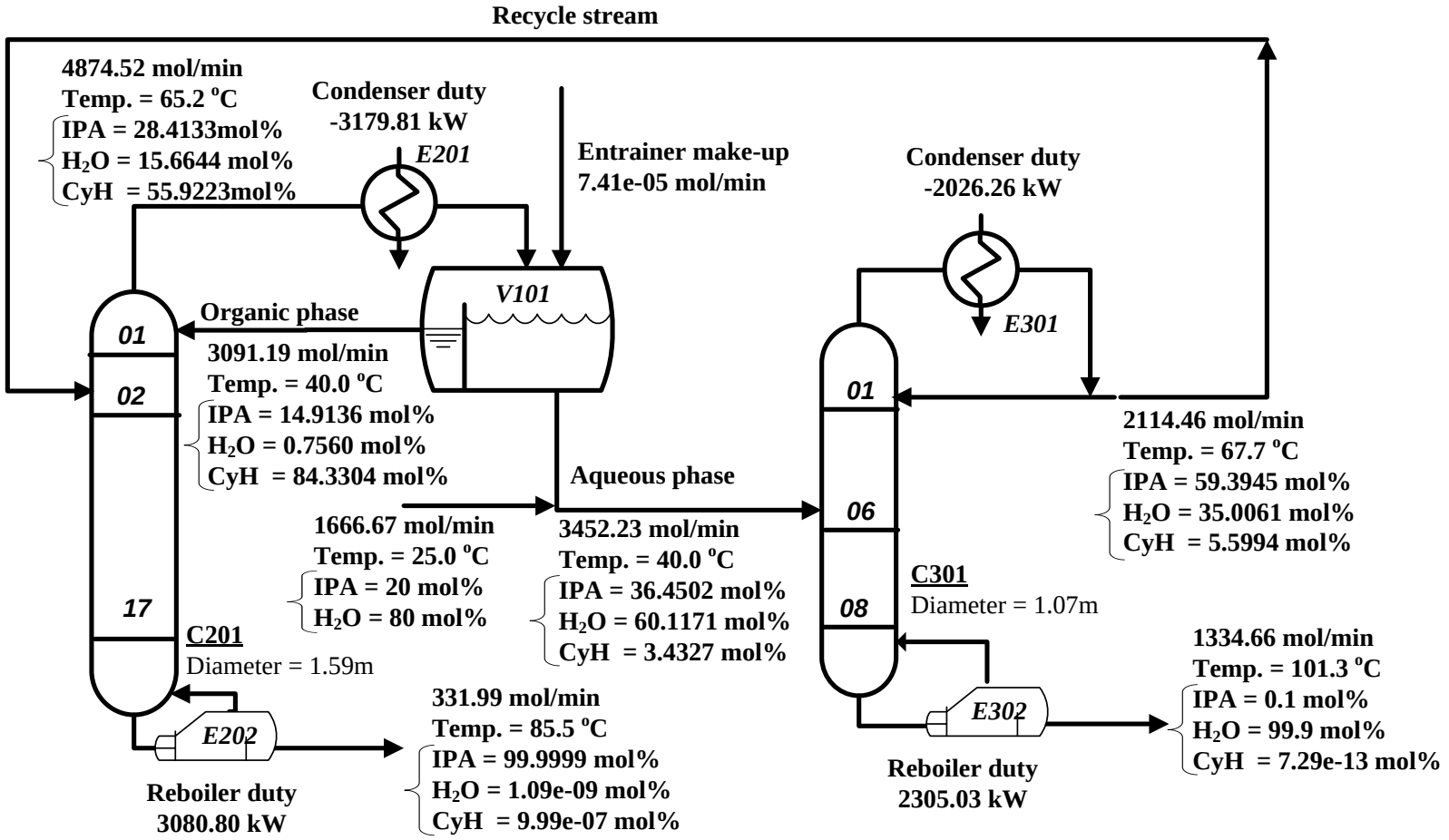

Figure 2-10 Operating conditions for Scheme 2 using 20 mol% IPA as feed.

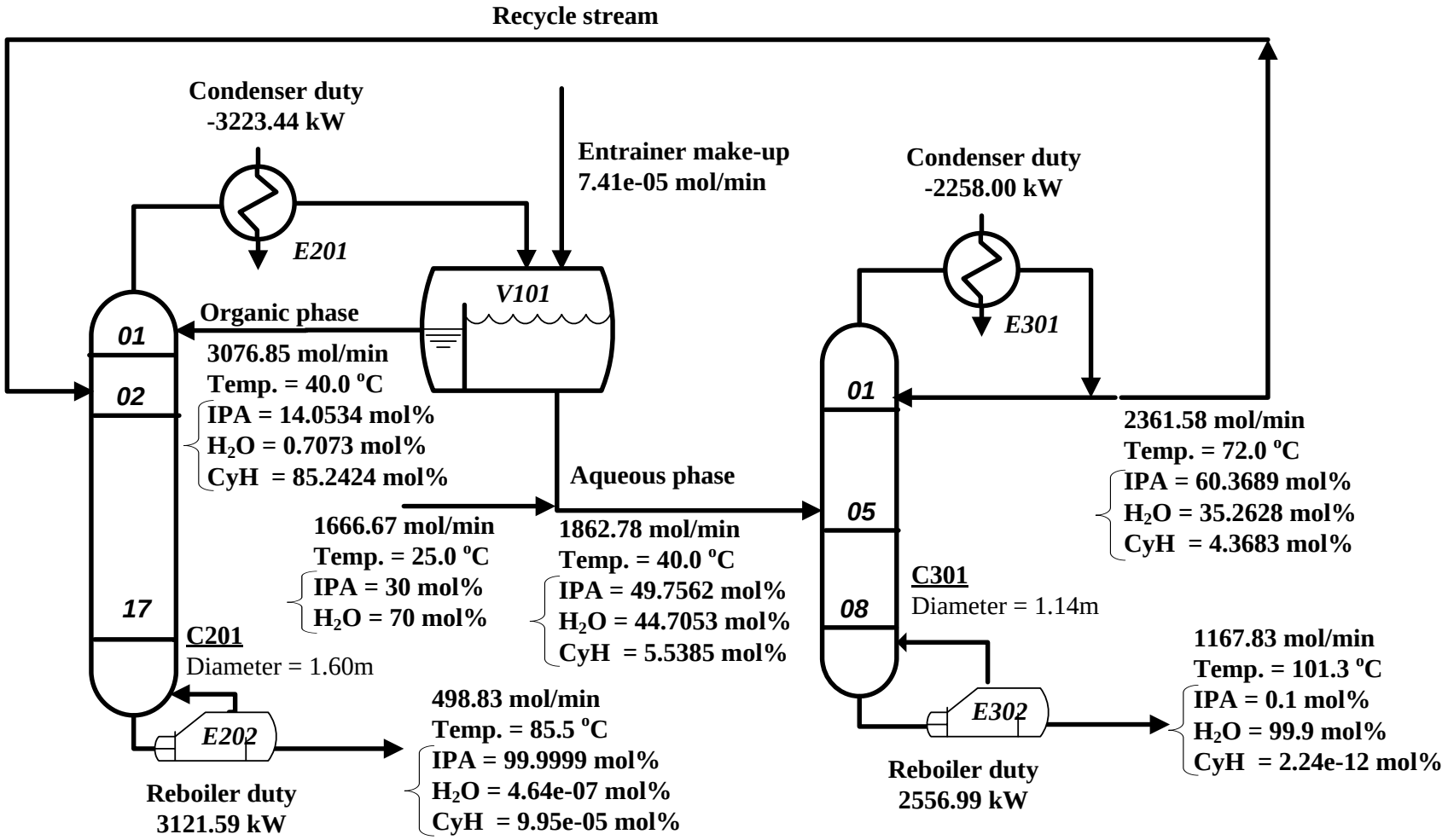

Figure 2-11 Operating conditions for Scheme 2 using 30 mol% IPA as feed.

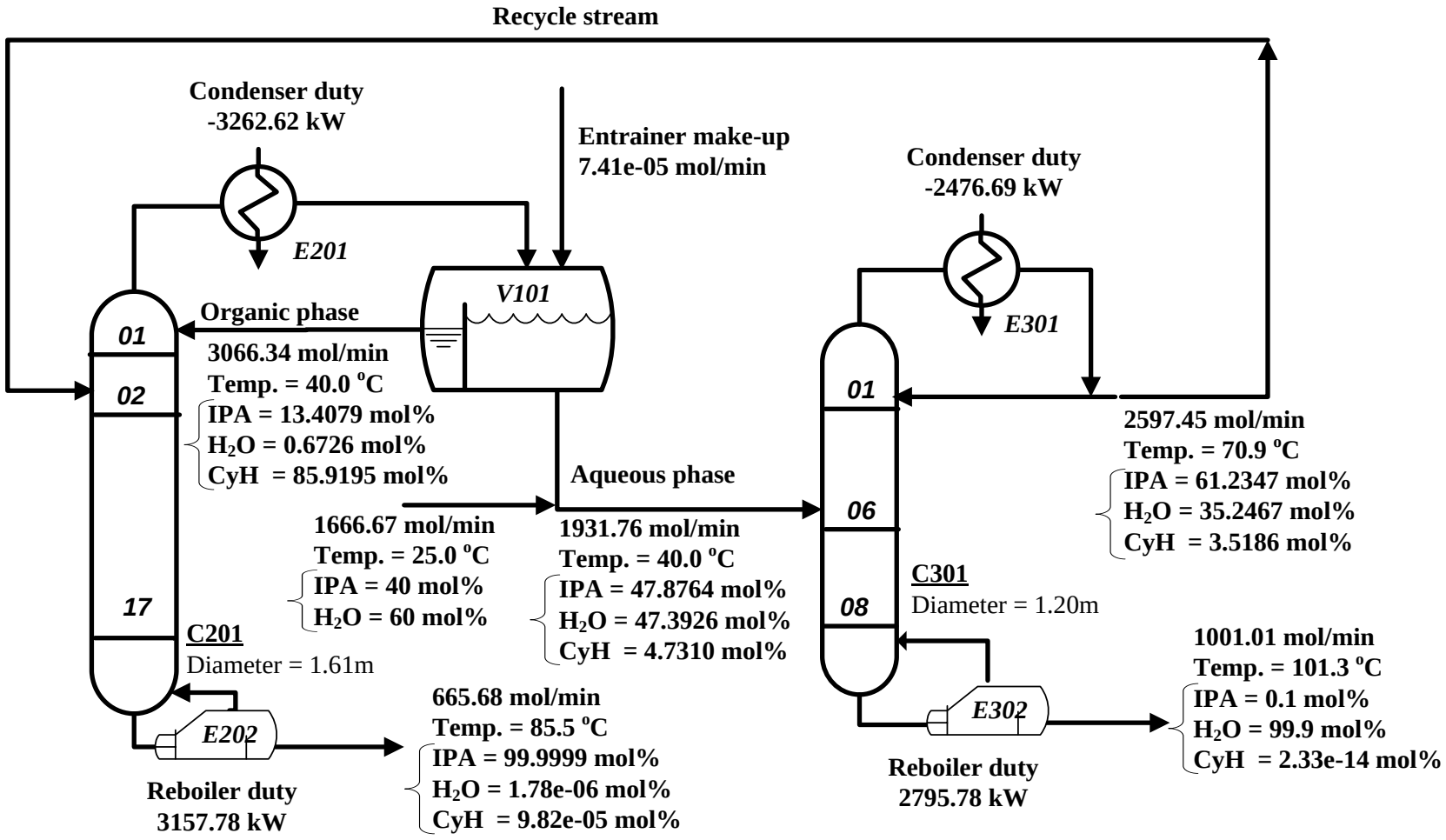

Figure 2-12 Operating conditions for Scheme 2 using 40 mol% IPA as feed.

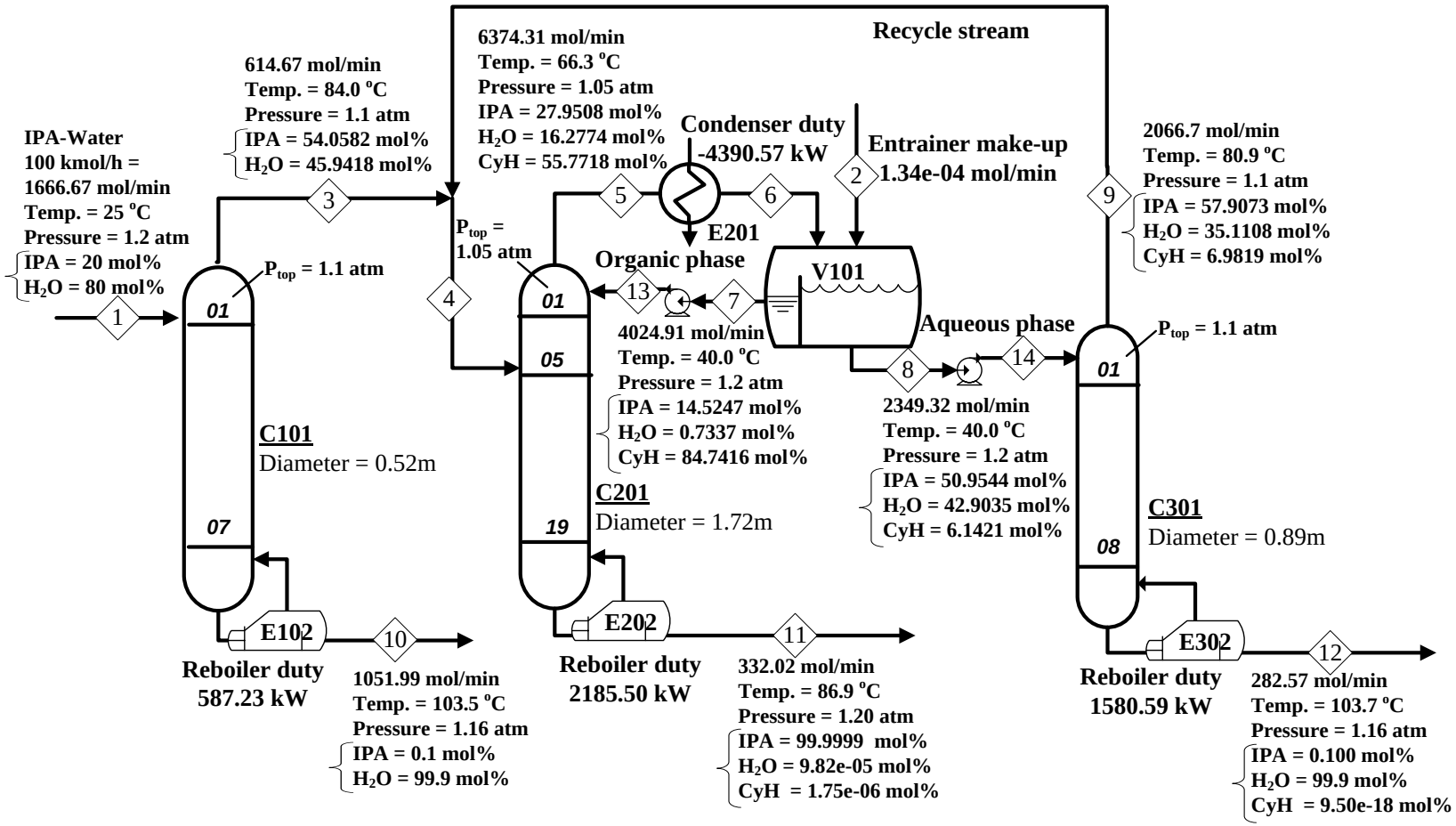

Figure 2-13 Operating conditions for Scheme 3 using 20 mol% IPA as feed.

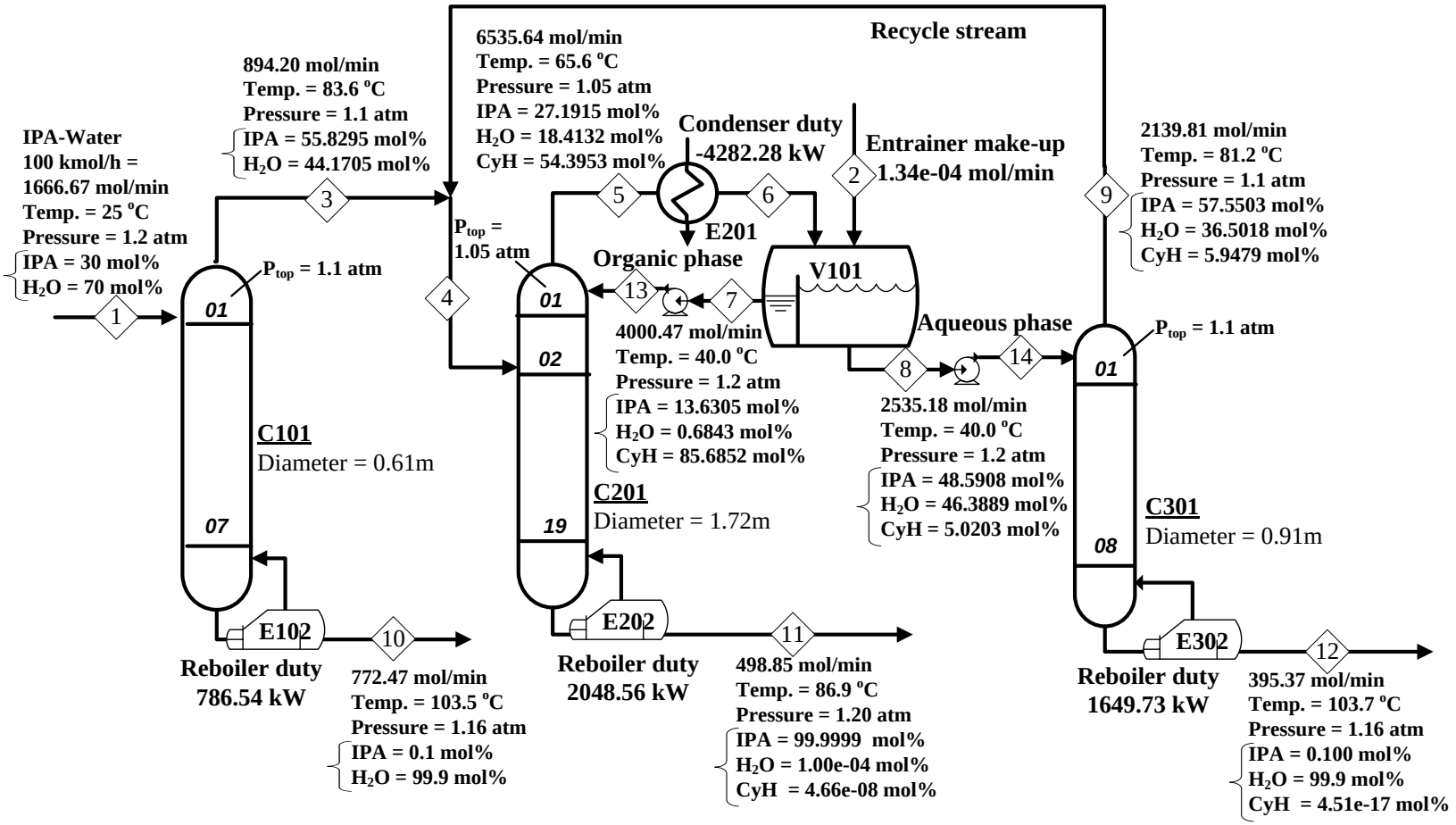

Figure 2-14 Operating conditions for Scheme 3 using 30 mol% IPA as feed.

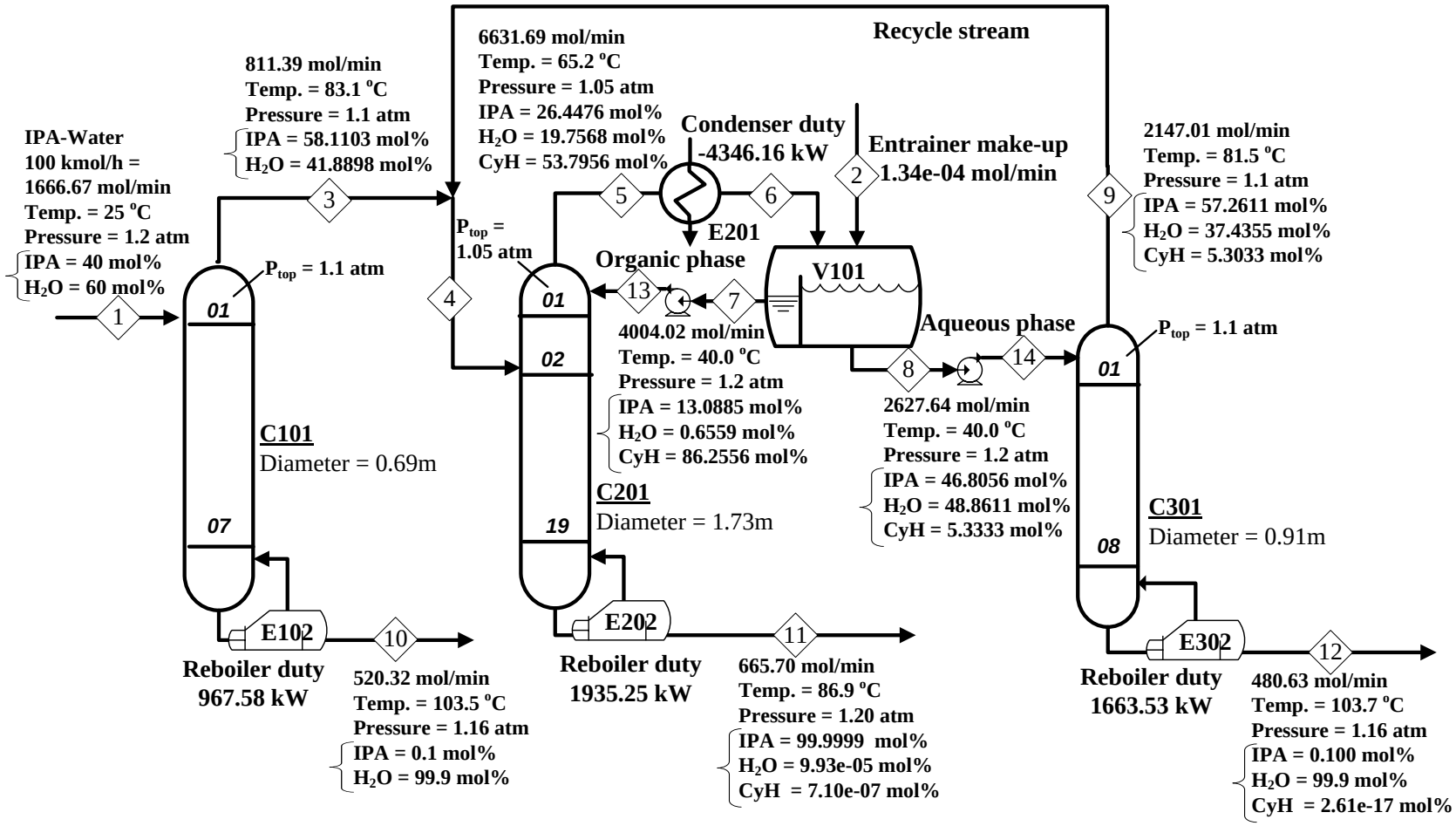

Figure 2-15 Operating conditions for Scheme 3 using 40 mol% IPA as feed.

Table 2-5. Comparison of reboiler duty of Scheme 2 and Scheme 3

	Scheme 2				Scheme 3			
Feed	Reboiler duty (kW)				Reboiler duty (kW)			
IPA purity	E102	E202	E302	total duty	E102	E202	E302	total duty
20 mol%	-	3080.83	2305.06	5385.89	587.23	2185.5	1580.59	4353.32
30 mol%	-	3121.59	2556.99	5678.58	786.54	2048.56	1649.73	4484.83
40 mol%	-	3157.78	2795.78	5953.56	967.58	1935.25	1663.53	4566.36
50 mol%	-	3194.48	3024.38	6218.86	1125.88	1830.46	1671.86	4628.2

2.3 Economic analysis

In order to evaluate the cost effectiveness of these three schemes, viz. the flowsheets in Figures 2-3, 2-4, 2-5, and 2-6, an economic analysis is performed in this study. All of these schemes are designed under the same operating conditions, i.e. the same inputs and outputs, the same cooling water temperature, and the same steam conditions, etc. These operating conditions in fact come from Arifin and Chien[7]. Column diameter for each distillation unit is estimated using the Aspen Plus, and a tray spacing of 0.6 m and flooding of 80% are assumed. The overall tray efficiency for each column is conservatively assumed to be 50%[6, 7]. Thus, the height of each column (H) is estimated from the number of actual plates (N_{actual}) and disengagement heights as

$$H = (N_{actual}-1)\,(\text{tray spacing}) + \text{disengagement height} + \text{skirt height} \quad (2\text{-}3)$$

According to Turton et al.[29], we add 1.2 m for vapor disengagement at the top,

and 1.8 m at the bottom for liquid level and reboiler return. In addition, the overall heat transfer coefficients are 850 and 1140 (W/m^{2}℃) for condenser and reboiler, respectively. The correction factor[29] of 0.9 for logarithmic mean temperature difference (LMTD) is used for each heat exchanger. Low pressure steam is assumed to be available at 5 barg (160 ^{o}C) and cooling water of 30 ^{o}C is employed. A stream factor[29] of 0.95, which is the fraction of working days in a year, is used for calculating the yearly cost of utilities. The decanter is sized with a liquid holdup of 20 min half full[29] and an aspect ratio (length-to-diameter ratio) of 3. It should be noted that the above design specifications together with utility costs are obtained from Turton et al.[29] Table 2-6 gives an equipment list with sizing results for all major equipment units.

Economic analysis in this study follows closely the method of Turton et al.[29] To estimate the capital cost, bare module equipment cost (C_{BM}) is calculated for each unit. The bare module cost (C_{BM}) is a function of purchased cost (C_p^0), bare module cost factor (F_{BM}), number of trays (N) in the column, and quantity factor (f_q) based on the number of trays in the column, i.e.

$$\begin{aligned} C_{BM} &= C_p^0 F_{BM} \quad \text{for vessels and heat exchangers} \\ C_{BM} &= C_p^0 F_{BM} N f_q \quad \text{for sieve trays in the column} \end{aligned} \tag{2-4}$$

The purchased cost for base conditions (C_p^0) is calculated by

$$\log_{10} C_p^0 = K_1 + K_2 \log_{10}(A) + K_3 [\log_{10}(A)]^2 \tag{2-5}$$

where K_1, K_2, and K_3 are constants specific to the type of equipment and A is capacity/ size parameter of the equipment.

The bare module cost factor (F_{BM}), a function of operating pressure and the construction materials, is calculated as:

$$F_{BM} = B_1 + B_2 F_M F_P \quad \text{for vessels and heat exchanger}$$
$$F_{BM} = 1 \quad \text{for sieve trays in the column} \tag{2-6}$$

where B_1 and B_2 are constants depending on the equipment type. F_M is material factor, and F_P is pressure factor. Carbon steel is chosen as the material of construction throughout, since the process under study is operating near ambient pressure and no corrosive chemicals are present.

The quantity factor (f_q) based on the number of trays (N) in the column, is calculated as:

$$\log_{10} f_q = 0.4771 + 0.08516 \log_{10} N - 0.3473 (\log_{10} N)^2 \quad \text{for } N < 20$$
$$f_q = 1 \quad \text{for } N \geqq 20 \tag{2-7}$$

The Constants of bare module costs (C_{BM}) for all of the major equipment units are shown in Table 2-7. The total bare module cost for each scheme is also presented in Table 2-8. In addition, the unit cost of 13.28 ($/GJ) for low-pressure steam and the unit cost of 0.354 ($/GJ) for cooling water are used according to Turton et al.[29] The annual steam and cooling water costs, together with the total annual utility

cost for each scheme are given in Table 2-8. It should be noted that the utility cost here, which is equivalent to the operating cost in Arifin and Chien[7], is the sum of steam cost and cooling water cost. On the other hand, the total annual cost (TAC) is employed here as a measure of economic potential, which does not involve sales revenues for products and is used for preliminary cost estimates when comparing alternative flowsheets during process synthesis. According to Seider et al.[30], the TAC in this study, with which several alternative distillation sequences are examined, can be calculated as:

$$TAC = Annual\ utility\ cost + \frac{Total\ capital\ cost}{i_{\min}} \tag{2-8}$$

The term i_{min} is payback period. The total capital cost is, in fact, the total bare-module costs for all columns and their auxiliaries based on the current Chemical Engineering Plant Cost Index (CEPCI). The bare module cost (C_{BM}) shown in Table 2-8 is based on the CEPCI of 397, which is an average value during the period of May to September of 2001[29].The current CEPCI on December of 2010 is found to be 560.4. Thus, the total capital cost for each scheme can be calculated as:

$$\text{Total capital cost} = \text{Total bare module cost} \times 560.4 / 397 \tag{2-9}$$

Furthermore, Seider et al.[30] recommend that i_{min} be taken as five years. Based on a three-year payback period, Arifin and Chien[7] adopt i_{min} = 3. Olujic et al.[31] consider that i_{min} = 10, according to an assumed plant life time of 10 years.

Table 2-6. Comparison of Equipment Specifications of the schemes

	Scheme 1	Scheme 2	Scheme 3	Scheme 4
Column 1 (C101)				
Total no. of trays	14	-	14	-
Diameter (m)	0.83	-	0.75	-
Height (m)	10.8	-	10.8	-
Condenser (E101)				
Heat transfer area (m^2)	27.94	-	-	-
Reboiler (E102)				
Heat transfer area (m^2)	21.98	-	19.43	-
Column 2 (C102)				
Total no. of trays	34	34	38	34
Diameter (m)	1.63	1.61	1.73	1.99
Height (m)	22.8	22.8	25.2	22.8
Condenser (E201)				
Heat transfer area (m^2)	191.78	186.66	243.12	311.74
Reboiler (E202)				
Heat transfer area (m^2)	42.43	42.03	24.42	34.67
Column 3 (C103)				
Total no. of trays	16	16	16	16
Diameter (m)	0.9	1.25	0.91	1.3
Height (m)	12	12	12	12
Condenser (E301)				
Heat transfer area (m^2)	39.1	72.59	-	-
Reboiler (E302)				
Heat transfer area (m^2)	26.27	50.09	28.95	57.53
Decanter				
Total flow rate (m^3/min)	0.43	0.418	0.552	0.728
Diameter (m)	1.94	1.92	2.11	2.31
Height (m)	5.82	5.76	6.33	6.94

Table 2-7. Constants of Bare Module Equipment Cost

	Equipment*	Type	K_1	K_2	K_3	B_1	B_2	F_m	F_p
E101	HEX	Multiple-pipe	2.7652	0.7282	0.0783	1.74	1.55	1.0	1.0
E201	HEX	Fixed-tube	4.3247	-0.303	0.1634	1.63	1.66	1.0	1.0
E301	HEX	Multiple-pipe	2.7652	0.7282	0.0783	1.74	1.55	1.0	1.0
E102	HEX	Kettle reboiler	4.4646	-0.5277	0.3955	1.63	1.66	1.0	1.0
E202	HEX	Kettle reboiler	4.4646	-0.5277	0.3955	1.63	1.66	1.0	1.0
E302	HEX	Kettle reboiler	4.4646	-0.5277	0.3955	1.63	1.66	1.0	1.0
V101	DC	Horizontal vessel	3.5565	0.3776	0.0905	1.49	1.52	1.0	1.0
C101	COL	Vertical vessel	3.4974	0.4485	0.1074	2.25	1.82	1.0	1.0
	Tray	Sieve	2.9949	0.4465	0.3961	-	-	-	-
C201	COL	Vertical vessel	3.4974	0.4485	0.1074	2.25	1.82	1.0	1.0
	Tray	Sieve	2.9949	0.4465	0.3961	-	-	-	-
C301	COL	Vertical vessel	3.4974	0.4485	0.1074	2.25	1.82	1.0	1.0
	Tray	Sieve	2.9949	0.4465	0.3961	-	-	-	-

* HEX: heat exchanger, DC: decanter, COL: column.

Table 2-8. Comparison of Costs of the schemes

C_{BM} ($)	Scheme 1	Scheme 2	Scheme 3	Scheme 4
Column 1 (C101)	61,900	-	56,000	-
Condenser (E101)	44,500	-	-	-
Reboiler (E102)	137,000	-	128,000	-
Column 2 (C102)	277,000	272,000	333,000	390,000
Condenser (E201)	142,000	140,000	158,000	179,000
Reboiler (E202)	209,000	208,000	145,000	181,000
Column 3 (C103)	73,400	109,200	74,300	115,000
Condenser (E301)	61,700	114,000	-	-
Reboiler (E302)	151,000	238,000	160,000	268,000
Decanter	63,000	61,600	75,200	91,800
Total capital cost ($)	1,220,500	1,142,800	1,129,500	1,224,800
Annual steam cost ($/year)	2,464,500	2,474,300	1,843,000	2,360,000
Annual cooling water cost ($/year)	63,200	63,600	47,000	60,000
Annual utility cost ($/year)	2,527,700	2,537,900	1,890,000	2,420,000

Table 2-9. Comparison of TAC's and Cost Ratios of the schemes

		Scheme 1	Scheme 2	Scheme 3	Scheme 4
i_{min} = 10	TAC ($)	2,649,750	2,652,180	2,002,950	2,542,480
	Cost ratio	1.000 (Base)	1.001	0.756	0.960
i_{min} = 5	TAC ($)	2,771,800	2,766,460	2,115,900	2,664,960
	Cost ratio	1.000 (Base)	0.998	0.763	0.961
i_{min} = 3	TAC ($)	2,934,533	2,918,833	2,266,500	2,828,267
	Cost ratio	1.000 (Base)	0.995	0.772	0.964

A comparison of all the calculated TAC's as well as cost ratios (determined with reference to the cost of Scheme 1) is summarized in Table 2-9 and sketched in Figure 2-16 for the three alternative schemes using various values of i_{min}. Pump costs however are not included in the TAC, like those in the work of Arifin and Chien[7], as they are relatively small when compared with the costs of other equipment.

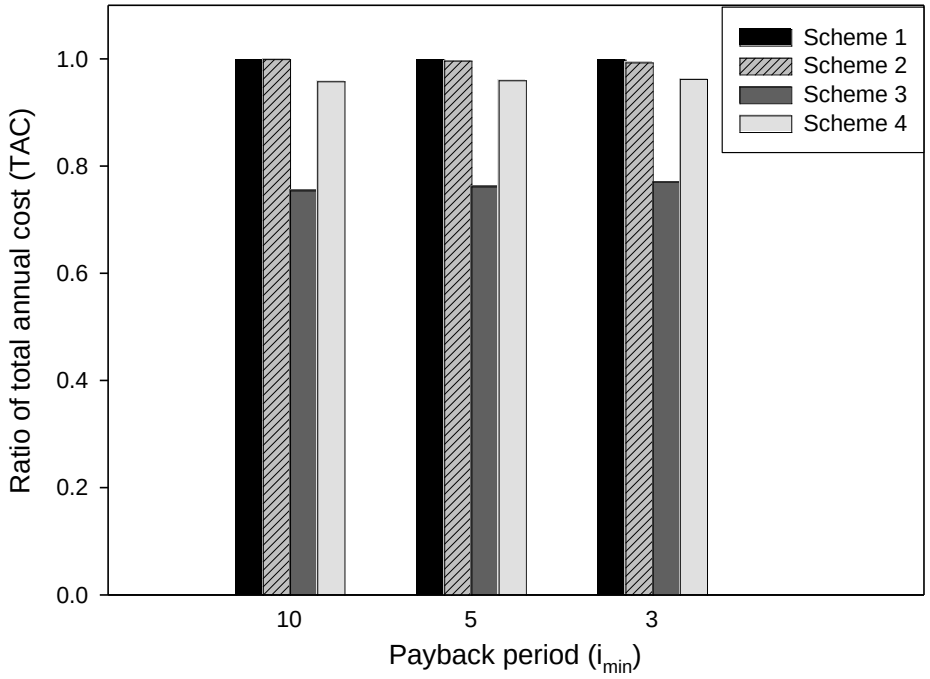

Figure 2-16 Ratio of total reboiler duties of four schemes.

Besides TAC based on Turton et al.[29], this work also present TAC based on Douglas[32] used by Arifin and Chien[7]. The capital cost and the annual utility cost are estimated the equations (2-10) where latent heat of steam (λ) is 955.41 Btu/lb at 1 atm and 229.33°F.

$$\text{Column cost} = \frac{\text{M \& S}}{280} \times 101.9 \times \left(D_c \times \frac{1\text{ft}}{0.305\text{m}} \right)^{1.066} \times \left(L_c \times \frac{1\text{ft}}{0.305\text{m}} \right)^{0.802} \times (2.18 + 1 \times 1)$$

$$\text{Tray cost} = \frac{\text{M \& S}}{280} \times 4.7 \times \left(D_c \times \frac{1\text{ft}}{0.305\text{m}} \right)^{1.55} \times \left(L_c \times \frac{1\text{ft}}{0.305\text{m}} \right) \times (1 + 0 + 0)$$

$$\text{Reboiler cost} = \frac{\text{M \& S}}{280} \times 101.3 \times \left((2.29 + ((1.35 + 0) \times 1)) \times \left(A_R \times \frac{1\text{ft}^2}{0.093\text{m}^2} \right)^{0.65} \right) \quad (2\text{-}10)$$

$$\text{Condenser cost} = \frac{\text{M \& S}}{280} \times 101.3 \times \left((2.29 + ((1 + 0) \times 1)) \times \left(A_R \times \frac{1\text{ft}^2}{0.093\text{m}^2} \right)^{0.65} \right)$$

$$\text{Decanter cost} = \frac{\text{M \& S}}{280} \times 101.9 \times \left(D_c \times \frac{1\text{ft}}{0.305\text{m}} \right)^{1.066} \times \left(L_c \times \frac{1\text{ft}}{0.305\text{m}} \right)^{0.82} \times (2.18 + 1 \times 1)$$

Table 2-10. Comparison of Costs of the schemes based on Douglas[32]

C_{BM} (\$)	Scheme 1	Scheme 2	New scheme	Scheme 3
Column 1 (C101)	94,643	-	84,766	-
Condenser (E101)	74,596	-	-	-
Reboiler (E102)	70,614	-	65,175	-
Column 2 (C102)	363,624	358,718	421,324	453,068
Condenser (E201)	260,908	256,359	304,403	357,792
Reboiler (E202)	108,283	107,618	75,615	94,960
Column 3 (C103)	112,589	161,129	113,952	168,189
Condenser (E301)	92,807	138,751	-	-
Reboiler (E302)	79,290	120,617	84,458	131,978
Decanter	136,009	133,402	159,116	188,662
Total capital cost (\$)	1,393,363	1,276,594	1,308,810	1,394,650

Table 2-11. Comparison of TAC's and Cost Ratios of the schemes based on Douglas[32].

		Scheme 1	Scheme 2	Scheme 3	Scheme 4
i_{min} = 10	TAC (\$)	2,667,036	2,665,559	2,020,881	2,559,465
	Cost ratio	1.000 (Base)	0.999	0.758	0.960
i_{min} = 5	TAC (\$)	2,806,373	2,793,219	2,151,762	2,698,930
	Cost ratio	1.000 (Base)	0.995	0.767	0.962
i_{min} = 3	TAC (\$)	2,992,154	2,963,431	2,326,270	2,884,883
	Cost ratio	1.000 (Base)	0.990	0.777	0.964

The capital cost and the annual utility cost estimated by Douglas[32] shown in Table 2-10 is based on the M&S of 1536.5 on 4th 2011 and a comparison of all the calculated TAC's as well as cost ratios is summarized in Table 2-11. According to Table 2-9 and Table 2-11, TAC of Scheme 3 in this study is the best and least whether based on Turton et al.[29] or Douglas[32].

Chapter 3 Dynamic Simulation

It is futile if a distillation sequence is difficult to control, even though the sequence is most energy-saving. Hence, dynamic simulation of Scheme 3 is established with a program written in FORTRAN language and Aspen Dynamics.

For dynamic simulation using FORTRAN, a computational flowchart of a distillation column is established illustrated in Figure 3-1, consisted of number of trays (N), fresh feed at j stage (F_j), vapor flow rate leaving stage j (V_j), liquid flow rate leaving stage j (L_j), liquid molar fraction of component i (x_i), vapor molar fraction of component i (y_i). Each stage of a column is assumed as equilibrium stage and the liquid holdup of a stage maybe divided into vapor-liquid-liquid-equilibrium (VLLE) or vapor-liquid-liquid-equilibrium (VLE). Figure 3-2 shows sketches of an equilibrium stage j for VLLE and VLE and input and output information is illustrated clearly.

3.1 MESH equation

Dynamic characteristic of a equilibrium stage can be calculated by following equations:

- Material balance equations, abbreviated M equation.
- Phase equilibrium equations, abbreviated E equation.

- Summation equations of mole fraction, abbreviated S equation.
- Heat balance equations, abbreviated H equation.

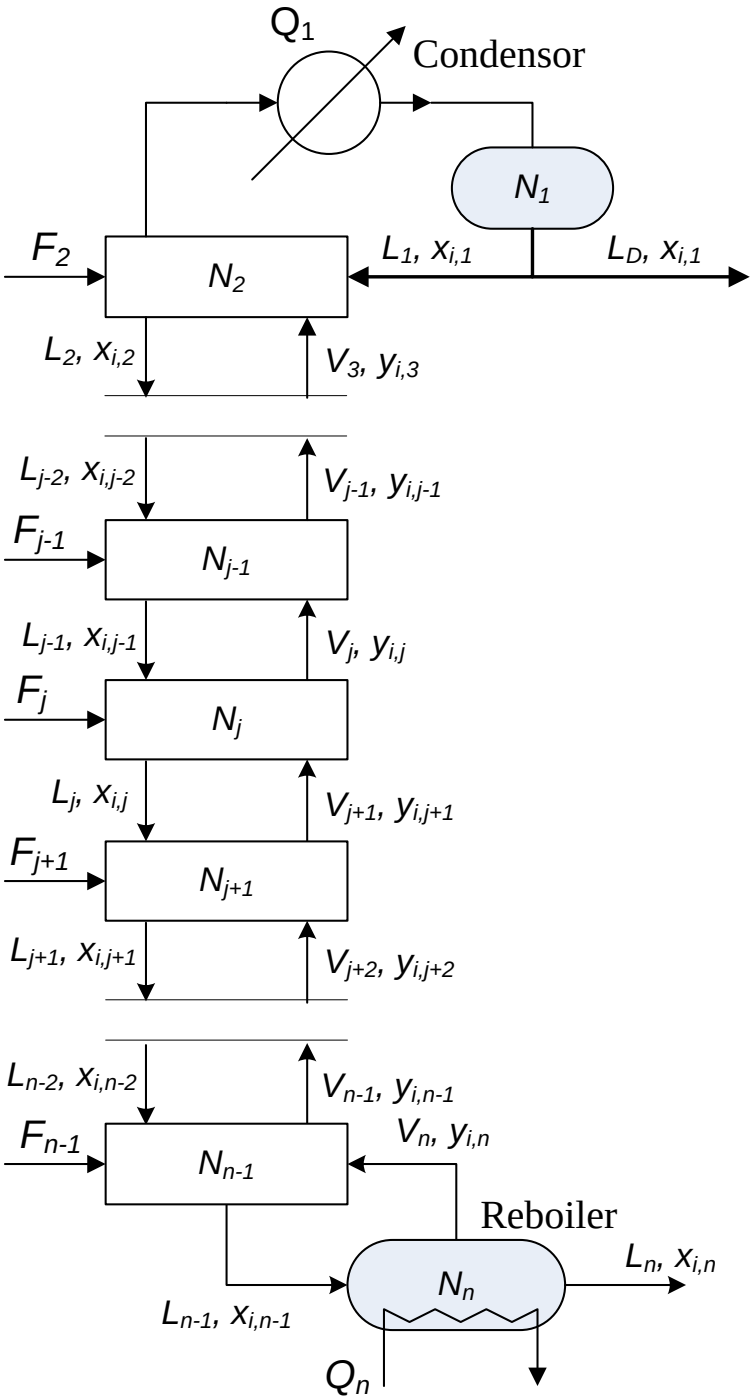

Figure 3-1 Computational flowchart of a distillation column.

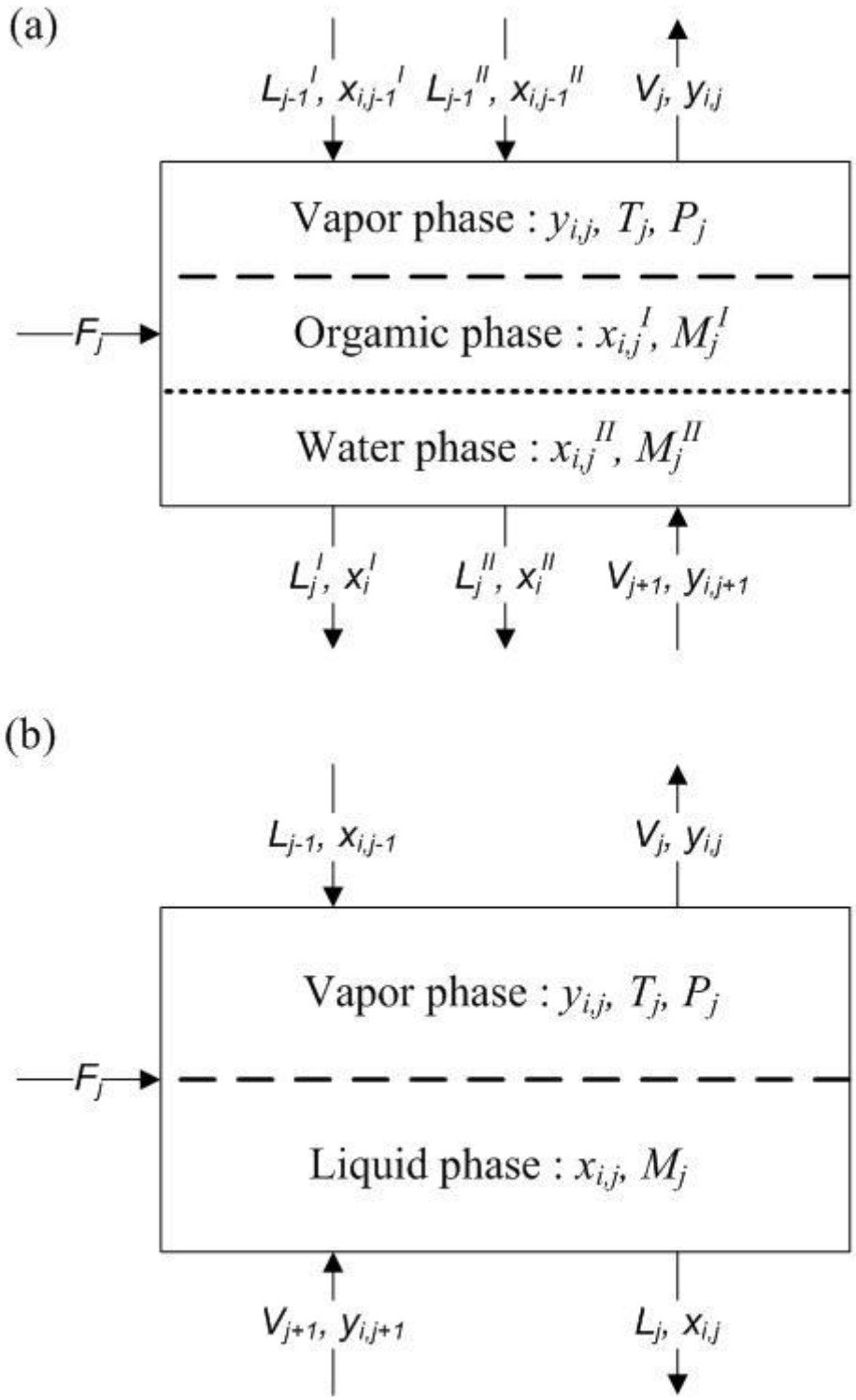

Figure 3-2 Sketches of an equilibrium stage *j* for (a) VLLE and (b) VLE.

Material balance equations

For mass balance of holdup on stage *j*:

$$\begin{aligned} \frac{dM_j}{dt} &= L_{j-1} + V_{j+1} + F_j - L_j - V_j \\ \frac{dM_j x_{i,j}}{dt} &= L_{j-1}x_{i,j-1} + V_{j+1}y_{i,j+1} - L_j x_{i,j} - V_j y_{i,j} + F_j z_{i,j} \end{aligned} \tag{3-1}$$

For mass balance for component *i* on stage *j*:

$$\frac{dM_j x_{i,j}}{dt} = L_{j-1}x_{i,j-1} + V_{j+1}y_{i,j+1} - L_j x_{i,j} - V_j y_{i,j} + F_j z_{i,j} + R_{i,j} \tag{3-2}$$

Phase equilibrium equations

For VLE:

$$y_i = \frac{\gamma_i P_i^{sat} x_i}{P} = K_i x_i \tag{3-3}$$

For VLLE:

$$y_i = \frac{\gamma_i^I P_i^{sat} x_i^I}{P} = \frac{\gamma_i^{II} P_i^{sat} x_i^{II}}{P} \tag{3-4}$$

Heat balance equations

For *j* stage, the heat balance relationship:

$$\frac{dM_j H_j^L}{dt} = L_{j-1}H_{j-1}^L + V_{j+1}H_{j+1}^V - L_j H_j^L - V_j H_j^V + F_j H_j^F + Q_{R,j} \tag{3-5}$$

Summation equations of mole fraction

The sum of liquid molar fraction and vapor molar fraction of component *i* flow out *j* stage:

$$\begin{aligned} \sum x_i &= 1 \\ \sum y_i &= 1 \end{aligned} \tag{3-6}$$

3.2 Physical properties

Physical properties and model parameters used in the dynamic simulation, such as critical properties, heat capacity coefficients, and Antoine constants, are taken from the Aspen Plus data bank[27] and binary parameters of NRTL model are obtained from Wang et al.[26]. Their values are the same as those used in the steady-state simulation for Scheme 3 using Aspen Plus.

Basic physical properties

Basic physical properties of these three components include molecular weight (*MW*, unit: g/mol), heat of vaporization (H_{vap}, unit: J/mol), critical temperature (T_c, unit: K), critical pressure (P_c, unit: bar), critical volume (V_c, unit: m^3/mol), and critical compressibility factor (Z_c). They are taken from Aspen Plus data bank[27] and summarized in Table 3-1.

Saturated vapor pressure

Saturated vapor pressure of a pure substance can be calculated by extended Antoine equation as:

$$\ln(P^{sat}) = A_1 + \frac{A_2}{T + A_3} + A_4 T + A_5 \ln(T) + A_6 T^{A_7}, \quad A_8 < T < A_9 \tag{3-7}$$

where P^{sat} is the saturated vapor pressure and A_i are the extended Antoine equation parameters. A_i are also taken from Aspen Plus data bank[27] and summarized in Table 3-2.

Table 3-1. Basic Physical Properties for IPA/CyH/H_2O System[27]

	IPA	CyH	H2O
MW (g/mol)	60.09592	84.16128	18.01528
H_0 (J/mol)	39383.7	29909.0	40799.2
T_c (K)	508.3	553.8	647.13
P_c (bar)	47.64	40.8	220.55
V_c (m^3/mol)	220.0	308.0	55.9478
Z_c	0.25	0.273	0.229

Table 3-2. Extended Antoine Equation Parameters for IPA/CyH/H_2O System[27]

	CyH	IPA	H2O
A_1	39.57407	64.91707	62.13607
A_2	-5226.4	-7607	-7258.2
A_3	0	0	0
A_4	0	0	0
A_5	-4.2278	-7.4086	-7.3037
A_6	9.76E-18	4.40E-18	4.17E-06
A_7	6	6	2
A_8	279.69	185.28	273.16
A_9	553.8	508.3	647.13

* Unit: temperature: K, pressure: bar.

Liquid mixture density

For liquid bubble-point density (ρ_m, unit: mol/m^3) of a mixture, it can be calculated by modified Rackett equation[33] as:

$$\frac{1}{\rho_m} = R\left(\sum_i \frac{x_i T_{ci}}{P_{ci}}\right) Z_{cm}^{\left[1+(1-T_r)^{2/7}\right]}$$

$$\phi_i = \frac{x_i V_{ci}}{\sum_i x_i V_{ci}}$$

$$Z_{cm} = \sum_i x_i Z_{ci}$$

$$T_r = T / T_{cm} \qquad \text{(3-8)}$$

$$T_{cm} = \left[\sum_i \sum_j \phi_i \phi_j T_{cij}\right]$$

$$T_{cij} = \left(1 - k_{ij}\right)\left(T_{ci} T_{cj}\right)^{1/2}$$

$$\left(1 - k_{ij}\right) = \frac{8\left(V_{ci} V_{cj}\right)^{1/2}}{\left(V_{ci}^{\,1/3} + V_{cj}^{\,1/3}\right)^3}$$

where universal gas constant (R) is 83.144 ($\mathrm{bar \cdot cm3/mole\text{-}K}$). x_i and ϕ_i are mole fraction and volume fraction for i component. For component i, critical temperature (T_{ci}), critical pressure (P_{ci}), critical volume (V_{ci}), and critical compressibility factor (Z_{ci}) are same Table 3-1. Z_{cm} is compressibility factor of a mixture and T_r is reduced temperature.

Mixture enthalpies

Liquid enthalpy of component *i* (H^L_i, unit: J/mol) is reference enthalpy plus a integration of liquid heat capacity over a given temperature range. And vapor molar enthalpy of component *i* (H^V_i, unit: J/mol) is liquid molar enthalpy plus molar heat of vaporization (H_i^{evp}, unit: J/mol). If the heat of mixing is ignored, and liquid mixture molar enthalpy (H^L_m, unit: J/mol) and vapor mixture molar enthalpy (H^V_m) are therefore the sum of product of liquid mole fraction (x_i) and liquid enthalpy of component *i* and the sum of product of vapor mole fraction (y_i) and vapor enthalpy of component *i*, respectively.

$$\begin{aligned} H_i^L &= H_{0,i} + \int_{T_0}^{T} C_{PL,i}\,dT \\ H_i^V &= H_i^L + H_i^{evp} \\ H_m^L &= \sum_i x_i H_i^L \\ H_m^V &= \sum_i y_i H_i^V \end{aligned} \tag{3-9}$$

$$C_{PL,i} = C_{p1,i} + C_{p2,i}T + C_{p3,i}T^2 + C_{p4,i}T^3 + C_{p5,i}T^4$$

The reference enthalpy is set zero at a reference temperature (T_0) of 298.15 K. $C_{PL,,i}$ is liquid heat capacity of component *i* and the parameters of liquid heat capacity are taken from Aspen Plus data bank[27] listed in Table 3-3.

Table 3-3. A Set of the Parameters of Liquid Heat Capacity for IPA/CyH/H_2O System[27]

	CyH	IPA	H2O
C_{p1}	-220.6	723.55	276.37
C_{p2}	3.1183	-8.095	-2.0901
C_{p3}	-0.0094216	0.036662	0.008125
C_{p4}	1.07E-05	-6.64E-05	-1.41E-05
C_{p5}	4.41E-08	0	9.37E-09

*Unit: J/mole·K

3.3 Equilibrium-related computation algorithms

For liquid-liquid equilibrium (LLE), vapor-liquid equilibrium (VLE), and vapor-liquid-liquid equilibrium (VLLE) computation mode in this study, a activity coefficient (γ_i) of the component is calculated using NRTL and binary parameters of NRTL model are obtained from Wang et al.[26]. Computational flowchart of LLE[34], VLE, and VLLE are shown in Figure 3-3, Figure 3-4, and Figure 3-5, sequentially. For bubble-point calculation of VLE, the convergence method of King (1980)[35] is used in this work and shown as:

$$f(T) = \left[\sum y_i\right] - 1 = \left[\sum x_i K_i(T)\right] - 1$$
$$\psi\left(\frac{1}{T}\right) = \ln f\left(\frac{1}{T}\right) = \ln \sum y_i = \ln \sum x_i K_i\left(\frac{1}{T}\right) \quad (3\text{-}10)$$

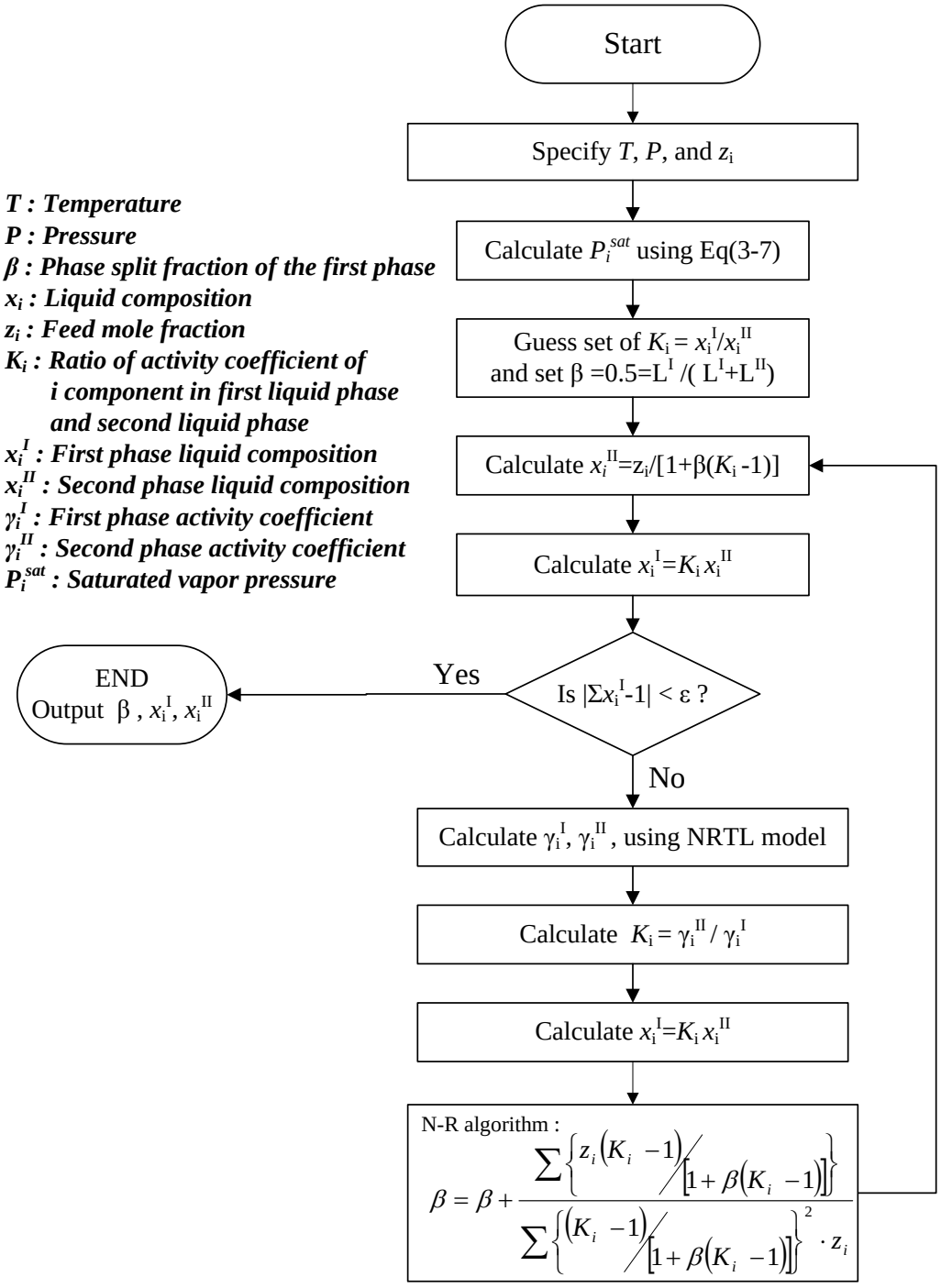

T : Temperature
P : Pressure
β : Phase split fraction of the first phase
x_i : Liquid composition
z_i : Feed mole fraction
K_i : Ratio of activity coefficient of i component in first liquid phase and second liquid phase
x_i^I : First phase liquid composition
x_i^{II} : Second phase liquid composition
γ_i^I : First phase activity coefficient
γ_i^{II} : Second phase activity coefficient
P_i^{sat} : Saturated vapor pressure

Figure 3-3 Computational flowchart of liquid-liquid-equilibrium[34].

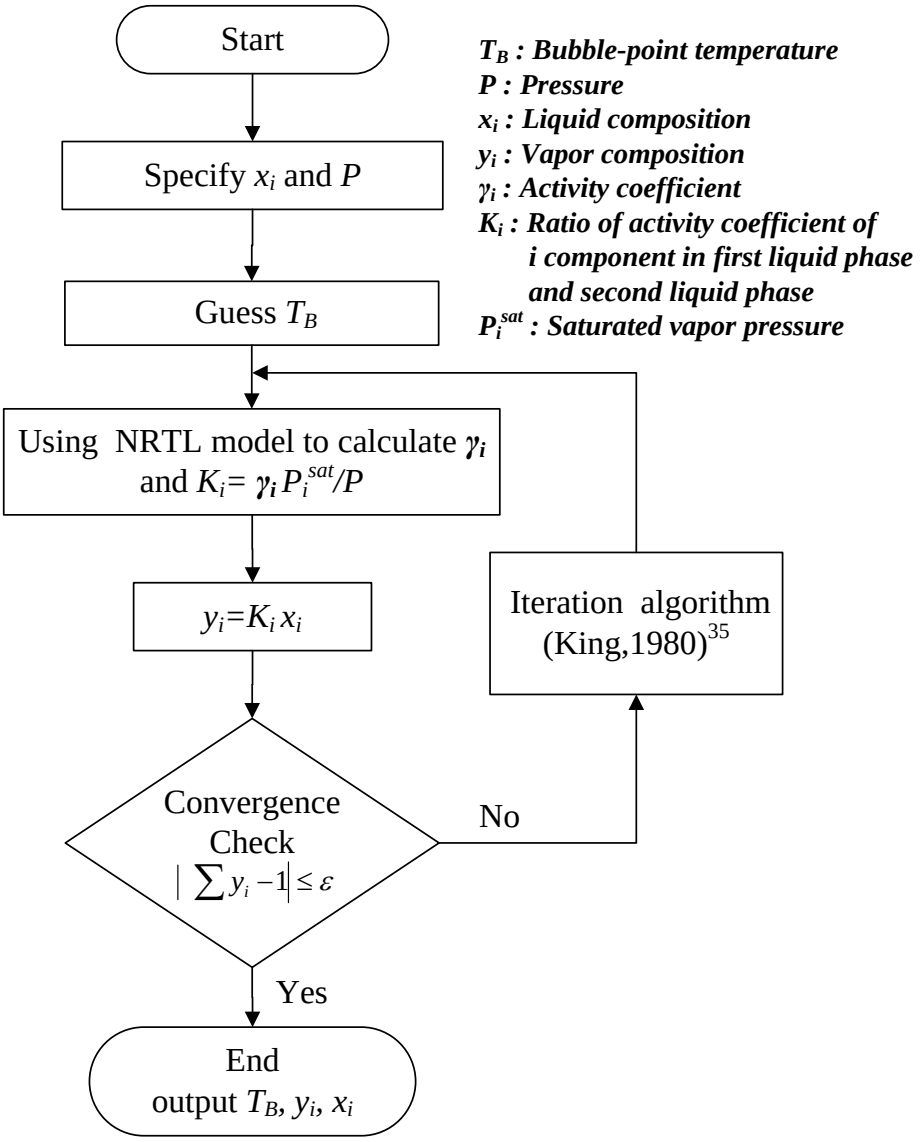

Figure 3-4 Computational flowchart of vapor-liquid-equilibrium[34].

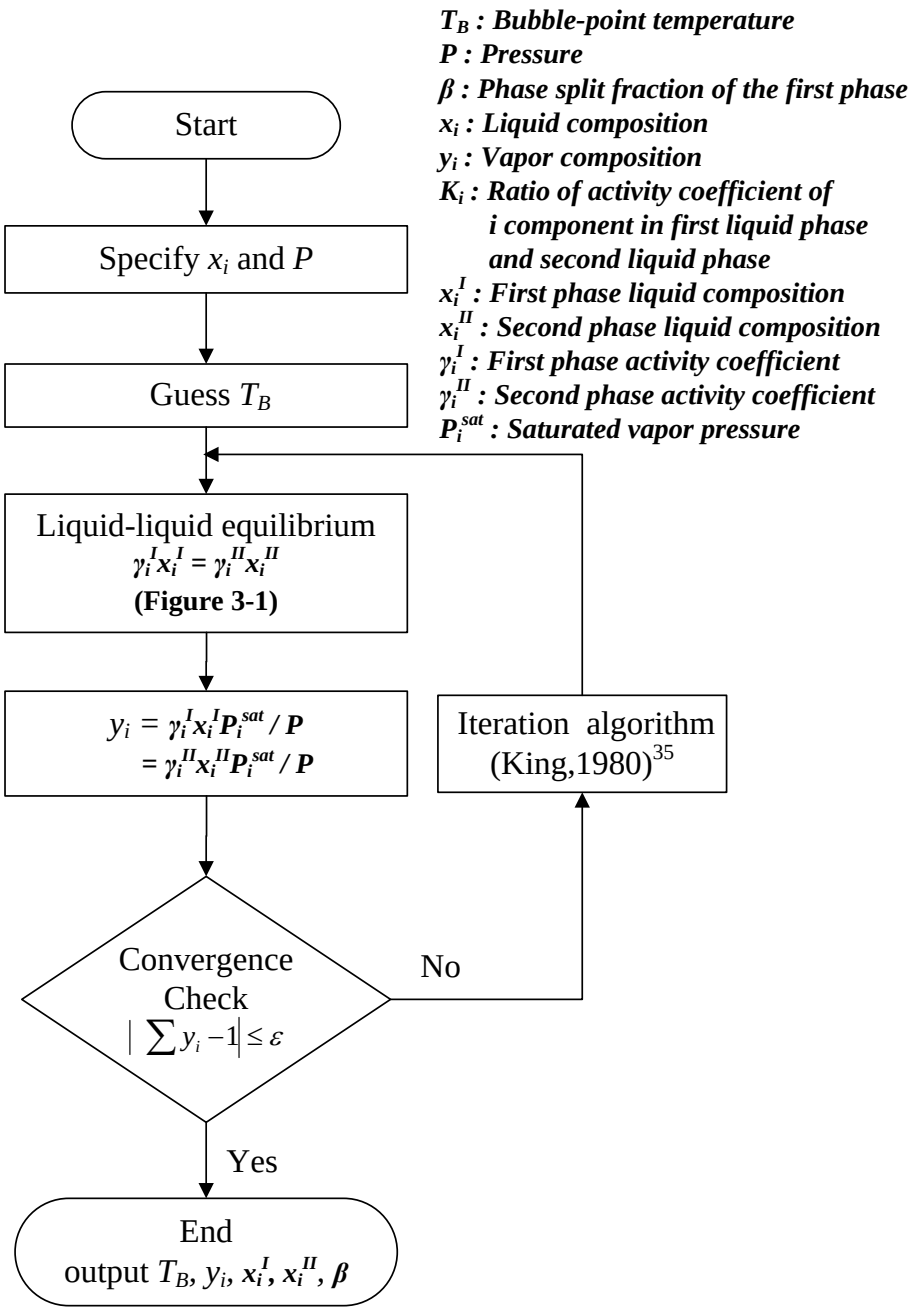

Figure 3-5 Computational flowchart of vapor-liquid-liquid-equilibrium[34].

Figure 3-6(a) shows a plot of *f(T)* versus *T*. The function *f(T)* is monotonic and hence will not give spurious solutions. However, there is a substantial amount of non-linearity to *f(T)* because of K_i which are related to vapor pressure not being linear in *T*. Because $\ln(K_i)$ is more nearly linear in *T*, it is reasonable to anticipate that a more nearly linear function will be $\Psi(T) = \ln[f(T)]$. Since $\ln(K_i)$ will usually be even more nearly linear in *1/T*, an even more rapid convergence can be achieved if $\Psi(1/T) = \ln[f(1/T)]$ shown in Figure 3-6(b). Hence, a sufficiently accurate bubble-point temperature can be obtained by computing at two values of temperature T_0 and T_1 and then calculating the bubble-point by linear interpolation or extrapolation using equation 3-11.

$$\frac{1}{T_{BP}} = \frac{1}{T_0} + \left(\frac{1}{T_1} - \frac{1}{T_0}\right)\frac{\psi\left(1/T_0\right)}{\psi\left(1/T_0\right) - \psi\left(1/T_1\right)} \tag{3-11}$$

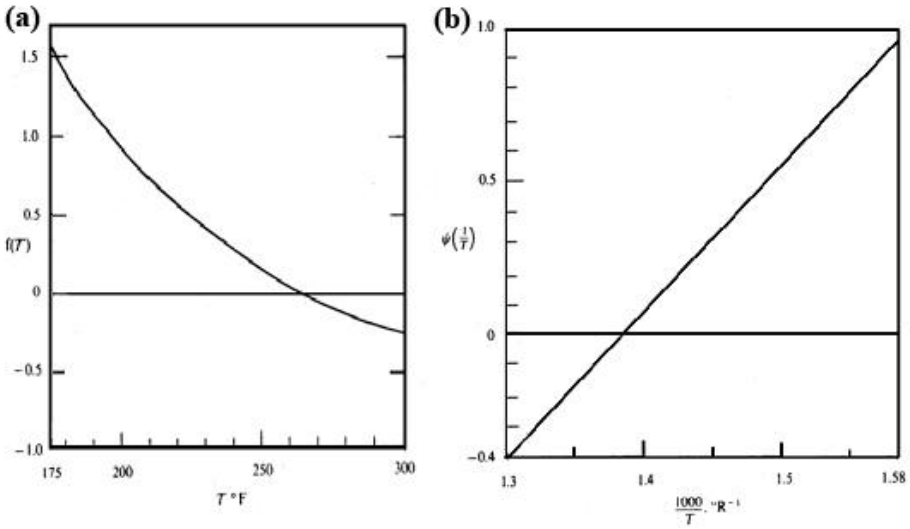

Figure 3-6 Convergence characteristics of *f(T)* given by equation 3-11[35].

3.4 Modularized simulation

The dynamic simulation program is built on an equilibrium-stage model of Franks[36], and Figure 3-7 shows the computational flowchart associated with the model for stage *j*. First, a cubic spline interpolation[37] can be used to fit the data and a binodal curve can thus be generated, with which liquid composition on each tray will be checked to see whether it is located inside the phase envelop or not (i.e., phase splitting). If phase splitting takes place on a tray, the VLLE computation mode will be adopted. Otherwise, the VLE computation mode is used. Given a stage pressure and initial liquid composition of component *i*, the vapor composition of component *i* leaving stage *j* and the temperature on stage *j* can both be computed based on a bubble-point temperature calculation. Once the stage temperature is known, the density of liquid mixture at bubble-point condition (ρ_m) is estimated by modified Rackett equation[33] (equation 3-8).

The liquid flow rate leaving stage *j* (L_j, unit: mol/min) can then be calculated by Francis weir formula.

$$L_j = 110.3067 \rho_m W_L W_{HO}^{1.5}$$
$$W_{HO} = \frac{M_j}{\rho_m A_w} - W_H \qquad (3\text{-}12)$$

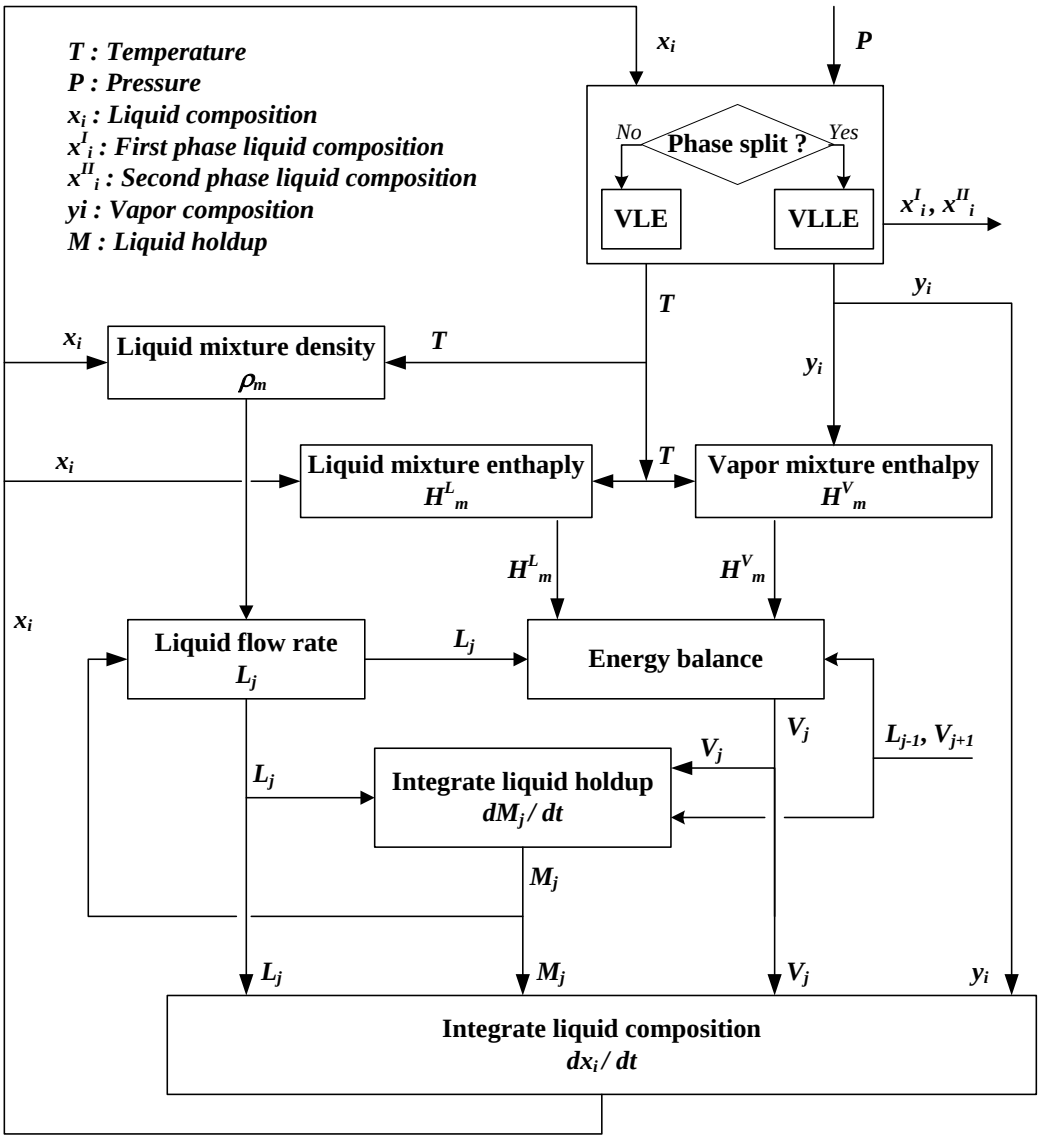

Figure 3-7 Computational flowchart of equilibrium stage *j*.

The value of side weir length (W_L, unit: m) is from the results of tray sizing by Aspen Plus. Effective area of a stage (A_w, unit: m^2) is calculated by subtracting downcomer area from cross sectional area (or 90% tower area). The value of weir height (W_H, unit: m) is 0.05. The value of head on the weir (W_{HO}, unit: m) is calculated by holdup on the stage (M_j, unit: mol) divided by the product of liquid bubble-point density (ρ_m, unit: mol/m^3) and effective area of a stage (A_w, unit: m^2) to subtract value of weir

height (W_H, unit: m). The liquid and vapor mixture molar enthalpies (H^L_j, unit: J/mol and H^V_j, unit: J/mol) at the j stage temperature can be estimated by assuming ideal mixing using equation 3-9.

By energy balance on the stage, the flow rate of leaving vapor stream is calculated by assuming that the change amount of liquid mixture enthalpy (dH_j^L/dt) is smaller than vapor mixture enthalpy. All stages are assumed adiabatic, $Q_{R,j}$= 0, except for condenser and reboiler.

$$\begin{aligned}\frac{dM_j H_j^L}{dt} &= H_j^L \frac{dM_j}{dt} + M_j \cancel{\frac{dH_j^L}{dt}} \\ &= L_{j-1}H_{j-1}^L + V_{j+1}H_{j+1}^V - L_j H_j^L - V_j H_j^V + F_j H_j^F + Q_{R,j} \\ \xrightarrow{equation\ 3\text{–}1\ substituted} V_j &= \frac{L_{j-1}\left(H_{j-1}^L - H_j^L\right) + V_{j+1}\left(H_{j+1}^V - H_j^L\right) + F_j\left(H_j^F - H_j^L\right) + Q_{R,j}}{H_j^V - H_j^L}\end{aligned} \tag{3-13}$$

Through the use of overall and component material balances, liquid holdup and liquid composition on the stage are integrated with explicit 4th-order Runge-Kutta method with a time interval of 0.01 minute, even as 0.6 second, to solve likely stiffness problems and control data acquisition (note: sampling time of a controller in the industry is 0.3-0.6 second generally).

$$\begin{aligned}\frac{dM_j x_{i,j}}{dt} &= M_j \frac{dx_{i,j}}{dt} + x_{i,j}\frac{dM_j}{dt} \\ &= L_{j-1}x_{i,j-1} + V_{j+1}y_{i,j+1} - L_j x_{i,j} - V_j y_{i,j} + F_j z_{i,j} + R_{i,j} \\ \xrightarrow{equation\ 3\text{–}1\ substituted} \frac{dx_{i,j}}{dt} &= \left[L_{j-1}\left(x_{i,j-1} - x_{i,j}\right) + V_{j+1}\left(y_{i,j+1} - x_{i,j}\right) - V_j\left(y_{i,j} - x_{i,j}\right)R_{i,j}\right. \\ &\quad \left. + F_j\left(z_{i,j-1} - x_{i,j}\right)\right]\frac{1}{M_j}\end{aligned} \tag{3-14}$$

3.5 Controllers

In this study, the reset-feedback algorithm PID controller which is generally used in the industries is used. The reset-feedback algorithm PID controller[38] which integrated portion of PID controller is modified shown in Figure 3-8 and used to prevent reset windup condition when the process is out of control and the error reaches a saturated condition. In addition, the derivative action of PID is modified using the negative of the derivative of the controlled variable instead of the derivative of the error to prevent a drastic change of the derivative change based on the error (or called "derivative kick") when a step change is introduced a set point change. And the derivative portion of PID controller is multiplied by the term $1/(\alpha\tau_d s+1)$ which is referred to as a filter to avoid the interference with high frequency noise and the value of α is set 10 in this study. The controller output is limited to between 0 and 100%. The equations of the modified PID controller can be written in the Laplace domain, as:

$$\begin{aligned} \%CO(s) &= P(s) + I(s) + D(s) \\ P(s) &= K_c E(s) \\ I(s) &= \frac{1}{\tau_I s + 1} \%CO(s) \\ D(s) &= \frac{-K_c \tau_D s}{\frac{\tau_D}{\alpha} s + 1} \%TO(s) \end{aligned} \tag{3-15}$$

In writing FORTRAN program, the equations of the modified PID controller in s-domain are transformed to *z*-domain and these equations can be rewritten in time-domain as[39]:

$$\%CO_{nT} = P_{nT} + I_{nT} + D_{nT}$$

$$P_{nT} = K_c E_{nT}$$

$$I_{nT} = I_{(n-1)T} + \frac{\left[\%CO_{(n-1)T} - I_{(n-1)T}\right]T}{\tau_I + T} \tag{3-16}$$

$$D_{nT} = \frac{\tau_D D_{(n-1)T} - K_c \tau_D \alpha \left[\%TO_{nT} - \%TO_{(n-1)T}\right]}{\tau_D + \alpha T}$$

where T is the sampling time and is set 0.01 minute in this study.

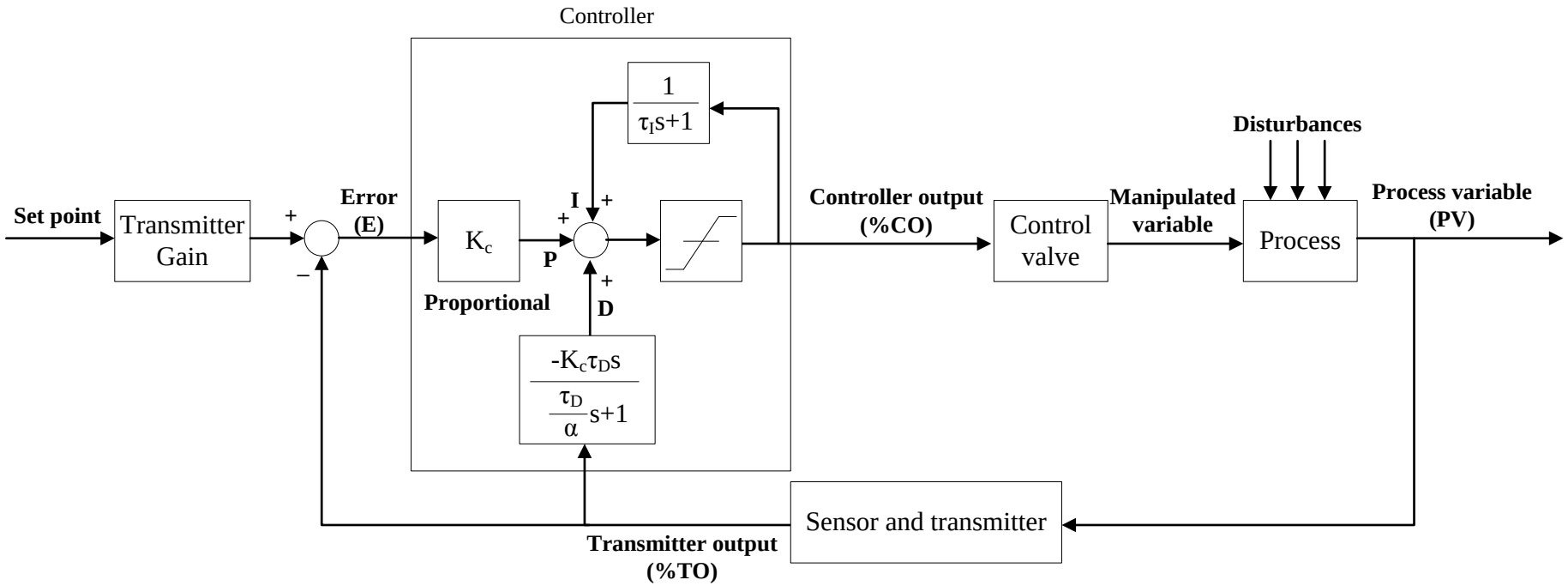

Figure 3-8 Reset-feedback PID controller.[38]

Chapter 4 Control Strategy

For dynamic simulation, Scheme 3 is modularized using a FORTRAN program in this study and shown in Figure 4-1. From the steady-state simulation results of Aspen Plus, on the basis of 80% flooding and a tray spacing of 0.6 m, Columns C101, C201, and C301 are designed to have diameters of 0.75, 1.73, and 0.92 m, respectively. The weir height of each tray in every column is assumed to be 0.05 m. In addition, the column base volumes for the three columns are all sized for a liquid hold-up of 10 minutes. Pressure drops per tray for the three columns are set to at 0.007 bar. A holdup time of 20 minutes[29] in the decanter is assumed to allow for two liquid phases to separate.

A dynamic simulation run is done using the FORTRAN program, and the operating conditions of the proposed scheme at steady state are computed until the conditions of the system do not change with time. Also, the steady state results of all streams from the dynamic simulator in FORTRAN shown in Table 4-1 are about the same as the results from the design study using Aspen Plus as shown in Table 4-2. Moreover, Aspen Dynamics is also used to run dynamic simulations with the tuning of temperature PID controllers.

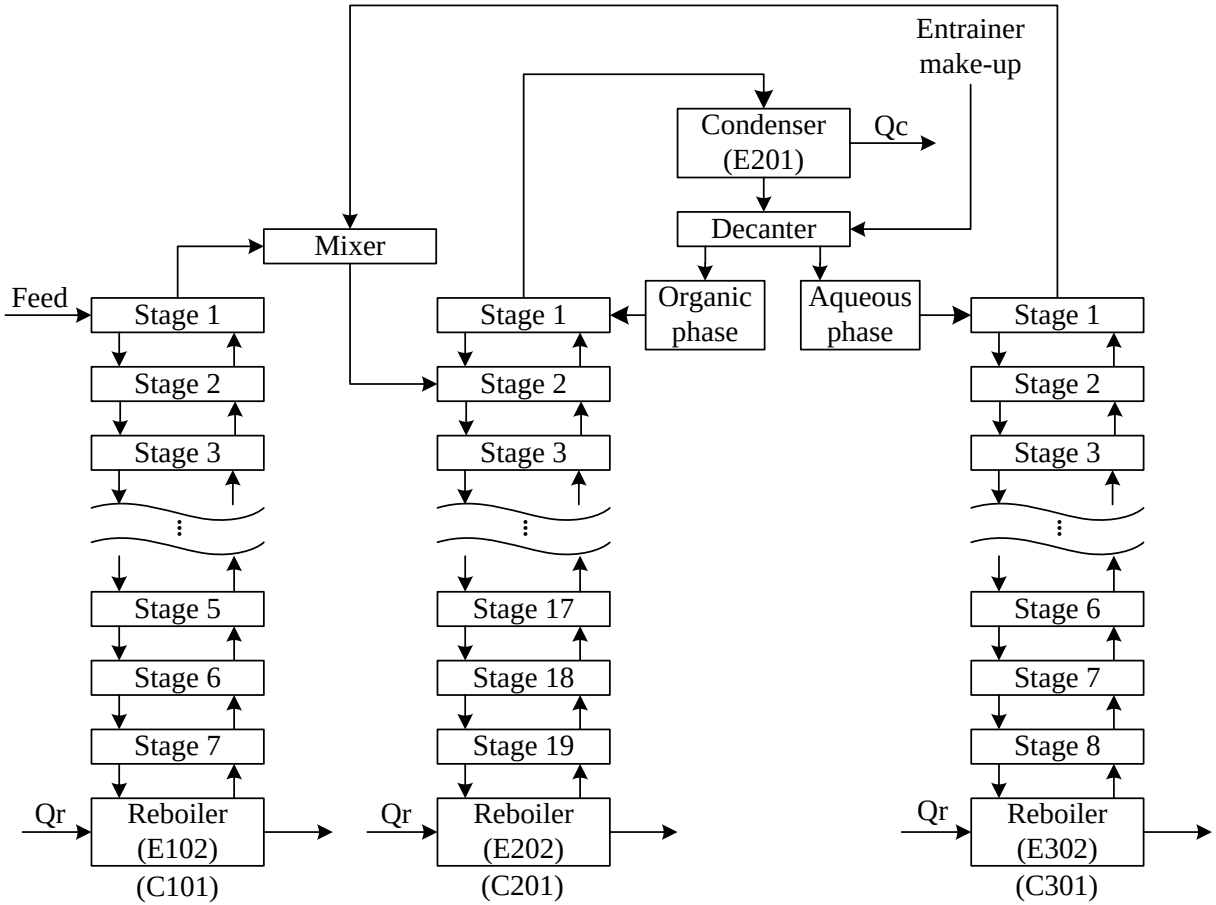

Figure 4-1 Modularized simulation of Scheme 3.

Table 4-1. Summary of Steady-State Stream Data Using Dynamic Simulation Program (FORTRAN)

	feeds		decanter flows		C101 top and bottom flows	
	1	2	7	8	10	3
Pressure (atm)	1.2	1	1	1	1.16	1.1
Temperature (℃)	25	25	40	40	103.5	82.7
CyH	0	1	0.865663	0.039713	0	0
IPA	0.5	0	0.127928	0.457328	0.001001	0.609906
H2O	0.5	0	0.006409	0.502959	0.998999	0.390094
Total Flow mol/min	1666.67	1.34E-04	4013.6	2683.09	301.2	1365.84

	C201 top and bottom flows		C301 top and bottom flows	
	11	5	12	9
Pressure (atm)	1.2	1.05	1.16	1.1
Temperature (℃)	86.9	65	103.7	81.6
CyH	trace	0.53475	trace	0.049576
IPA	0.999999	0.259895	0.001	0.570526
H2O	0.000001	0.205355	0.999	0.379898
Total Flow mol/min	832.31	6696.75	532.42	2149.73

Table 4-2. Summary of Stream Data Based on the Steady-State Simulation with Aspen Plus

	feeds		decanter flows		C101 top and bottom flows	
	1	2	7	8	10	3
Pressure (atm)	1.2	1	1	1	1.16	1.1
Temperature C	25	25	40	40	103.5	82.7
CyH	0	1	0.86544	0.039899	trace	0
IPA	0.5	0	0.12814	0.457875	0.001	0.61032
H2O	0.5	0	0.00642	0.502227	0.999	0.38968
Total Flow mol/min	1666.67	1.34E-04	4014.73	2683.97	301.76	1364.91

	C201 top and bottom flows		C301 top and bottom flows	
	11	5	12	9
Pressure (atm)	1.2	1.05	1.16	1.1
Temperature C	86.9	65	103.7	81.6
CyH	trace	0.534671	trace	0.049771
IPA	0.999999	0.260252	0.001	0.570925
H2O	0.000001	0.205077	0.999	0.379304
Total Flow mol/min	832.52	6698.69	532.39	2151.57

4.1 Basic control strategy

The basic control for Scheme 3 is investigated and Figure 4-2 depicts its plant-wide control structure. In order to maintain the column head pressures, three pressure control loops have been employed. For providing effective control the purities of the product streams of the distillation columns, composition control loops can be used. However, many industrial columns use temperatures for composition control because direct composition analyzers can be expensive, high-maintenance, and unreliable. Although temperature is uniquely related to composition only in a binary system at known pressure, it is still often possible to use the temperature controller on the trays of the column to maintain approximate composition control, even in multi-component systems. Temperature control of some tray is used to hold the composition profile in the column to prevent the light-key impurities from dropping out the bottom and the heavy-key impurities from going overhead. Dual composition or temperature control is not recommended for high-purity columns because of interaction of this control[40]. Single-end temperature control is used in this study. Hence, the bottom product qualities of the three columns are maintained by adjusting reboiler duty and a tray temperature control loop is used for each column. Open-loop sensitivity analysis for the tray temperature control loop in each column is carried out using Aspen Plus.

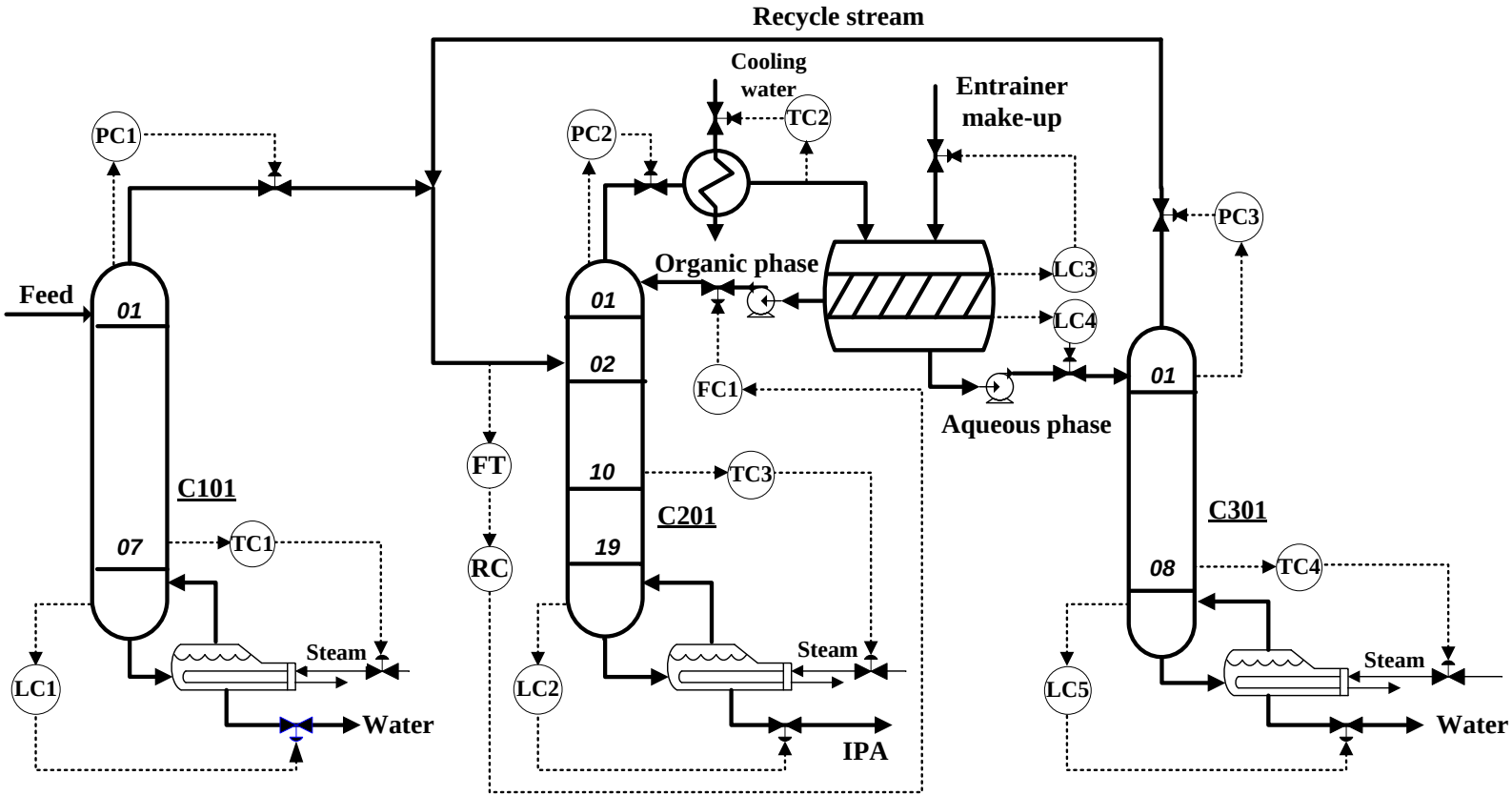

Figure 4-2 Plant-wide control structure for Scheme 3.

Figure 4-3 and Figure 4-4 shows open-loop sensitivity analysis results of the three columns by changing ±0.5% and ±0.05% of reboiler duties. According to Figure 4-5 shown temperature difference distribution of the three columns as ±0.05% of reboiler duties change, the temperature control trays are easily to decide. Tray #7 of the C101 column, tray #10 of the C201 column, and tray #8 of the C301 column are chosen as three temperature control points, in view of the high sensitivity of tray temperature with respect to variations in reboiler duty. PID control is used in these three tray temperature control loops. The tuning constants are K_c (proportional gain) = 0.8, τ_I (integral time) = 8.0, and τ_D (derivative time) = 0.125 for these three tray temperature control loops.

The heterogeneous azeotropic column (C201) can be operated to distillate high purity IPA based on enough ratio of organic phase flow rate and feed flow rate of the azeotropic column to cross the distillation boundary. Hence, ratio control scheme is implemented to reject feed rate disturbance of the C201 column similar as Arifin and Chien[7] and the ratio of the organic reflux flow to the feed flow rate of the C201 column is kept constant.

The organic-phase liquid level of the decanter is controlled by manipulating entrainer make-up flow, and the aqueous-phase level of the decanter is controlled by manipulating aqueous flow rate. For the organic-phase level loop and the

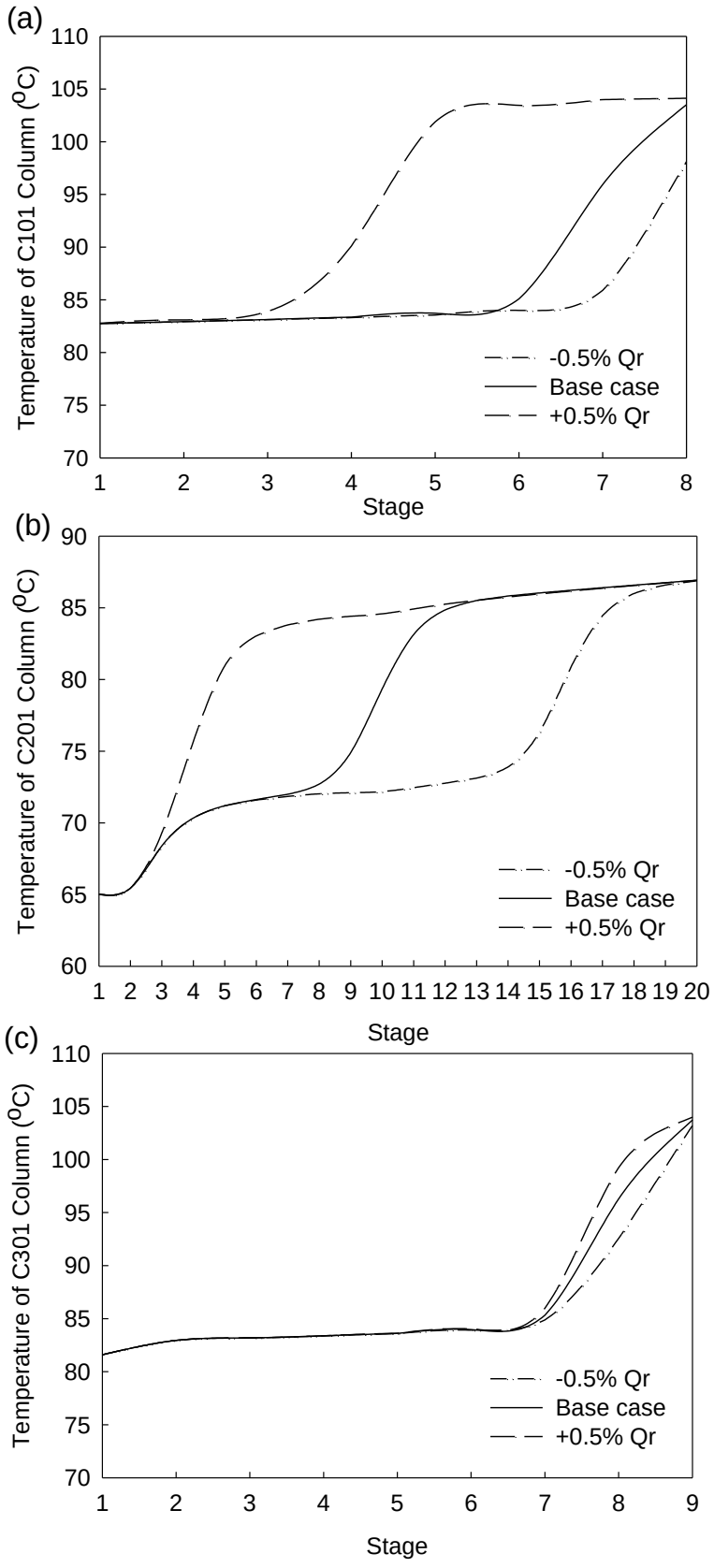

Figure 4-3 Open-loop sensitivity analysis for the three columns in Scheme 3 by changing ±0.5% of reboiler duties (a) C101, (b) C201, (c) C301

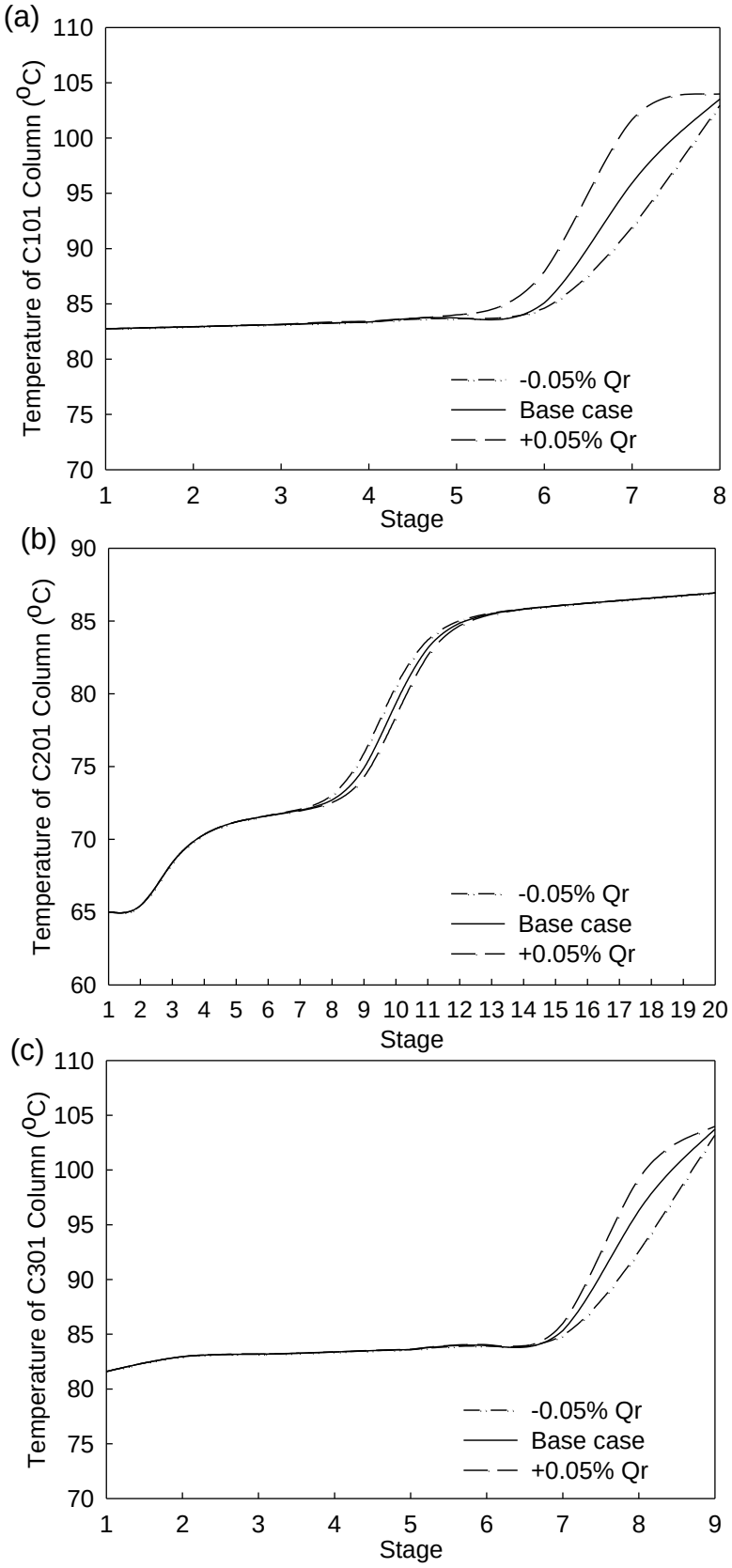

Figure 4-4 Open-loop sensitivity analysis for the three columns in Scheme 3 by changing ±0.05% of reboiler duties (a) C101, (b) C201, (c) C301

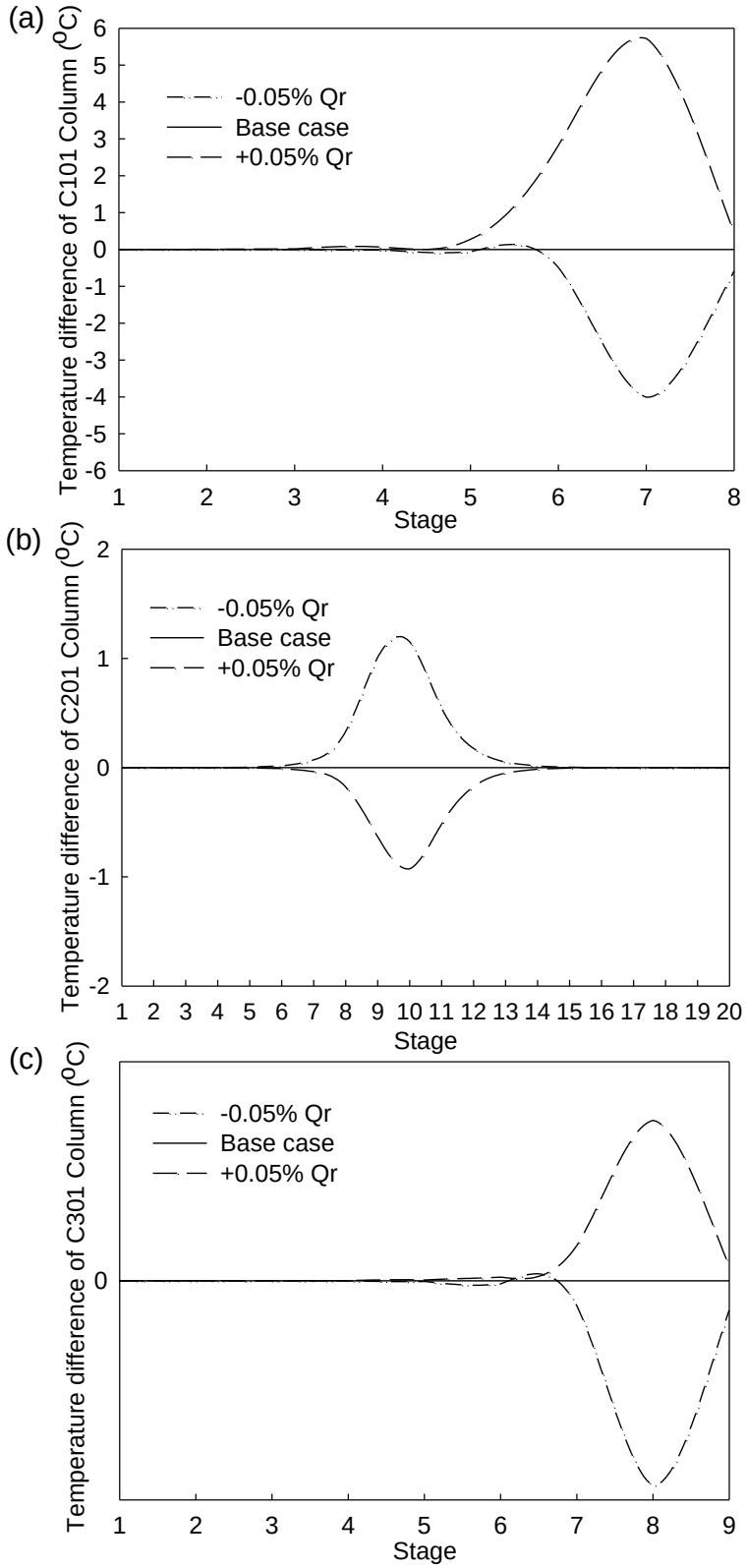

Figure 4-5 Temperature difference for the three columns in Scheme 3 by changing ±0.05% of reboiler duties (a) C101, (b) C201, (c) C301

aqueous-phase level loop of the decanter, the P-only controllers are used and K_c = 10 is used as in Arifin and Chien[7]. The bottom liquid levels of the three columns are controlled by manipulating the bottom product flow. The column bottom level control loops are considered to be ideal. The tuning constants of all controllers are summarized in Table 4-3.

As the overhead vapor of Column C201 is condensed into liquid, the condensate temperature is controlled at 40℃ by manipulating cooling water flow. The top temperature control loop of the C201 column is also assumed to be ideal control (or called perfect control). All ranges of measuring instrument and control are summarized in Table 4-4.

Table 4-3. Constants of Controllers Based on Heuristics Used in FORTRAN Program

Code	Kind of controller	K_c	τ_I	τ_D	Reference
PC1	ideal control	-	-	-	-
PC2	ideal control	-	-	-	-
PC3	ideal control	-	-	-	-
TC1	PID controller	0.8	8	0.125	heuristic
TC2	ideal control	-	-	-	-
TC3	PID controller	0.8	8	0.125	heuristic
TC4	PID controller	0.8	8	0.125	heuristic
LC1	ideal control	-	-	-	-
LC2	ideal control	-	-	-	-
LC3	P controller	10	9999	0.0001	[7]
LC4	P controller	10	9999	0.0001	[7]
LC5	ideal control	-	-	-	-
FC1	ideal control	-	-	-	-

Table 4-4. Ranges of Measuring Instrument and Control

Instrument measurement range	Maximum	Normal	Minimum	Unit
Temperature sensor of C101	105.9	95.9	85.9	℃
Temperature sensor of C102	89.4	79.4	69.4	℃
Temperature sensor of C103	106.3	96.3	86.3	℃
Organic phase level	2.5	2.4	2.3	m
Control range				
Duty of E102	2251.76	1125.88	0	kW
Duty of E202	3660.92	1830.46	0	kW
Duty of E302	3343.72	1671.86	0	kW
Flow rate of entrainer make-up	0.00027	0.0001337	0	mol/min

For comparison, Aspen Dynamics is used for dynamic control test showed as Figure 4-6 and the control structure for Scheme 3 is the same as Figure 4-2. The constants of all PID controllers based on heuristics are summarized in Table 4-5. Two types of disturbances, namely ±20% changes in both fresh feed rate and fresh feed H_2O composition, are also used to test the proposed plant-wide control structure in Aspen Plus Dynamics process flowsheet.

Luyben[41] considers that the tuning of temperature controllers is more involved than simply using heuristics as is done for flow and level controllers, and some effective tuning procedure is required. In order to eliminate excessively large overshoot, the Integral of Absolute Error (IAE) tuning method is used. Minimum IAE

tuning parameters for load disturbance is[38]:

$$K_c = \frac{1.435}{K_p}\left(\frac{T_D}{\tau}\right)^{-0.921}$$

$$\tau_I = \frac{\tau}{0.878}\left(\frac{T_D}{\tau}\right)^{0.749} \quad (4\text{-}1)$$

$$\tau_D = 0.482\tau\left(\frac{T_D}{\tau}\right)^{1.137}$$

Analysis of the open loop response and tuning parameters of three tray temperatures are summarized in Table 4-6.

Table 4-5. Constants of PID Controllers based on Heuristics in Aspen Plus Dynamics

Code	Kind	Action	K_c	τ_I	τ_D	*others*	Reference
FC1	PI	reverse	0.5	0.3	-	-	Heuristic, [43]
FC2	PI	reverse	0.5	0.3	-	-	Heuristic, [43]
RC	-	-	-	-	-	2.06	-
PC1	PI	direct	20	12	-	-	Heuristic, [7], [43]
PC2	PI	direct	20	12	-	-	Heuristic, [7], [43]
PC3	PI	direct	20	12	-	-	Heuristic, [7], [43]
TC1	PID	reverse	0.8	8	0.125	-	Heuristic
TC2	PID	reverse	0.8	8	0.125	-	Heuristic
TC3	PID	reverse	0.8	8	0.125	-	Heuristic
TC4	PID	reverse	0.8	8	0.125	-	Heuristic
LC1	P	direct	2	9999	-	-	Heuristic, [43]
LC2	P	direct	2	9999	-	-	Heuristic, [43]
LC3	P	reverse	10	9999	-	-	Heuristic, [7]
LC4	P	direct	2	9999	-	-	Heuristic, [43]
LC5	P	direct	2	9999	-	-	Heuristic, [43]

Table 4-6. Constants of Controllers based on IAE Tuning in Aspen Plus Dynamics

Code	Kind	Action	K_p	τ	T_D	K_c	τ_I	τ_D	*others*	Reference
FC1	PI	reverse	-	-	-	0.5	0.3	-	-	Heuristic, [43]
FC2	PI	reverse	-	-	-	0.5	0.3	-	-	Heuristic, [43]
RC	-	-	-	-	-	-	-	-	2.06	
PC1	PI	direct	-	-	-	20	12	-	-	Heuristic, [7], [43]
PC2	PI	direct	-	-	-	20	12	-	-	Heuristic, [7], [43]
PC3	PI	direct	-	-	-	20	12	-	-	Heuristic, [7], [43]
TC1	PID	reverse	8.25	1.94	1.2	0.271	1.543	0.542	-	IAE
TC2	PID	reverse	-	-	-	0.8	8	0.125	-	Heuristic
TC3	PID	reverse	3.67	1.16	3.87	0.128	3.263	2.023	-	IAE
TC4	PID	reverse	8.06	2.11	0.6	0.568	0.937	0.243	-	IAE
LC1	P	direct	-	-	-	2	9999	-	-	Heuristic, [43]
LC2	P	direct	-	-	-	2	9999	-	-	Heuristic, [43]
LC3	P	reverse	-	-	-	10	9999	-	-	Heuristic, [7]
LC4	P	direct	-	-	-	2	9999	-	-	Heuristic, [43]
LC5	P	direct	-	-	-	2	9999	-	-	Heuristic, [43]

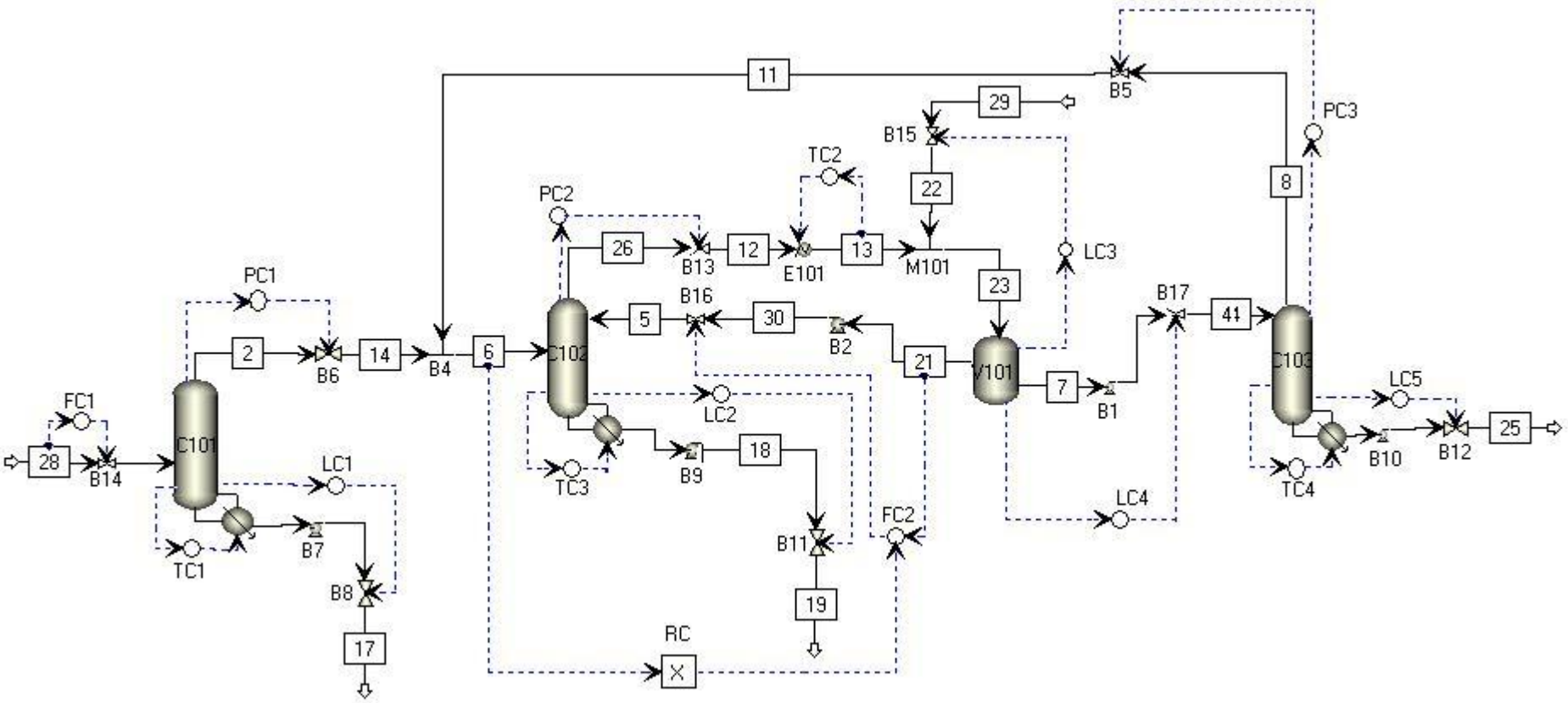

Figure 4-6 Plant-wide control structure for Scheme 3 using Aspen Plus Dynamics

4.2 Result and discussion

Two types of disturbances are used to test the proposed plant-wide control structure, namely ±20% changes in both fresh feed rate and fresh feed H_2O composition. Figure 4-7 shows the dynamic responses using FORTRAN program for ±20% step change in fresh feed rate. The plots in the first and second rows show responses of top vapor flow and bottom product flow of the three columns. Due to the ±20% change in the fresh feed rate, the vapor flow and the product flow, for the most part, increase or decrease over time before reaching their steady-state values. The water product flows (from C101 and C301) and IPA product flow also increase (or decrease) and reach their new values in 80 min. with a +20% (or -20%) change in fresh feed rate. For +20% change in fresh feed rate, the total water product flow rate changes from 834.20 to 1001.03 mol/min and the IPA product flow rate changes from 832.49 to 998.65 mol/min. The plots in the third row show that the three tray temperatures are brought back to their desired set-points. The plots in the last row show that the stabilized product compositions of the three columns are very near their purity specifications. The water product compositions are back to 99.9 mol% and the IPA product composition is also greater than 99.99989 mol%.

Figure 4-8, on the other hand, shows the dynamic responses using FORTRAN program for ±20% changes of water composition in the feed. The plots in the first row

show that top vapor flows of the three columns all generally decrease over time with an increase in the water composition in the feed. However, as shown in the second-row plots, the response to a positive step change in the H_2O composition is such that the product flow of Column C101 generally increases over time before finally approaching a steady-state value, whereas the steady-state product flows of Columns C201 and C301 decrease with the same step change. The plots in the third row also show that the three tray temperatures can be effectively brought back to their set-point values. The plots in the last row show that the product compositions of the three columns are still in the ultra-pure region. The water product compositions of the C101 column is greater than 99.88 mol% and the water product compositions of the C301 column is very near to 99.9 mol%. The IPA composition in the product stream is greater than 99.99987 mol%. All results of two types of disturbances control tests, namely ±20% changes in both fresh feed rate and fresh feed H_2O composition, are summarized in Table 4-7.

Figure 4-9 and Figure 4-10 shows the dynamic responses using Aspen Plus Dynamic with constant of controllers based on heuristics for ±20% step change in fresh feed rate and in fresh feed H_2O composition. Figure 4-11 and Figure 4-12 shows the dynamic responses using Aspen Plus Dynamic with constant of controllers based on IAE for ±20% step change in fresh feed rate and in fresh feed H_2O composition.

The results of Figure 4-8 and Figure 4-9 show that the three tray temperatures can be effectively brought back to their set-point values and show that the product compositions of Column C101, C201 and, C301 are still in the ultra-pure region. However, the overshoots of the three tray temperatures are too large. In Figure 4-10 and Figure 4-11, the large overshoots of the three tray temperature are eliminated, and the overshoots of the product compositions of the three columns are decreased for the dynamic responses for the load disturbances of ±20% step change in fresh feed rate and in fresh feed H_2O composition. In Figure 4-9 and Figure 4-11, there are some small gap away from 99.9 mol% for water product composition of C301, because change in feed causes pressure drop oscillation at each stage in C301 at ±20% step change in fresh feed rate condition.

As using FORTRAN program to simulate dynamic response for Scheme 3, ideal controls are set at pressure control, level control, and flow control shown as Table 4-3. Because these ideal controls are not affected by dynamic fluctuations, time achieved steady-state using FORTRAN program (about 80 min) shorter than using Aspen Plus Dynamic (about 400 min) by comparing Figure 4-7 and Figure 4-8 with Figure 4-9 and Figure 4-10,

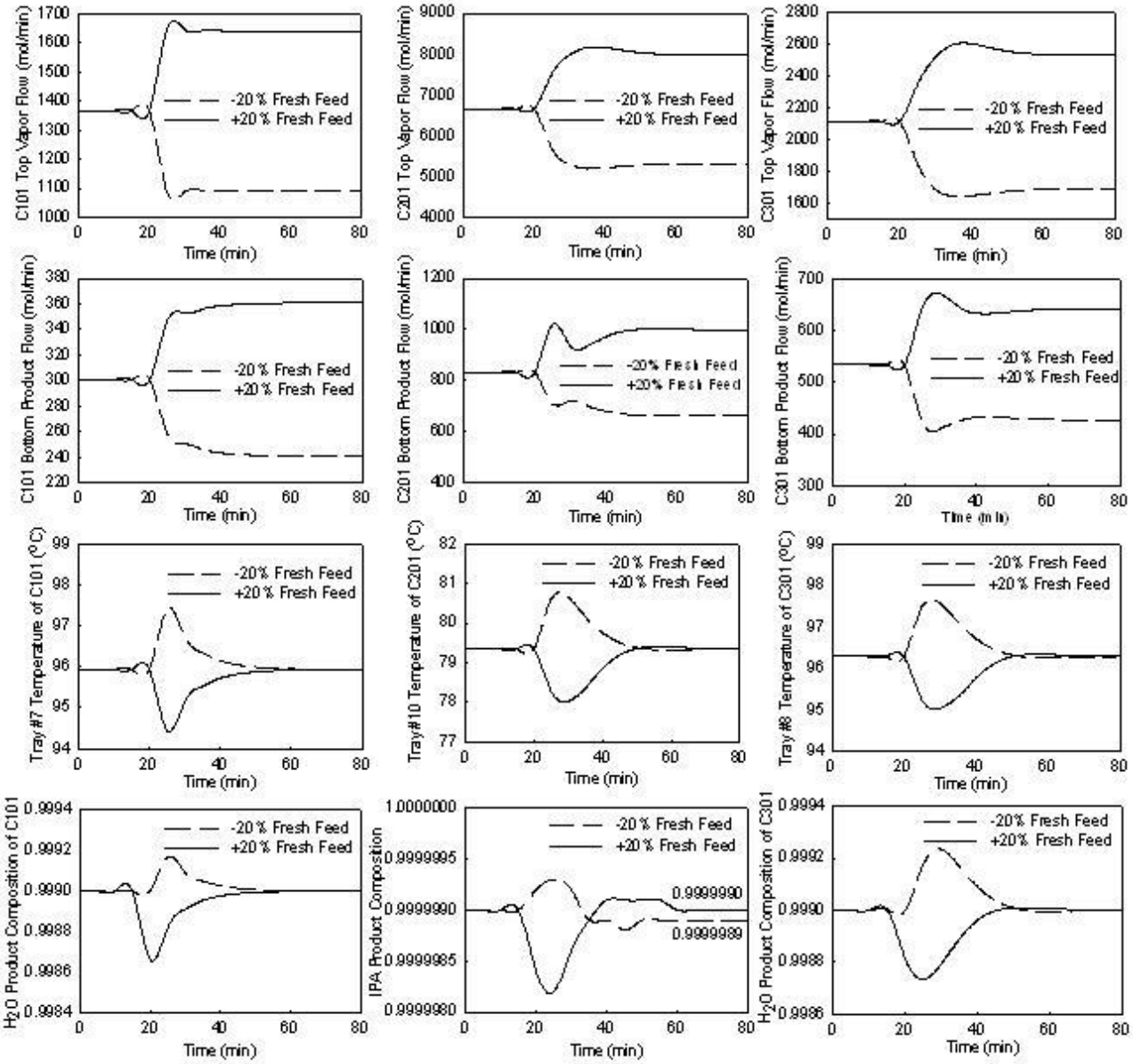

Figure 4-7 Closed-loop responses with ±20% fresh feed rate changes (dashed lines, -20%; solid lines, +20%) using FORTRAN program.

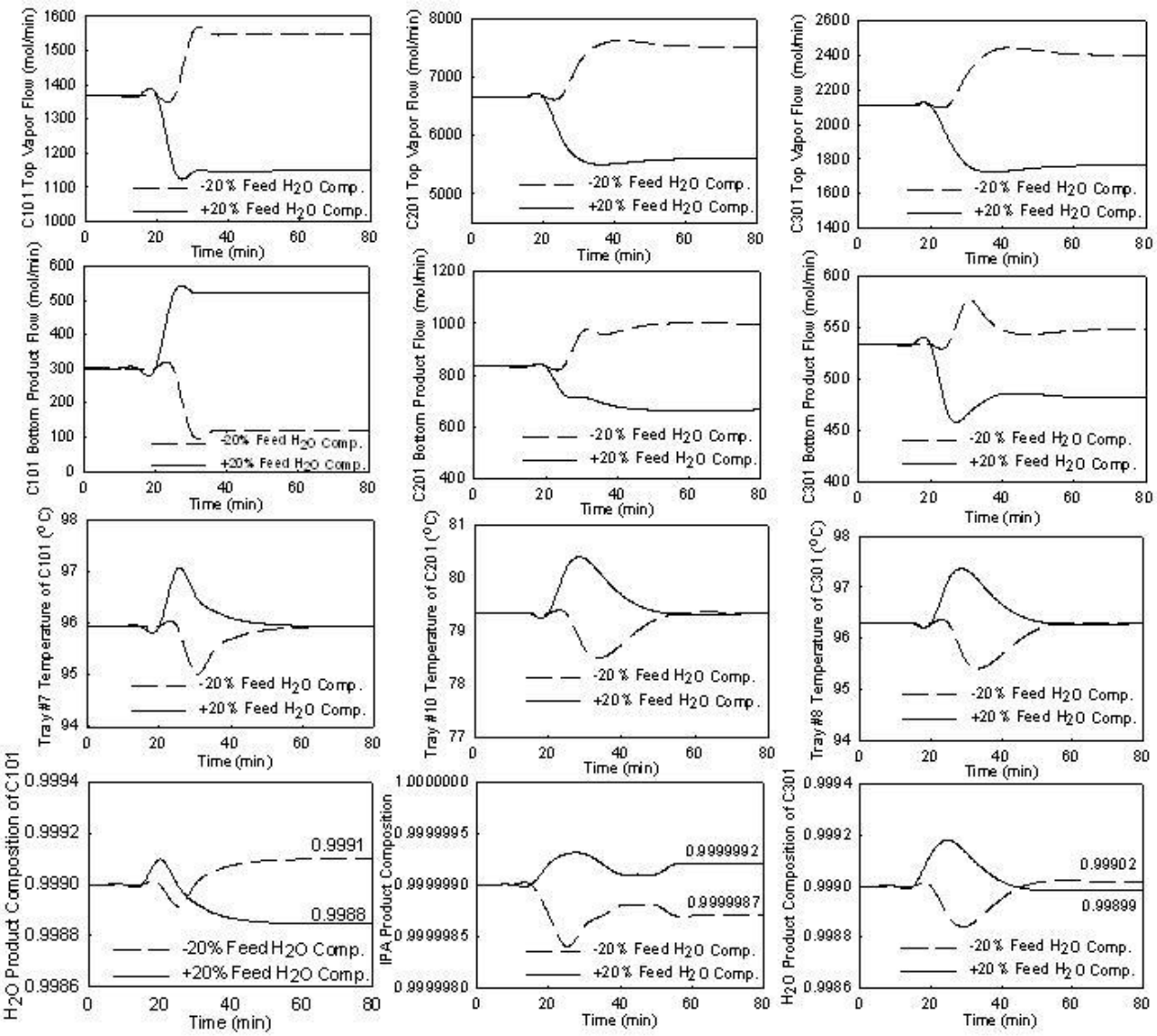

Figure 4-8 Closed-loop responses with ±20% feed H_2O composition changes (dashed lines, -20%; solid lines, +20%) using FORTRAN program.

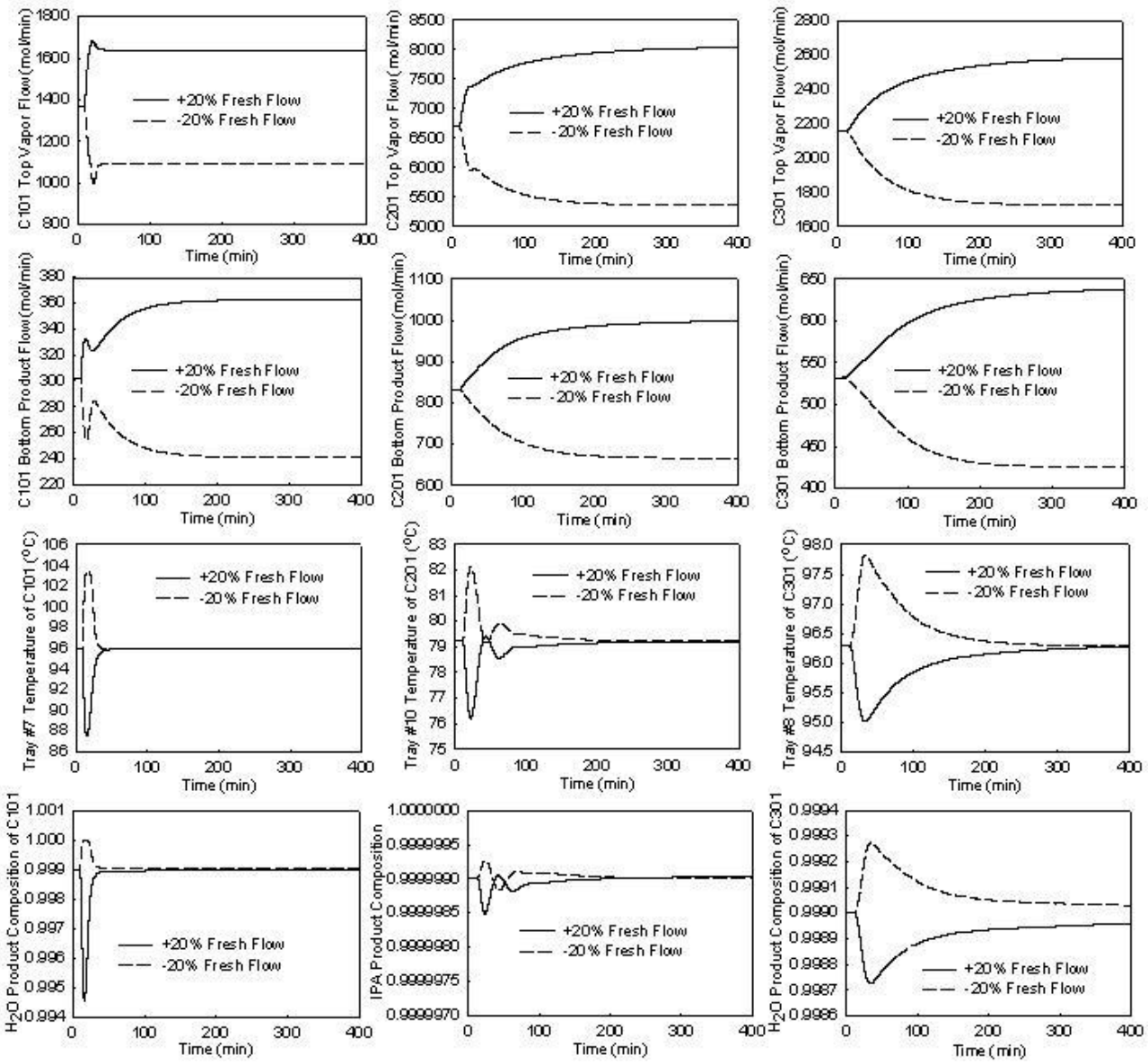

Figure 4-9 Closed-loop responses with ±20% fresh feed rate changes (dashed lines, -20%; solid lines, +20%) based on heuristics using Aspen Plus Dynamics.

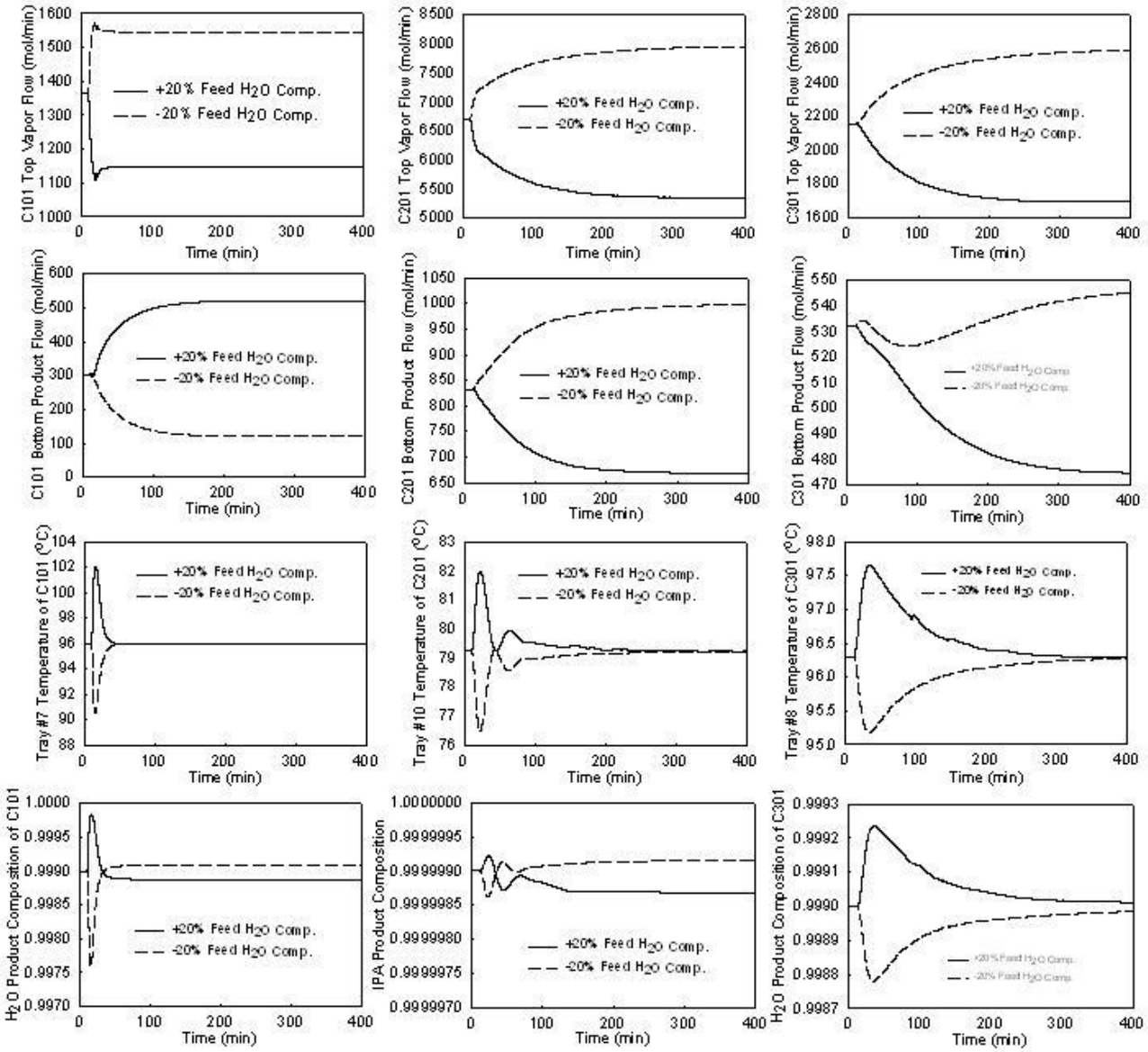

Figure 4-10 Closed-loop responses with ±20% feed H_2O composition changes (dashed lines, -20%; solid lines, +20%) based on heuristics using Aspen Plus Dynamics.

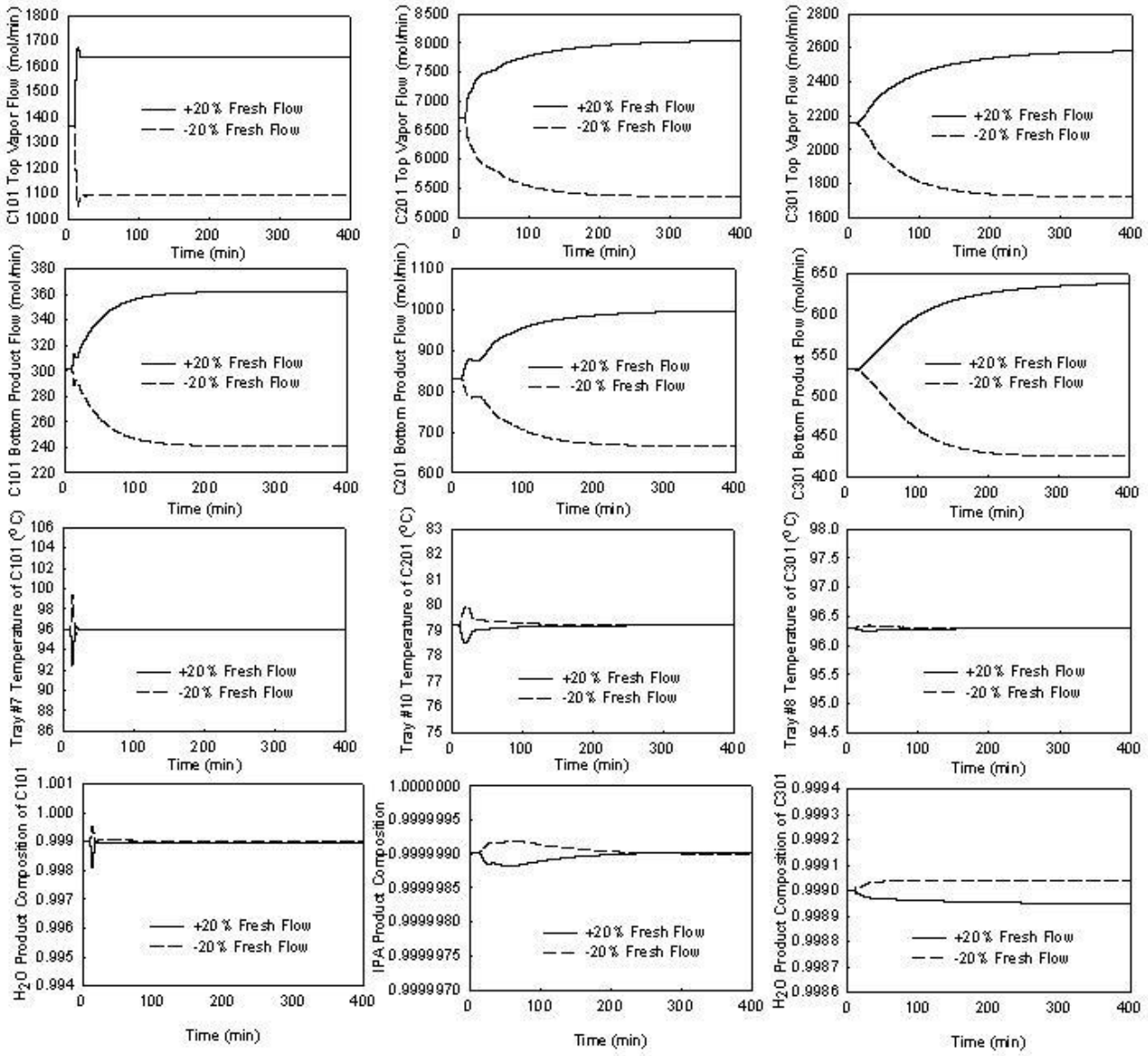

Figure 4-11 Closed-loop responses with ±20% fresh feed rate changes (dashed lines, -20%; solid lines, +20%) based on IAE tuning using Aspen Plus Dynamics.

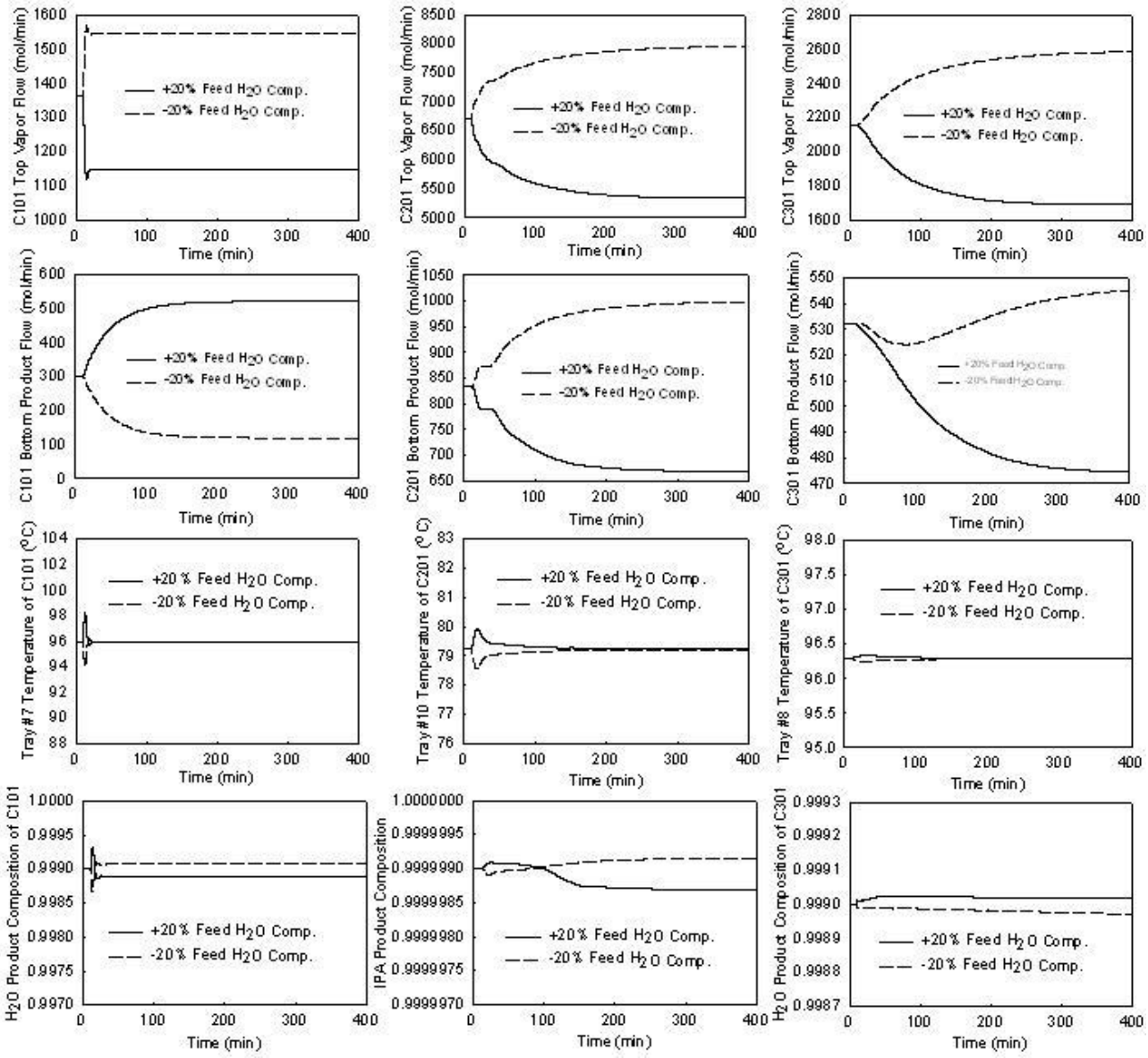

Figure 4-12 Closed-loop responses with ±20% feed H_2O composition changes (dashed lines, -20%; solid lines, +20%) based on IAE tuning using Aspen Plus Dynamics.

Table 4-7. Results of Two Types of Disturbances Control Tests Using FORTRAN Program

Case	Product composition of C101			Product composition of C102			Product composition of C101		
	X_{IPA}	X_{CyH}	X_{H2O}	X_{IPA}	X_{CyH}	X_{H2O}	X_{IPA}	X_{CyH}	X_{H2O}
Base condition	0.001	0	0.999	0.999999	0.000001	trace	0.001	trace	0.999
+20 % fresh feed rate	0.001	0	0.999	0.999999	0.000001	trace	0.001001	trace	0.998999
-20 % fresh feed rate	0.000999	0	0.999001	0.999999	0.000001	trace	0.001001	trace	0.998999
+20 % fresh feed H_2O composition	0.001154	0	0.998846	0.999999	0.000001	trace	0.001015	trace	0.998985
-20 % fresh feed H_2O composition	0.000901	0	0.999099	0.999998	0.000001	0.000001	0.000983	trace	0.999017

Chapter 5 Conclusions

This study presents a study of designing a three-column heterogeneous azeotropic distillation configuration to separate IPA and water using cyclohexane as the entrainer, featuring energy saving and cost effective. Due to low reflux ratios, a pre-concentration column and an entrainer recovery column employed in the previous works are replaced by stripping columns. This proposed scheme, essentially a three-column sequence using stripping columns in place of conventional distillation columns, saves more energy and is more cost effective than other schemes in the literature. Regardless of the payback period on investment being used (i.e., 3, 5 or 10 years), the total annual cost of the proposed scheme is less than that of the other schemes.

The basic control for the proposed scheme has also been examined. A tray temperature control loop implemented in each of these three columns can be used to maintain the bottom product compositions. In addition, ratio control of the organic reflux flow to the feed flow of the IPA purification column is capable of rejecting feed rate disturbances. Furthermore, if fresh feed rate or water composition in the feed is subject to a ±20% change, the simulation results of the closed-loop system reveal that the control strategy for the proposed scheme can yield good control performance. According to the above results, this proposed scheme can be achieved three goals that

are more energy saving, less total annual cost, and process easily controlled.

Three-column heterogeneous distillation sequence is more energy saving as demonstrated by Pham and Doherty[3] and Arifin and Chien[7]. Hence, thermally coupled distillation of the three-column sequence, dividing-wall distillation with two dividing walls for IPA dehydration process, this is worth to discuss in the future. And the DWC structure will be compared with Scheme 3 in this study about energy-saving and control strategy.

Nomenclature

Letters		Unit
A	capacity / size parameter of the equipment	[-]
A_i	extended Antoine equation parameters	[-]
a_{ij}	non-randomness parameters of NRTL	[-]
A_w	effective area of a stage	[m^2]
B_1	constants depending on the equipment type	[-]
B_2	constants depending on the equipment type	[-]
b_{ij}	non-randomness parameters of NRTL	[-]
C_{BM}	bare module equipment cost	[$]
C_p^0	purchased cost	[$]
$C_{PL,,I}$	liquid heat capacity of component *i*	[J/mol·K]
F_{BM}	bare module cost factor	[-]
F_j	fresh feed at j stage	[mol/min]
F_M	material factor	[-]
F_P	pressure factor	[-]
$H^L{}_i$	liquid molar enthalpy of component *i*	[J/mol]
$H^L{}_m$,	liquid mixture molar enthalpy	[J/mol]
$H^L{}_j$	liquid mixture molar enthalpy at the *j* stage temperature	[J/mol]

H^V_i	vapor molar enthalpy of component *i*	[J/mol]
H^V_j	vapor mixture molar enthalpy at the *j* stage temperature	[J/mol]
H^V_m	vapor mixture molar enthalpy	[J/mol]
H_{vap}	molar heat of vaporization	[J/mol]
H_i^{evp}	molar heat of vaporization of component *i*	[J/mol]
f_q	quantity factor	[-]
i_{min}	payback period	[year]
MW	molecular weight	[g/mol]
i_{min}	payback period	[year]
K_1	constants specific to the type of equipment	[-]
K_2	constants specific to the type of equipment	[-]
K_3	constants specific to the type of equipment	[-]
K_c	proportional gain	[%MV/%TO]
L_j	liquid flow rate leaving stage *j*	[mol/min]
M_j	holdup on the *j* stage	[mol]
N	number of trays	[-]
P	pressure	[atm]
P_c	critical pressure	[bar]
P^{sat}	saturated vapor pressure	[bar]

R	universal gas constant	$[\,\mathrm{bar}\cdot\mathrm{cm}^3/\mathrm{mol}\cdot\mathrm{K}\,]$
T	sampling time	[min]
T_0	reference temperature	[K]
T_c	critical temperature	[K]
T_D	dead time	[min]
T_r	reduced temperature	[-]
V_c,	critical volume	[m^3/mol]
V_{ci}	critical volume of component *i*	[m^3/mol]
V_j	vapor flow rate leaving stage *j*	[mol/min]
W_H	weir height	[m]
W_{HO}	head on the weir	[m]
W_L	side weir length	[m]
x_i	liquid molar fraction of component *i*	[-]
y_i	vapor molar fraction of component *i*	[-]
Z_c	critical compressibility factor	[-]
Z_{ci}	critical compressibility factor of component *i*	[-]
Z_{cm}	compressibility factor of a mixture	[-]

Greek letters		Unit
α_{ij}	non-randomness parameters of NRTL	[-]
γ_i	activity coefficient of the component *i*	[-]
ρ_m	liquid bubble-point density	[mol/m^3]
τ	Time constant	[min]
τ_{ijj}	dimensionless interaction parameters of NRTL	[-]
τ_I	integral time	[min]
τ_D	derivative time	[min]
ϕ_i	volume fraction for *i* component	[-]
λ	latent heat of steam	[Btu/lb]

Subscripts

$_i$	component *i*
j	stage *j*

Reference

(1) Gmehling, J., Onken, U., *Vapor-liquid equilibrium data collection aqueous-organic system, chemistry data series*. DECHMA, Vol.1, Part1, 1977.

(2) Widagdo, S.; Seider, W. D. Azeotropic distillation. *AIChE J.* **1996**, *42*, 96.

(3) Pham, H. N.; Doherty, M. F. Design and Synthesis of Heterogeneous Azeotropic Distillation – III. Column Sequences. *Chem. Eng. Sci.*, **1990**, *45*, 1845.

(4) Ryan, P. J.; Doherty, M. F. Design/Optimization of Ternary Heterogeneous Azeotropic Distillation Sequences. *AIChE J.* **1989**, *35*, 1592.

(5) Luyben, W. L. Control of a Multiunit Heterogeneous Azeotropic Distillation Process. *AIChE J*. **2006**, *52*, 623.

(6) Chien, I. L.; Zeng, K. L.; Chao, H. Y. Design and Control of a Complete Heterogeneous Azeotropic Distillation Column System. *Ind. Eng. Chem. Res.* **2004**, *43*, 2160.

(7) Arifin, S.; Chien, I. L. Combined Preconcentrator/Recovery Column Design for Isopropyl Alcohol Dehydration Process. *Ind. Eng. Chem. Res.* **2007**, *46*, 2535.

(8) Luyben, W. L. Plantwide Control of an Isopropyl Alcohol Dehydration Process. *AIChE J*. **2006**, *52*, 2290.

(9) Arifin, S.; Chien, I. L., Design and Control of an Isopropyl Alcohol Dehydration Process via Extractive Distillation Using Demethyl Sulfoxide as an Entrainer. *Ind. Eng. Chem. Res.* **2008**, *47*, 790.

(10) Abu-Eishah, S. I.; Luyben, W.L. Design and Control of a Two-column Azeotropic System. *Ind. Eng. Chem. Process Des. Dev.* **1985**, *24*, 132.

(11) Luyben, W. L. Design and Control of a Fully Heat-integrated Pressure-swing Azeotropic Distillation System. *Ind. Eng. Chem. Res.* **2008**, *47*, 2681.

(12) Breure, B., Kinetic Separation of Vaporous Alcohol-Water Mixtures; Doctor's thesis of Technische Universiteit Eindhoven, 2010.

(13) Lin, F. L. Internally Heat-Integrated Distillation Column (HIDiC) Design by Mathematical Programming Approach; Master's thesis of National Taiwan University, 2007.

(14) Halvorsen, I. J.; Skogestad, S., Shortcut Analysis of Optimal Operation of Petlyuk Distillation. *Ind. Eng. Chem. Res.* **2004**, *43*, 3994.

(15) Bravo-Bravo, C. Segovia-Hernández, J. G., Gutiérrez-Antonio, C., Durán, A. L., Bonilla-Petriciolet, A., Briones-Ramírez, A., Extractive Dividing Wall Column: Design and Optimization. *Ind. Eng. Chem. Res.* **2010**, *49*, 3672.

(16) Sun, L. Y., Chang, X. W., Zhang, Y. M., Li, J., Li, Q. S., Reducing Energy Consumption and CO_2 Emissions in Thermally Coupled Azeotropic Distillation. *Chem. Eng. Technol.* **2010**, 33, 395.

(17) Wang, S. J.; Wong, D. S. H., Controllability and Energy Efficiency of a High-purity Divided Wall Column. *Chem. Eng. Sci.* **2007**, *62*, 1010.

(18) Ling, H.; Luyben, W. L. New Control Structure for Divided-Wall Columns. *Ind. Eng. Chem. Res.* **2009**, *48*, 6034.

(19) Ling, H.; Luyben, W. L. Temperature Control of the BTX Divided-Wall Column. *Ind. Eng. Chem. Res.* **2010**, 49, 189.

(20) Vane, L. M., A review of pervaporation for product recovery from biomass fermentation processes. *J. Chem. Technol. Biotechnol.* **2005**, *80*, 603.

(21) Lipnizki, F., Hausmanns S., Ten, P. K., Field, R. W., Laufenberg, G., Organophilic pervaporation: prospects and performance. *Chem Eng. J.* **1990**, *73*, 113.

(22) Lipnizki, F., Field, R. W., Ten, P. K., Pervaporation-based hybrid process: a review of process design, applications and economics. *J. Memb. Sci.* **1999**, *153*, 183.

(23) Brschke, H.E.A., Industrial application of membrane separation processes. *Pure Appl. Chem.* **1995**, 67, 993.

(24) Cho, J., Joen, J. K., Optimization study on the azeotropic distillation process for isopropyl alcohol dehydration. *Korean J. Chem. Eng.* **2006**, 23(1), 1.

(25) Renon, H.; Prausnitz, J. M. Local Compositions in Thermodynamic Excess Function for Liquid Mixtures. *AIChE J.* **1968**, *14*, 135.

(26) Wang, C. J.; Wong, D. S. H.; Chien, I.-L.; Shih, R. F.; Liu, W. T.; Tsai, C. S. Critical Reflux, Parametric Sensitivity, and Hysteresis in Azeotropic Distillation of Isopropyl Alcohol+Water+Cyclohexane. *Ind. Eng. Chem. Res.* **1998**, *37*, 2835.

(27) Aspen Plus and Aspen Plus Dynamic V7.3. Aspen Technology, Inc.: U.S.A., 2011.

(28) Dean, J. A. *Lange's Handbook of Chemistry*; 15th ed., McGraw-Hill Book Company: New York, 1999.

(29) Turton, R.; Bailie, R. C.; Whiting, W. B.; Shaeiwitz, J. A. *Analysis, Synthesis, and Design of Chemical Processes*; 3rd ed., Pearson Education: Boston, 2009.

(30) Seider, W. D.; Seader, J. D.; Lewin, D. R. *Product and Process Design Principles: Synthesis, Analysis, and Evaluation*; 2nd ed., John Wiley and Sons: New York, 2004.

(31) Olujic, Z.; Sun, L.; de Rijke, A.; Jansens, P. J. Conceptual Design of an Internally Heat Integrated Propylene-Propane Splitter. *Energy* **2006**, *31*, 3083.

(32) Douglas J. M., *Conceptual Design of Chemical Processes*, McGraw-Hill Book Company, 1988.

(33) Reid R. C.; Prausnitz, J. M.; Poling, B. E., *Properties of Gases and Liquids*, 4th ed., McGraw-Hill Book Company, 1987.

(34) Walas, S. M. *Phase Equilibrium in Chemical Engineering*, Butterworth Publishers, Bostom, 1985.

(35) King, C. J., *Separation Processes*, 2nd ed., McGraw-Hill Book Co., New York, 1980.

(36) Franks, R. G. E. *Modeling and Simulation in Chemical Engineering*; John Wiley and Sons: Canada, 1972.

(37) Rovaglio, M.; Doherty, M. F. Dynamics of Heterogeneous Azeotropic Distillation Columns. *AIChE J.* **1990**, *36*, 39.

(38) Smith, C. A.; Corripio, A., *Principles and Practice of Automatic Process Control*, 3nd ed., John Wiley &Sons, Inc., New York, 1997.

(39) Smith, C. A.; Corripio, A., *Principles and Practice of Automatic Process Control*, 2nd ed., John Wiley &Sons, Inc., New York, 1997.

(40) Luyben W. L., B. D. Tyreus, and M. L. Luyben, *Plantwide Process Control*, McGraw-Hill Book Company, New York, 1999.

(41) Luyben, W. L., *Distillation Design and Control Using Aspen^{TM} Simulation*, John Wiley & Sons, Inc., New Jersey, 2006.